

abstracts

Hot Topics in Molecular Imaging – TOPIM 2012

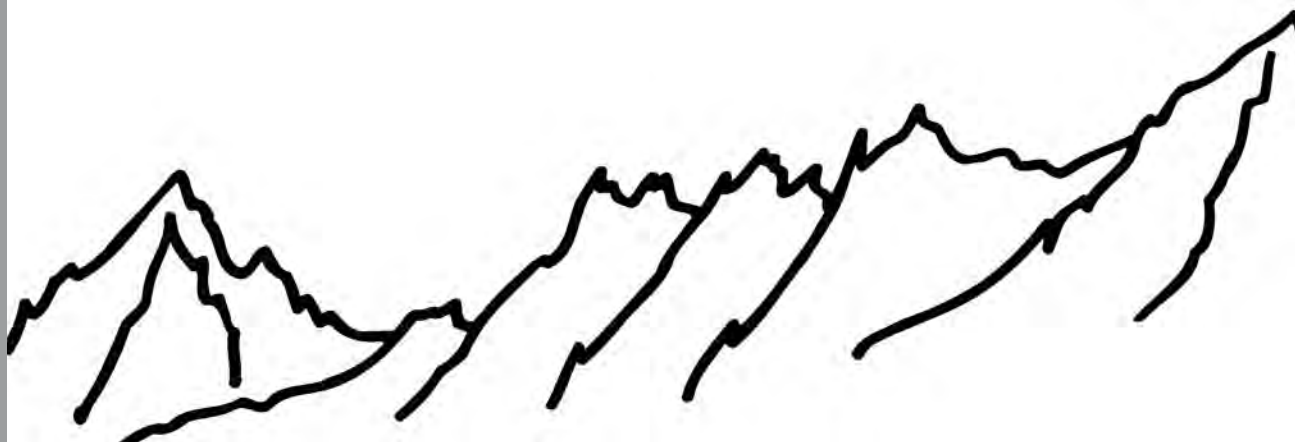
PROCESSING BIOMEDICAL IMAGES –

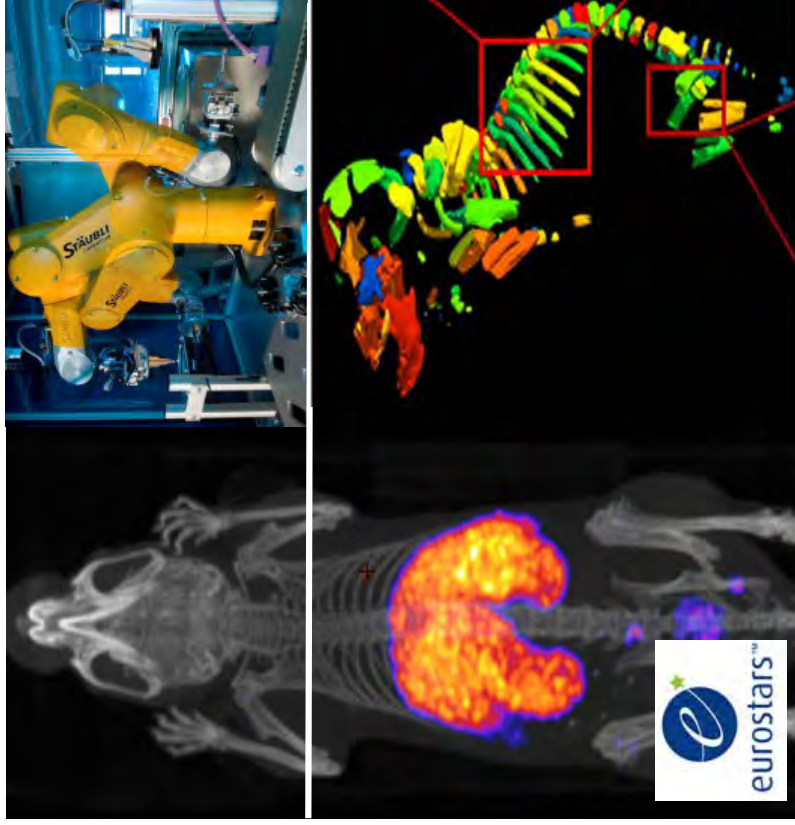
Visualisation, Modelling, Segmentation, Quantification, Registration

April 15 to 20, 2012

Ecole de Physique des Houches, France







Animascope

Innovation in Preclinical Imaging

Animascope innovates by developing new imaging agents, a new scanner and high throughput toxicological studies by means of medical imaging. In partnership with local French and international companies.

www.animascope.eu

THE „ECOLE DE PHYSIQUE DES HOUCHES“, FRANCE

...is a resort village in the Chamonix valley in the French Alps. Established in 1951, the Physics School is located in a group of chalets surrounded by meadows and woods, at an altitude of 1150 m facing the Mont-Blanc range - a very favourable environment for intellectual activity in ideal surroundings for skiing, hiking or mountaineering. The Mont Blanc is the highest mountain in the Alps, Western Europe and the European Union. It rises 4,810.45 m above sea level and is ranked 11th in the world in topographic prominence.

Ecole de Physique des Houches

La Côte des Chavants

74310 Les Houches, France

+33 (0)4 50 54 40 69

HOW TO GET TO LES HOUCHES

By plane: Geneva Airport is 1 hour drive from Les Houches. The simplest way is to use a shuttle service (approximately 25€ up to the school, book at least three days in advance). Please find here an overview of the different providers:

www.chamonix.net/english/transport/transfers.htm

There is also a regular bus service between Geneva and Les Houches (max. twice a day). You should then take a taxi for the last 5 km from the Les Houches village to the school. You can also travel from Geneva to Les Houches by train (+ taxi from the train station to the School), but it is rather complicated and long (go through Annemasse on the French side or through Martigny on the Swiss side).

By train: arrival at the Les Houches station, with one change at Saint-Gervais (from France), or at Martigny (from Switzerland). There are about 10 trains per day between St Gervais and Les Houches. Then we strongly recommend to take a taxi and to pre-reserve by calling one of the following providers: taxi Garny: +33 6 12 35 30 72, taxi Persault : +33 4 50 54 41 09 and taxi Servoz : +33 6 84 66 86 73 to go up to the school ~5km.

By car: Les Houches are easily accessible from France (A41 highway), from Switzerland (Martigny and Col des Montets) and from Italy through the Mont Blanc Tunnel.

From Geneva and Le Fayet: 8km before Chamonix, 300 m after passing under the tunnel, bear right by the first road out for "Les Houches Bellevue". When arriving at the cable car station "Bellevue", turn right and continue upwards (roughly 2 km starting from the teleferic). 500m after the cable car station "Prarion", turn left and follow small arrows at crossroads. Continue up to the end of Route de la Côte des Chavants. Here you are! From Chamonix: bear right for "Les Houches-Chef-Lieu", turn right in Les Houches, and go ahead at the cable car station "Bellevue". Then proceed as above.

Winter equipment for the car is recommended (snow chains). Please park your car at the parking place above the Ecole de Physique.

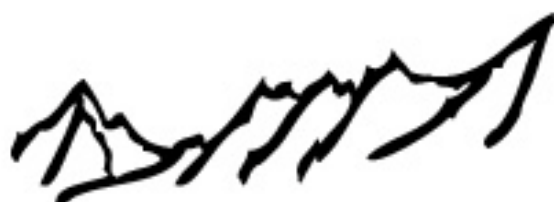
AT THE ECOLE DE PHYSIQUE DES HOUCHES

Arriving is possible on **Sunday April 15, 2012 from 15:00h** onwards. Please note that the school is closed before 15:00h. Within the foyer of the main building you will find a plan of the allocation of rooms as well as the instructions how to get in the chalets. Participants are housed in individual "chalets" (electricity: AC, 50Hz, 220V). The first joint meal will be the dinner at 19:30h.

Breakfast is from 8:00 am to 8:45 am; **Lunch:** at 12:30h; and **Dinner:** 19:30h

Meals are taken at the school dining room. Drinks are not included. Coffee, tea (free!) and other drinks are available at the cafeteria.

ÉCOLE DE PHYSIQUE
des HOUCHES



WELCOME TO TOPIM 2012 – THE 6TH "HOT TOPIC IN MOLECULAR IMAGING" CONFERENCE OF THE ESMI

by Bertrand Tavitian – Chair of the TOPIM 2012 committee

Dear Participant,

PROCESSING BIOMEDICAL IMAGES – VISUALISATION MODELLING SEGMENTATION QUANTIFICATION REGISTRATION

TOPIM – hot TOPics in molecular Imaging is the annual Winter Conference of the European Society for Molecular Imaging. Every year, TOPIM focuses on one hot topic chosen for its pertinence and timeliness, which is an exciting aspect, application or technique at the forefront of Molecular Imaging.

TOPIM takes place at the foot of the Mont Blanc, the highest mountain in Europe, in the village of Les Houches in the Chamonix valley with deep-rooted mountain traditions of hospitality and solidarity. The grandiose surroundings are a unique source of inspiration for visionary ideas, while the warmth and comfort of the remote chalet settings serve inter-disciplinary cross connections and informal discussions between participants. By combining expert descriptions of the most up-to-date imaging technologies and applications, TOPIM contributes in collectively describing and categorizing imaging approaches, and draws the landscape of in vivo imaging approaches of a given scientific issue.

A glance at past hot topics of the previous years

The first **TOPIM** took place in **2007** on Imaging in Neurodegeneration and Neuroinflammation. What was pretty much a bench test for a new style of conference turned out into a tremendous success. For many of the participants it was a revelation that much added value and drive could stem from warm, friendly and informal discussions. Collaborations were started, future programmes were elaborated and TOPIM was on its way!

TOPIM 2008 followed with an ambitious programme on the Imaging of Nano Objects, groundbreaking food-for-thought at a time when the field of nanomedicine was beginning to bloom. TOPIM contributed in installing the complex but fruitful dialogue between material scientists, chemists and imaging scientists.

In **2009**, Dual and Innovative Imaging Modalities continued the tradition of TOPIM to focus on subjects on the verge of swinging from bench to bedside. Again, this was an eye-opener towards the fantastic inventiveness of imaging physicists and their capacity to translate it into in vivo (pre)clinical applications.

TOPIM 2010 was special in two respects: it took place on the Italian side of the Alps in Bardonecchia, and it dealt with Imaging and Systems Biology, a beautiful demonstration of how interdisciplinarity can sparkle new modes of thinking and new avenues.

Last year, **TOPIM 2011** returned to Les Houches and to a translational topic. Emerging Imaging Methods in Medicine opened a unique window on the implementation of sophisticated modern imaging into medical arts, and evidenced that today more than ever, the eye guides the hand.

The hot topic for TOPIM 2012

PROCESSING BIOMEDICAL IMAGES – Visualisation, Modelling, Segmentation, Quantification, Registration has a foot in both camps: on the one hand, incredibly realistic image rendering from the entertainment industry is entering the bio-medical field and will without any doubt change scientists' and doctors' practice. On the other hand, progress in image computing science applied to image calculation, analysis and modelling are building up previously unseen images of biomedical parameters.

How can one extract the relevant information from biomedical in vivo images? In other words, if images speak for themselves, exactly what language are they speaking? TOPIM 2012 will bring together prominent specialists from both worlds to discuss the state of the art and the future in modern processing of biomedical images.

The production of an image aims at building a representation of the real world accurate enough to allow a useful connection with that world. The process by which biomedical images are built follows successive steps, basically the same as those used by the human visual system (Figure 1). The first step is perception, which is bordered by the capacities of the acquisition system, i.e. the part of the real world to which the acquisition system is sensitive. For biomedical imaging this corresponds to image acquisition and registration. The second step applies pre-established, memory built-in schemes, memorized recognition patterns in humans, and for biomedical images, application of various filters and reconstruction algorithms to the raw image data. Segmentation and co-registration are also typical parts of the processes conducted during this second step. It is important to realize that this step is both additive since it calls upon memorized schemes or algorithms that were not initially present in the data, and subtractive since it filters and rejects a significant part of the raw data. The third step consists in the extraction of relevant parameters from the pre-treated data. Humans do this by a priori interpretations (fantasies), imaging scientists do it by introducing operating paradigms: models for quantification. The result is a series of relevant parameters predefined by the operator; often, but not necessarily, an image. This step, as the previous one, adds a priori information in the process, and eliminates much of the original data.

The final step is the production of a representation of reality by retro-projection, through a feedback loop, of the processed image onto the real world. All along the image processing chain, a large part of reality has been removed, and external data has been added. The final output is therefore a cognitive synthesis of reality into an image, whose qualities defining its usefulness as a proper representation are completeness, coherence, constancy and stability. Importantly, the quality and relevance of the representation depend on the initial intention of the end user.

The popular quote from Teilhard de Chardin (quoted in Henry Wagner's classical textbook 'Principles of Nuclear medicine') "The history of the living world is the elaboration of ever more perfect eyes within a cosmos in which there is always more to be seen", can easily be paraphrased to define the practice of image processing: elaborate more perfect eyes to describe the cosmos. TOPIM 2012 has the ambition to present how image processing makes this happens. The scientific committee has set up an attractive programme to take you through a journey along the tricks and treats of this fascinating domain. We hope that you will enjoy it. Similarly to Paul Klee's statement 'Art does not reproduce the visible; rather, it makes visible' (Figure 2), we believe that accurate knowledge of the art of processing biomedical images can only improve our awareness of what can be seen of a biological situation in an individual. It is after all biological situations that we want to explore and describe, and the more this is mastered the better if, as Philip K Dick wrote, 'Reality is that which, when you stop believing in it, doesn't go away'.



Figure 2:
The Future man
(Paul Klee, 1933)

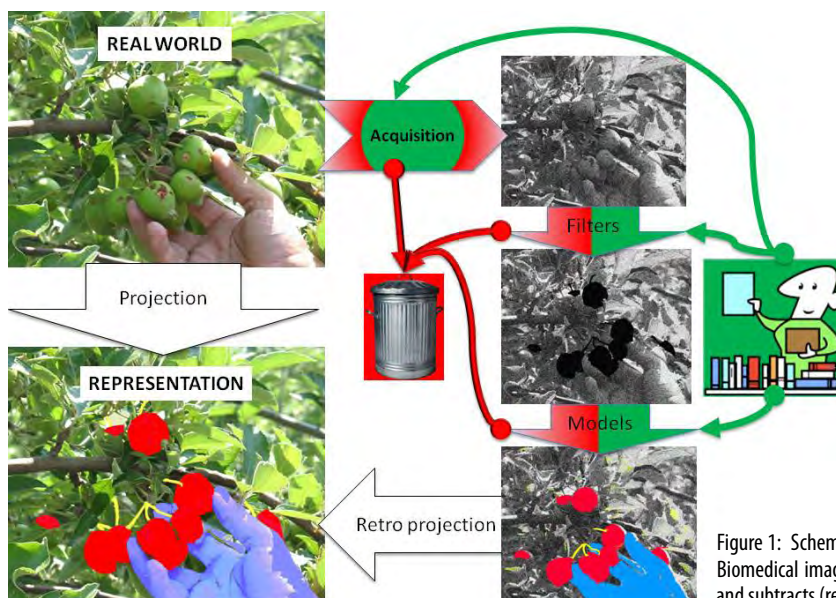














Figure 1: Schematic view of how representations of the real world (left) are built by Biomedical image processing (right). Note that image processing both adds (green) and subtracts (red) information.

HOT TOPIC IN MOLECULAR IMAGING – TOPIM 2012

Thursda

| | Monday, 16th April | Tuesday, 17th April | Wednesday, 18th April |
|---------------|--|--|--|
| 08:00 - 08:45 | breakfast | | |
| 08:45 - 08:50 | Welcome - Bertrand Tavitian | Automatic region of interest delineation and Partial volume correction - Claus Svarer, Copenhagen  | Implementation and analysis of a list-mode algorithm using tubes of response on a dedicated breast PET - Laura Moliner, Torino |
| 08:50 - 08:55 | | | 3D Inversion Recovery MEMRI using Super- Resolution Reconstruction - Esben Plenge, Rotterdam  |
| 08:55 - 09:00 | Educational Keynote Lecture Quantification of biomedical images using tracer kinetic modelling Adriaan Lammertsma  | Parametric analysis of dynamic PET studies - Ronald Boellard, Amsterdam  | Iterative Reconstruction Techniques for Faster Scan Speed in Magnetic Resonance Imaging - Tobias Block, NY |
| 09:00 - 09:05 | | | coffee break |
| 09:05 - 09:10 | | | |
| 09:10 - 09:15 | | | Image Reconstruction: What makes optical imaging an ill-posed problem - Jorge Ripoll, Heraklion |
| 09:15 - 09:20 | | | |
| 09:20 - 09:25 | | | Fast edge-preserving iterative image reconstruction method for fluorescence diffuse optical tomography using anatomical prior information - Teresa Correira |
| 09:25 - 09:30 | | | |
| 09:30 - 09:35 | | | Improving FMT reconstruction accuracy using CT-based shape and numerically determined optical tissue properties - Felix Gremse, Aachen |
| 09:35 - 09:40 | | | |
| 09:40 - 09:45 | | | Bioimage Analysis of Cellular and Molecular Dynamics - Erik Meijering, Rotterdam  |
| 09:45 - 09:50 | | | |
| 09:50 - 09:55 | coffee break | High-resolution small animal PET imaging - Klaus Schäfers, Münster  | lunch break |
| 09:55 - 10:00 | | | |
| 10:00 - 10:05 | | | |
| 10:05 - 10:10 | | | |
| 10:10 - 10:15 | | | |
| 10:15 - 10:20 | | | |
| 10:20 - 10:25 | | | |
| 10:25 - 10:30 | | | |
| 10:30 - 10:35 | | | |
| 10:35 - 10:40 | | | |
| 10:40 - 10:45 | Educational Keynote Lecture Quantification of biomedical images using tracer kinetic modelling Adriaan Lammertsma  | Quantification of presynaptic cardiac sympathetic function Using 11C-HED and PET: analysis and interpretation of simplified approaches - Sofia Goncalves Antunes | Multi-parametric phenotype profiling of 3D cell cultures for the classification of biologically active molecules - Zi Di, Leiden |
| 10:45 - 10:50 | | | |
| 10:50 - 10:55 | | | |
| 10:55 - 11:00 | | | |
| 11:00 - 11:05 | | | |
| 11:05 - 11:10 | | | |
| 11:10 - 11:15 | | | |
| 11:15 - 11:20 | | | |
| 11:20 - 11:25 | | | |
| 11:25 - 11:30 | | | |
| 11:30 - 11:35 | Principles of Optical Imaging: light emission, propagation and absorptionl by Jorge Ripoll, Heraklion | Key Note Lecture The Past Achievements of Brain PET and the Role of Quantification - Terry Jones | Automated Segmentation and Tracking of Caenorhabditis Elegans Embryogen-esis in Fluorescence Microscopy - Oleh Dzyubachyk |
| 11:35 - 11:40 | | | |
| 11:40 - 11:45 | | | |
| 11:45 - 11:50 | | | |
| 11:50 - 11:55 | | | |
| 11:55 - 12:00 | | | |
| 12:00 - 12:05 | | | |
| 12:05 - 12:10 | | | |
| 12:10 - 12:15 | | | |
| 12:15 - 12:20 | | | |
| 12:20 - 12:25 | coffee break | Modelling in DCE-MRI - Paul Tofts, Brighton and Sussex | Beyond one's nose lecture Staffan Strömblad "A systems microscopy platform for studying cell adhesion and migration" |
| 12:25 - 12:30 | | | |
| 12:30 - 13:00 | | | |
| 13:00 - 15:45 | | | |
| 15:45 - 15:50 | | | |
| 15:50 - 15:55 | | | |
| 15:55 - 16:00 | | | |
| 16:00 - 16:05 | | | |
| 16:05 - 16:10 | | | |
| 16:10 - 16:15 | | | |
| 16:15 - 16:20 | The General PET Compartment Model - Vincent Cunningham, Aberdeen | coffee break and Poster Session 1 (poster #16-29) | coffee break and Poster Session 2 (poster #1-15) |
| 16:20 - 16:25 | | | |
| 16:25 - 16:30 | | | |
| 16:30 - 16:35 | | | |
| 16:35 - 16:40 | | | |
| 16:40 - 16:45 | | | |
| 16:45 - 16:50 | | | |
| 16:50 - 16:55 | | | |
| 16:55 - 17:00 | | | |
| 17:00 - 17:05 | | | |
| 17:05 - 17:10 | Determination of the arterial input function in mice using the beta microprobe system - Florian Buether, Muenster | The GATE Monte Carlo simulation platform: An opensource tool for medical imaging and radiation therapy applications - Sebastien Jan, CEA | best poster presentation - poster walk 1 |
| 17:10 - 17:15 | | | |
| 17:15 - 17:20 | | | |
| 17:20 - 17:25 | | | |
| 17:25 - 17:30 | | | |
| 17:30 - 17:35 | | | |
| 17:35 - 17:40 | | | |
| 17:40 - 17:45 | | | |
| 17:45 - 17:50 | | | |
| 17:50 - 17:55 | | | |
| 17:55 - 18:00 | break | Optimal selection of imaging wavelengths for spectral unmixing - Martijn van de Giessen, Leiden | Seeing the invisible; Predicting the unexpected - Michal Irani, Rehovot |
| 18:00 - 18:05 | | | |
| 18:05 - 18:10 | | | |
| 18:10 - 18:15 | | | |
| 18:15 - 18:20 | | | |
| 18:20 - 18:25 | | | |
| 18:25 - 18:30 | | | |
| 18:30 - 18:35 | | | |
| 18:35 - 18:40 | | | |
| 18:40 - 18:45 | | | |
| 18:45 - 18:50 | Application of non-steady state FDG-PET to study dynamic processes in vivo - Delphine Feuerstein, Cologne  | Image reconstruction from projections in SPECT, PET and TOF-PET - Johan Nuyts, Leuven | Setup for simultaneous measurement of laser speckle flowmetry, rgb reflectometry and PET: validation and in vivo application - Markus Gramer, Cologne |
| 18:50 - 18:55 | | | |
| 18:55 - 19:00 | | | |
| 19:00 - 19:05 | | | |
| 19:05 - 19:10 | | | |
| 19:10 - 19:15 | | | |
| 19:15 - 19:20 | | | |
| 19:20 - 19:25 | | | |
| 19:25 - 19:30 | | | |
| 19:30 - 19:45 | | | |
| 19:35 - 19:40 | | | |
| 19:40 - 19:45 | | | |
| 19:45 - 20:15 | Champagne Reception by BiospaceLab | | |
| | dinner | | dinner |
| 20:15 - end | come together | come together | Discussion on the Future of PET - Terry Jones |

| | Thursday, 19th April | Friday, 20th April | |
|---------------|---|--|--|
| 08:00 - 08:45 | | | |
| 08:45 - 08:50 | | | |
| 08:50 - 08:55 | Data storage & analysis: "Opportunities and challenges in biomedical imaging research" - Wiro Niessen, Rotterdam  | Development of imaging biomarkers for neurodegenerative diseases - Sebastien Ourselin, London | |
| 08:55 - 09:00 | | | |
| 09:00 - 09:05 | | | |
| 09:05 - 09:10 | | | |
| 09:10 - 09:15 | | | |
| 09:15 - 09:20 | | | |
| 09:20 - 09:25 | | | |
| 09:25 - 09:30 | | | |
| 09:30 - 09:35 | Fully Automated Image Post-Processing of (f)MRI Data during an Imaging Session using a Remote Cluster - Eberhard Pracht, Cologne | Iterative Reconstruction Techniques for Faster Scan Speed in Magnetic Resonance Imaging - Daniel Bulte, Oxford | |
| 09:35 - 09:40 | | | |
| 09:40 - 09:45 | The Open Microscopy Environment: Open Image Informatics for the Biological Sciences Jason Swedlow, Dundee | | |
| 09:45 - 09:50 | | | |
| 09:50 - 09:55 | | | |
| 09:55 - 10:00 | | | |
| 10:00 - 10:05 | | | |
| 10:05 - 10:10 | | | |
| 10:10 - 10:15 | | | |
| 10:15 - 10:20 | | | |
| 10:20 - 10:25 | | | |
| 10:25 - 10:30 | | | |
| 10:30 - 10:35 | Automatic spectral clustering for segmentation of dynamic PET images - Hiba Zbib, Tours | | |
| 10:35 - 10:40 | | | |
| 10:40 - 10:45 | The Open Microscopy Environment: Open Image Informatics for the Biological Sciences - Jean-Marie Burel, Dundee | coffee break | |
| 10:45 - 10:50 | | | |
| 10:50 - 10:55 | | | |
| 10:55 - 11:00 | | | |
| 11:00 - 11:05 | coffee break | best poster presentation - poster walk 2 | |
| 11:05 - 11:10 | | | |
| 11:10 - 11:15 | Image analysis challenges in multi-modal pre-clinical imaging studies - Boudewijn Leliveldt, Leiden  | Contrast-enhanced 3-D ultrasound skeletonization for the quantitative imaging of tumor vascular pattern - Filippo Molinari, Torino | |
| 11:15 - 11:20 | | When Electrophysiology meets Neuroimaging: Magnetoencephalography - Jérémie Mattout, Lyon | |
| 11:20 - 11:25 | | | |
| 11:25 - 11:30 | | | |
| 11:30 - 11:35 | | | |
| 11:35 - 11:40 | | | |
| 11:40 - 11:45 | | | |
| 11:45 - 11:50 | | | |
| 11:50 - 11:55 | | | |
| 11:55 - 12:00 | | conclusion - Bertrand Tavitian | |
| 12:00 - 12:05 | | | |
| 12:05 - 12:10 | Optical Tracking System for Imaging Freely Moving Mice with the quadHIDAC Small Animal PET Scanner - Sonke Schmid, Münster  | lunch and departure | |
| 12:10 - 12:15 | | | |
| 12:15 - 12:20 | | | |
| 12:20 - 12:25 | | | |
| 12:25 - 12:30 | | | |
| 12:30 - 13:00 | | | |
| 13:00 - 15:45 | | | |
| 15:45 - 15:50 | Construction of a statistical mouse atlas for preclinical image analysis - Richard Tascherau, UCLA | | |
| 15:50 - 15:55 | | | |
| 15:55 - 16:00 | Chances and Challenges of PET/MR imaging - Hans Wehrl, Tübingen | | |
| 16:00 - 16:05 | | | |
| 16:05 - 16:10 | | | |
| 16:10 - 16:15 | | | |
| 16:15 - 16:20 | | | |
| 16:20 - 16:25 | | | |
| 16:25 - 16:30 | | | |
| 16:30 - 16:35 | | | |
| 16:35 - 16:40 | break | | |
| 16:40 - 16:45 | | | |
| 16:45 - 16:50 | | | |
| 16:50 - 16:55 | | | |
| 16:55 - 17:00 | | | |
| 17:00 - 17:05 | | | |
| 17:05 - 17:10 | VINCI - Co-Registration of Rat Brains (PET-MR) - Stefan Vollmar, Cologne | | |
| 17:10 - 17:15 | | | |
| 17:15 - 17:20 | Attenuation correction of preclinical PET images based on MRI scout pair segmentation - László Papp, Budapest | | |
| 17:20 - 17:25 | | | |
| 17:25 - 17:30 | Fast, Robust and Accurate extraction of time activity curves in rodent PET whole-body images - Renaud Maroy, Orsay  | | |
| 17:30 - 17:35 | | | |
| 17:35 - 17:40 | | | |
| 17:40 - 17:45 | | | |
| 17:45 - 17:50 | | | |
| 17:50 - 17:55 | | | |
| 17:55 - 18:00 | | | |
| 18:00 - 18:05 | | | |
| 18:05 - 18:10 | | | |
| 18:10 - 18:15 | | | |
| 18:15 - 18:20 | | | |
| 18:20 - 18:25 | | | |
| 18:25 - 18:30 | | | |
| 18:30 - 18:35 | | | |
| 18:35 - 18:40 | | | |
| 18:40 - 18:45 | | | |
| 18:45 - 18:50 | | | |
| 18:50 - 18:55 | | | |
| 18:55 - 19:00 | | | |
| 19:00 - 19:05 | | | |
| 19:05 - 19:10 | | | |
| 19:10 - 19:15 | | | |
| 19:15 - 19:20 | | | |
| 19:20 - 19:25 | | | |
| 19:25 - 19:30 | | | |
| 19:30 - 19:45 | | | |
| 19:35 - 19:40 | | | |
| 19:40 - 19:45 | | | |
| 19:45 - 20:15 | | | |
| 20:15 - end | reception by the Ecole | | |

welcome letter _____ 4

programme overview _____ 6

programme committee _____ 10

thanks for your support _____ 10

talks:

day one monday april 16, 2012 _____ 11

day two tuesday april 17, 2012 _____ 15

day three wednesday april 18, 2012 _____ 22

day four thursday april 19, 2012 _____ 30

day five friday april 20, 2012 _____ 36

posters _____ 42

author's index _____ 59

PROGRAMME COMMITTEE – TOPIM 2012

Bertrand Tavitian - Paris, France CHAIR

Marion de Jong - Rotterdam, The Netherlands

Adriaan Lammertsma - Amsterdam, The Netherlands

Boudewijn Lelieveldt - Leiden, The Netherlands

Renaud Maroy - Orsay, France

Michal Neeman - Rehovot, Israel

Vasilis Ntziachristos - Munich, Germany

Bernd Pichler - Tuebingen, Germany

THANKS FOR YOUR SUPPORT

Caliper *a PerkinElmer company*

BiospaceLab

Servier

Roche

carestream

TOPIM is also co-funded by the FP7 projects **ENCITE** - the European Network for Cell Imaging and Tracking Expertise and **INMiND** - Imaging of Neuroinflammation in Neurodegenerative Diseases.



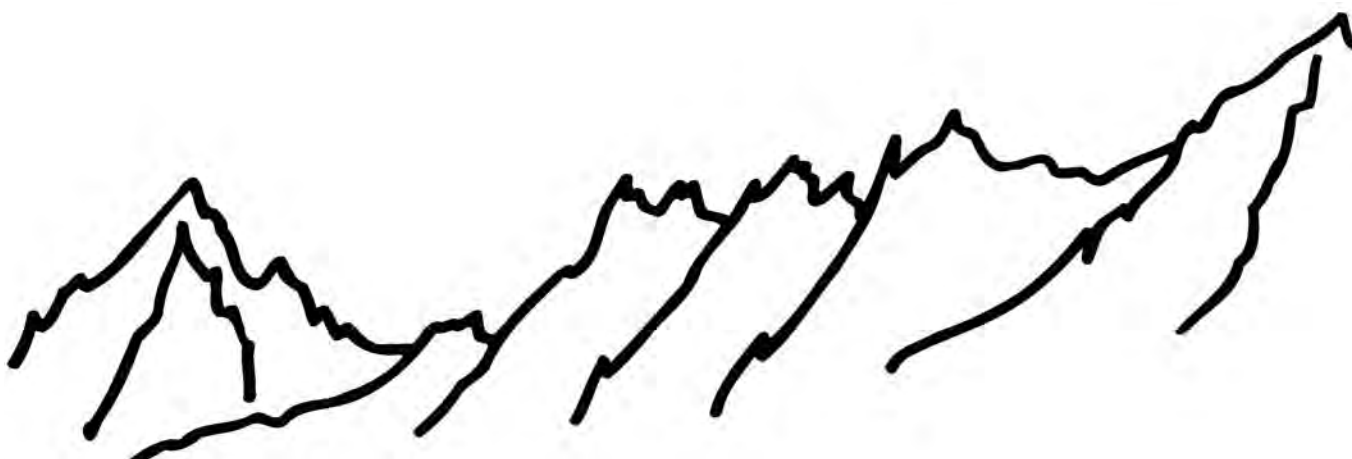
www.encite.org



www.inmind-project.eu

The project **ENCITE** co-funded by the European Commission within the 7th Framework Programme, is a strong collaboration of 29 different research groups from 10 European countries and Israel. The ambitious mission of the project is to develop and test new MR and optical imaging methods and biomarkers to draw a more comprehensive picture of cell fate and the reaction of the immune system. In the end, cell therapy shall be improved for the benefit of the European patient.

The large-scale integrating project **INMiND** co-funded by the European Commission (GA278850) within the 7th Framework Programme, is a collaboration of 27 research groups from 12 European countries and Australia. The goal of INMiND is to identify novel biological targets of neuroinflammation for both diagnostic and therapeutic purposes and to translate this knowledge into clinical application and patient benefit.



day one: monday april 16, 2012

educational keynote lecture

QUANTIFICATION OF BIOMEDICAL IMAGES USING TRACER KINETIC MODELLING

Lammertsma A.A.

Department of Nuclear Medicine & PET Research
 VU University Medical Center, Amsterdam, The Netherlands
 (aa.lammertsma@vumc.nl)

The net uptake of a tracer in tissue at a certain time after administration reflects the interplay between three distinct physiological processes: delivery to the tissue, (molecular) interactions within the tissue and clearance from the tissue. Delivery depends on (the time course of) arterial concentrations, tissue perfusion and extraction. Usually a tracer is selected because of its specific interactions in tissue, such as binding to a receptor or being a substrate for a metabolic pathway. It follows that in most cases the relationship between total signal (uptake) and specific signal (i.e. the signal related to the interaction under study) in an image will not be linear and that this relationship will vary with time.

Although imaging the distribution of a tracer at a certain time after administration may provide useful information, especially when uptake can be related to that in a reference region without specific signal (e.g. a region without receptors in case of a receptor study), it can also be misleading, as uptake depends on all factors mentioned above and the tissue specific signal is only one of them. For true quantification of a molecular process a tracer kinetic model is essential, together with dynamic scanning in which uptake and clearance (i.e. kinetics) of the tracer are followed over time.

A tracer kinetic model is a mathematical description of the fate of a tracer in the body, with emphasis on the organ of interest. Using such a model, observed tissue uptake and clearance can be related to various model parameters, provided the input function is also known. As most tracers are injected intravenously, they reach tissues through the bloodstream. Consequently, in most cases, measurement of the arterial concentration over time is also needed. Although other types of models have been proposed, in practice compartmental models are used. In these models, the distribution of activity is allocated to a number of (not necessarily physical) discrete compartments. The resulting operational equation primarily contains (unknown) rate constants, describing the rate of exchange of tracer between the various compartments, which are estimated by fitting the measured data to a suitable model.

In this contribution the basic principles of tracer kinetic modelling will be presented, together with the most commonly used compartment models, and concepts as volume of distribution and binding potential will be developed. Next, possibilities and limitations of reference tissue models will be discussed as a means to avoid arterial sampling. In addition, linearisations will be discussed, primarily as a tool to generate parametric images

Following this theoretical basis, more practical issues will be discussed, including limitations of tracer kinetic modelling. The focus here will be on the steps needed to generate a metabolite corrected arterial plasma input function. Next, procedures for selecting the most appropriate model for a new ligand will be discussed. Finally, specific issues related to quantification of small animal studies will be highlighted.

introductory talk on OI

PRINCIPLES OF OPTICAL IMAGING: LIGHT EMISSION, PROPAGATION AND ABSORPTIONRipoll, J.^{1,2}

¹University of Fribourg Department of Physics, Chemin du Musée 3, 1700 Fribourg, Switzerland; ²Foundation for Research and Technology-Hellas Institute for Electronic Structure and Laser, Vassilika Vouton, Heraklion, Greece
 (jripoll@iesl.forth.gr)

In this talk we shall cover the basic principles in any optical imaging setup. In particular, we shall discuss what are the mechanisms of light production (both in terms of fluorescent or bioluminescence and on light sources used for imaging), and how light propagates both in homogeneous (free space, for example) and inhomogeneous media (such as tissue). In order to understand light propagation in all possible situations we will cover the approach used to describe the mechanisms of absorption and scattering. Once these main concepts are understood, we will consider how they affect imaging in a real scenario and we will try to answer the following questions: what limits resolution in an optical imaging setup? How does scattering affect my image? How does this relate to current microscopy and whole-animal imaging approaches?

In particular the following concepts will be presented:

- The origins of color in nature: Mechanisms of light production, absorption and scattering
- Basics of light propagation
- Effects of scattering and absorption on light propagation
- Optical Imaging in practice: From ballistic (microscopy) to diffuse light (whole animal imaging)

THE GENERAL PET COMPARTMENT MODEL

Cunningham, V.

Aberdeen Biomedical Imaging Centre, School of Medical Sciences, University of Aberdeen, UK

(v.j.cunningham@abdn.ac.uk)

The kinetic behaviour of PET radiotracers *in vivo* is a reflection of their interaction with the underlying biochemical, physiological and pharmacological functions which govern their uptake and distribution in the organs and tissues of the body. In order to interpret the observed kinetics in blood and tissues on the one hand, and the biological function the tracer is designed to measure, on the other, a tracer kinetic model is required. These mathematical models embody the assumed relationship between the kinetics and the biological function.

The analysis of PET tracer kinetics is based mainly on compartmental models or on techniques derived from compartmental behaviour. The compartments usually refer to the 'state' of the radiotracer, free or bound etc, rather than, necessarily, differences in physical location. The biological interpretation of the fractional rate constants, linking the compartments, depends on the particular radiotracer being modelled. These rate constants may, for example, embody enzyme activity, as in the case of k_3 in the deoxyglucose model, or a combination of pharmacological and physicochemical properties, as in the case of models describing radioligand uptake and binding.

The biological interpretation of the particular rate constants, or microparameters, thus plays a vital role in setting up the compartmental models, and deciding whether the model can be a suitable description of the interaction of the radiotracer with the function it is to measure. However, there is no doubt that compartmental models are a simplification of complex biological behaviour, and over-interpretation and reliance on the quantitative estimates of individual microparameters should be avoided.

There are combinations of parameters, or macroparameters, which are much more robust, which are independent of particular compartmental configurations, are common across classes of compartmental models, for example reversible, or irreversible, but which can be derived from fitting individual compartmental models. These are Plasma Clearance, Irreversible Disposal Rates and tissue Volumes of Distribution, and these will be illustrated.

The general form of reversible and irreversible compartmental models with blood/plasma input functions and corresponding reference tissue models will be presented and discussed. The macroparameters will be related to the general forms of the equation and to observed tissue responses following bolus injection and constant infusion of radiotracers. The role that these macroparameters have played in the classic PET models for Blood Flow, Glucose Metabolic Rate and Radioligand Binding will be emphasised.

DETERMINATION OF THE ARTERIAL INPUT FUNCTION IN MICE USING THE BETA MICROPROBE SYSTEM

Buether, E., Reinhardt, D., Law, M., Schäfers, K.

European Institute for Molecular Imaging University of Muenster, Mendelstr. 11, 48151 Muenster, Germany

(butherrf@uni-muenster.de)

Introduction: Preclinical small animal PET imaging has become an important tool in the field of biomedical research. Of special interest for kinetic modeling of PET data is the concentration of the tracer in the arterial blood/blood plasma during the scan (arterial input function). Conventional methods to determine the input function in PET scans of mice are either based on several blood samples taken during the scan or on determining the blood tracer concentration from dynamic PET images. Both methods have difficulties caused by the small size of the animal and the fast dynamics involved. We present here an alternative method already introduced to determine the input function in rats [1] that directly measures the concentration of radioactivity in the blood *in vivo*.

Methods: The Biospace beta microprobe is a positron detection system consisting of a small plastic scintillator (0.25 mm diameter, 1 mm length) coupled to an optical fiber system and a registration unit. Due to the limited positron range in organic tissues (around 1 mm for F-18), it is well suited for local radioactivity measurements with high temporal resolution (1 s). In a study comprising four anesthetized mice one such probe was inserted into the aortic arch via the right carotid artery. Due to the small dimensions of the aorta, background activity from surrounding tissue potentially contaminates the measured signal, thus a second probe measuring only background activity was placed a few millimeters away from the aorta. The mice thus prepared received a bolus injection of 10 to 20 MBq of F-18-FDG into the tail vein. For both calibration and evaluation purposes, five blood samples were taken from the right femoral artery during the 45 minutes measurement period; their activity concentrations were determined in an automated well counter. The input function was then modeled as a smoothed and weighted difference of the aortic probe signal and the background probe signal, both corrected for dark counts and decay.

Results: In all studies, directly following the bolus injection of F-18-FDG, the aortic probe signal demonstrated very high radioactivity values followed by a fast decrease in signal and finally remaining on an almost constant level, while the background probe signal increased only slowly until reaching equilibrium. Using two blood samples for calibration, the arterial input function was obtained by subtracting the appropriately weighted background probe signal from the aortic probe signal. The determined smoothed curve demonstrated excellent agreement with the three other blood samples.

Conclusions: The beta microprobe is well suited for accurately determining the arterial input function in mice, minimizing the number of blood samples while additionally providing excellent timing resolution.

Acknowledgement/References: [1] Pain, F., Lanièce, P., Mastrippolito, R., et al. Arterial Input Function Measurement Without Blood Sampling Using a Beta Microprobe in Rats. *Journal of Nuclear Medicine* 2004, 45:1577-1582.

QUANTIFICATION OF CEREBRAL GLUCOSE CONSUMPTION IN PATHOLOGICAL TISSUE – FDG-PET BEYOND THE LUMPED CONSTANT

Backes, H.

MPI for neurological research Cologne, Germany

(backes@nf.mpg.de)

In positron emission tomography (PET) it is common to use tracer compounds that are chemically analog but not identical to the endogenous compound. The consequences of these differences on the determination of quantitative physiological values will be exemplified through the case of [^{18}F]-2-fluoro-2-deoxy-D-glucose (FDG), the most common tracer used in PET.

Based on the autoradiographic [^{14}C]-deoxyglucose (DG) method developed by Sokoloff, FDG is used for the *in vivo* quantification of cerebral glucose consumption. In the autoradiographic approach, the local glucose metabolic rate is calculated from tissue DG uptake 45 minutes after venous bolus injection and from the arterial tracer input function [1]. Differences between glucose and deoxyglucose include: (1) DG is no substrate for glycolysis after phosphorylation and is therefore trapped in the cells. (2) Glucose transporters are more efficient for transporting DG than glucose. (3) Phosphorylation efficiency by hexokinase of DG is half that of glucose. (1) simplifies quantification. (2) and (3) are summarized in the “lumped constant” (LC). Dividing the DG uptake by the LC provides the glucose consumption rate. This autoradiographic method is also commonly used for the quantification of FDG-PET. However, it requires the local LC to be known and it is common to assume the LC to be constant throughout the brain.

The LC can be expressed as a function of the rate constant for unidirectional transport of deoxyglucose from blood to tissue (K_1) and the net influx rate constant (K_i), i.e. it depends on the conditions of the tissue, whether activated or at rest, whether pathological or healthy [2,3]. This violates the assumption of a constant LC and thereby limits the applicability of the autoradiographic method for the quantification of glucose utilization. In contrast to autoradiography, dynamic PET data provide the time course of tracer uptake by the tissue, which allows to locally determine both K_1 and K_i by kinetic modelling. Hence the local LC and thereby the glucose consumption rate can be calculated as a function of the FDG rate constants K_1 and K_i [4]. This means that FDG-PET in contrast to autoradiography does not lose its validity in tissue with altered LC, provided the full kinetic model (instead of the autoradiographic method) is used for quantification.

In rats with acute cerebral ischemia, for example, K_1 in the ischemic tissue is decreased by the reduction of blood flow. In the so-called ischemic penumbra, cells compensate for the decrease in glucose supply from the blood by an increase in hexokinase activity in order to maintain energy consumption. Under these conditions FDG uptake can be elevated by up to a factor of 2 although glucose consumption is unchanged. Thus, due to the differences of FDG and glucose, a significant increase in FDG uptake does not necessarily imply an increase in glucose consumption rate [5].

The formalism and concepts discussed here with the example of FDG and glucose apply in principle to every situation where a chemical analogue is used as tracer. In order to quantify the physiological process of interest it is necessary to use kinetic models that take into account the chemical differences between tracer and endogenous compound.

References: [1] Sokoloff, Reivich, Kennedy et al. *J Neurochem.* 1977; 28: 897-916; [2] Kuwabara, Evans, Gjedde. *J Cereb Blood Flow Metab.* 1990; 10: 180-189; [3] Holden, Mori, Dienel et al. *J Cereb Blood Flow Metab.* 1991; 11: 171-182; [4] Backes, Walberer, Endepols et al. *J Nucl Med.* 2011; 52: 1252-1260; [5] Walberer, Backes, Rueger et al. *Stroke.* 2012; 43: 193-198

APPLICATION OF NON-STEADY STATE FDG-PET TO STUDY DYNAMIC PROCESSES IN VIVO

Feuerstein, D., Gramer, M., Takagaki, M., Graf, R., Backes, H.

MPI for neurological research Multimodal imaging, Gleueler strasse 50, 50931

Cologne, Germany

(dfeuerstein@nf.mpg.de)

Introduction: Accurate quantification of Positron Emission Tomography (PET) data typically requires steady-state conditions. Hence, dynamic events with time-scales smaller than the PET scan duration cannot be quantified using common methods. We here combine ^{18}F -fluoro-deoxy-glucose (FDG) -PET with high time-resolution optical imaging of cerebral blood flow and *in-situ* measurements of extracellular concentrations of glucose and lactate to develop a model for the time-dependent energy budget of cortical spreading depression (CSD). CSD is a wave of depolarization that spontaneously spreads across brain tissue after brain injury and is known for disturbing neurovascular and neurometabolic coupling [1,3].

Methods: Male Wistar rats were positioned in a custom-build holder for simultaneous optical imaging and PET measurement. Using laser speckle flowmetry (LSF) through thinned skull and dura mater [2], two-dimensional maps of surface cerebral blood flow were continuously recorded. A microdialysis probe was inserted through a small durotomy and the dialysate (sample of extracellular fluid) was assayed for glucose and lactate every minute using rapid-sampling microdialysis (rsMD) [3]. After baseline measurements of rsMD and LSF, FDG was injected and PET images were acquired for 90 min. SDs were induced 20 min after FDG injection by either a needle prick (single CSD, $n=10$) or by continuous epidural application of potassium chloride (multiple CSDs, $n=10$).

Results: SD waves were detected by LSF as hyperemic waves propagating over the cortex at a rate of ~ 3 mm/min and repeating at 3-7 minute intervals. The occurrence of CSDs and their associated rsMD concentration changes in glucose and lactate were compared to the local time-activity curves (TACs) of FDG uptake. One single CSD wave caused an immediate fall in glucose and rise in lactate concentrations. Simultaneously FDG uptake in the ipsi-lateral hemisphere was significantly increased above control uptake in the contra-lateral hemisphere. All measurements returned to baseline within 30 minutes after the CSD. Following multiple CSDs, FDG preferentially accumulated in regions with a high incidence of CSDs and the TACs showed a steady increase up to 45% above contra-lateral hemisphere. Similarly, dialysate glucose concentrations gradually decreased while lactate concentrations rose with the passage of CSD waves past the MD probe. Both responses were sustained and showed no apparent sign of recovery. On the basis of the measured data we developed a model for the energy budget of CSD. The model notably showed that the net energy consumption after the passage of a single CSD is increased only for about 2 minutes, after which, metabolism is reduced for a period of 30 min. Features of the FDG-TACs and glucose metabolite concentration changes could be explained in terms of glycogen breakdown and re-synthesis at a later time. When CSDs frequently occurred the number of repolarized cells decreased as a function of the number of CSDs.

Conclusions: In combination with *in-situ* measurements and imaging techniques, non-steady-state PET provides valuable information for the understanding of dynamic physiological events.

Acknowledgement/References: 1. Strong AJ et al. *Brain* (2007), 130,995-1008; 2. Dunn AK, *Ann Biomed Eng.* (2011); 3. Hashemi P, et al. *JCBFM* (2009) 29, 166-175



day two: tuesday april 17, 2012

AUTOMATIC REGION OF INTEREST DELINEATION AND PARTIAL VOLUME CORRECTION

Svarer, C., Knudsen, G.M.

Neurobiology Research Unit, Rigshospitalet, Copenhagen University Hospital, Denmark

(csvarer@nru.dk)

Introduction: One of the major limitations in PET molecular brain imaging is the limited scanner resolution. In state-of-the-art clinical scanners a resolution of down to 4.5 mm and with the Siemens HRRT scanner a resolution of 1.6 mm in center of the field of view have been reported. Unfortunately, these resolutions are reported under ideal experimental conditions and more realistic a resolution of 4-6 mm is achievable, due to low count statistics and movement artefacts. It is therefore essential to have precise algorithms for localization and grouping of voxels for parcellation of the brain into structural or functional areas and/or methods for correcting the scans for the low resolution in acquired scan data.

Methods: For parcellation of the brain two major different approaches have been used. The first one is where the individual brain images are normalized into a standard brain atlas like the approaches used in SPM (1) normally guided by a high resolution structural MR image. In other approaches the brain images is parcellated in acquisition space (2), (3), (4). In the latter case it is also shown that it is possible to achieve a higher precision in voxel labelling when working in subject space. Further, these methods working in subject space are especially well suited for correcting acquired PET scans for the low resolution - the so-called partial volume correction - as this has to be performed in acquisition space.

Different approaches for performing PVE corrections have been proposed. Most of them are using some kind of segmented high resolution structural MR image as a prior for where activity from PET acquisition can be placed, like the methods described in (5), (6), (7). Other methods will only work for quantification of dynamic PET images where assumptions about a difference in behaviour of the tracer kinetic model for different kinds of brain tissue is used (8). Finally, new approaches have been presented where the PET scanner is modelled more precisely for the iterative reconstruction method and in that way making it possible to enhance the resolution in the reconstructed PET images (9), (10). None of the latter methods requires structural MR scans for performing the PVE correction can be enhanced.

Discussion: Precise methods for labelling of brain images in subject space are available. Unfortunately, it makes it difficult to do voxel based analysis but the methods are very well suited for analysis of functional or structural connected volumes of interest as long as a suitable atlas is available. Regarding correction of acquired scanning data for the low resolution all proposed approaches will add noise to data due to the mechanisms used in the algorithms like MR-PET co-registration, MR-segmentation, kinetic modelling, and de-convolution techniques. But they have the potential to correct data for atrophy and other structural degenerations in studies where this could be a problem e.g. like longitudinal studies with a huge age span between subjects included, or studies including groupings of subjects with structural differences between the groups.

Reference List: (1) Ashburner J, Friston KJ. Nonlinear spatial normalization using basis functions. *Hum Brain Mapp.* 1999;7(4):254-66. (2) Hammers A, Allom R, Koeppe MJ et al. Three-dimensional maximum probability atlas of the human brain, with particular reference to the temporal lobe. *Hum Brain Mapp.* 2003;19(4):224-47. (3) Heckemann RA, Hajnal JV, Aljabar P, Rueckert D, Hammers A. Multiclassifier fusion in human brain MR segmentation: modelling convergence. *Med Image Comput Comput Assist Interv Int Conf Med Image Comput Comput Assist Interv.* 2006;9(Pt 2):815-822. (4) Svarer C, Madsen K, Hasselbalch SG et al. MR-based automatic delineation of volumes of interest

in human brain PET images using probability maps. *Neuroimage.* 2005;24(4):969-79. (5) Meltzer CC, Leal JP, Mayberg HS, Wagner HN, Frost JJ. Correction of PET data for partial volume effects in human cerebral cortex by MR imaging. *J Comput Assist Tomogr.* 1990;14(4):561-70. (6) Muller Gartner HW, Links JM, Prince JL et al. Measurement of radiotracer concentration in brain gray matter using positron emission tomography: MRI-based correction for partial volume effects. *J Cereb Blood Flow Metab.* 1992;12(4):571-83. (7) Rousset OG, Ma Y, Evans AC. Correction for partial volume effects in PET: principle and validation. *J Nucl Med.* 1998;39(5):904-11. (8) Iida H, Narita Y, Ardekani BA et al. [Evaluation of partial volume effect in quantitative measurement of regional cerebral blood flow in single photon emission computed tomography--effects of limited spatial resolution and first-pass extraction fraction]. *Kaku Igaku.* 1995;32(2):155-62. (9) Panin VY, Kehren F, Michel C, Casey M. Fully 3-D PET reconstruction with system matrix derived from point source measurements. *IEEE Trans Med Imaging.* 2006;25(7):907-921. (10) Sureau FC, Reader AJ, Comtat C et al. Impact of image-space resolution modeling for studies with the high-resolution research tomograph. *J Nucl Med.* 2008;49(6):1000-1008.

PARAMETRIC ANALYSIS OF DYNAMIC PET STUDIES

Boellaard, R.

Department of Nuclear Medicine & PET Research, VU University medical centre, Amsterdam, The Netherlands.

r.boellaard@vumc.nl

Quantification of dynamic PET studies usually starts with definition of volumes of interest (VOI) using manual or automated methodologies. Regional average time activity curves (TAC) are then extracted by projecting these VOIs onto the dynamic PET scan. Quantification of tracer kinetics is subsequently performed by fitting plasma input or reference tissue pharmacokinetic models to the TACs using non-linear regression. Regional analysis is a powerful approach to analyze studies in a standardized way. Yet, this approach depends on the specific VOI delineation being applied, usually based on an assumption of tracer uptake or binding distributions (hypothesis driven). Moreover, VOI based analysis may show less sensitivity to measure changes in tracer binding in case effect occur in an area not fully coinciding with VOI boundaries, i.e. partial VOI effects.

Parametric kinetic analysis is an alternative to avoid partial VOI effects. During parametric analysis the TAC of each voxel is analyzed and a pharmacokinetic parameter, such as binding potential or volume of distribution, is obtained for each voxel. In this way an image representing the 3D regional distribution of tracer binding or uptake is generated. These quantitative pharmacokinetic images can then be used to directly derive regional binding or uptake measures or within parametric statistical analysis methods to assess voxelwise differences in tracer binding or uptake between subjects or over time.

During this lecture various approaches and methods to obtain quantitative pharmacokinetic images will be discussed. Parametric methods need to provide accurate and precise results at higher noise levels (at a voxel level as opposed to regional TAC) and need to be computationally sufficiently fast to generate a 3D image (~1E6 voxels) within a reasonable amount of time. Methods are usually based on linearization of the pharmacokinetic model or can be implemented using so-called basis functions. Linearization is simply based on the integration of the differential equations describing the kinetic compartment model. Basis function methods are based on pre-computing the convolution term in the kinetic model equation for a range of plausible solutions and subsequently selecting the basis function that fits best onto the observed PET data (TAC).

Theoretical derivation of various parametric methods will be presented. Moreover, advantages and potential drawbacks of these methods will be summarized. Strategies to derive the most optimal method to be used will be discussed. In addition, methods that can be applied without assuming a specific underlying kinetic model, such as spectral analysis and basis pursuit will be addressed. Finally, various examples illustrating the benefits of using parametric analysis and images besides regional analysis will be shown.

HIGH-RESOLUTION SMALL ANIMAL PET IMAGING

Schäfers, K.

European Institute for Molecular Imaging – EIMI, University of Münster, Germany (schafkl@uni-muenster.de)

Small animal PET has become a widely used imaging tool in preclinical imaging offering high spatial resolution and sensitivity. High spatial resolution is needed to translate results from small animal studies to humans and vice versa. Positron emission tomography, however, has some fundamental limits to high spatial resolution imaging due to phenomena such as positron range, photon noncollinearity or detector Compton scatter. The challenge is to obtain high spatial resolution for imaging mice, the species that is most often used for research in biology, while at the same time providing adequate scanner sensitivity. Sensitivity is crucial to measure dynamic processes in vivo and to perform tracer kinetic modeling. A simulation is given for predicting the spatial resolution of a small animal PET scanner dependent on parameters such as positron energy, scanner geometry, detector size etc. Noise properties are shown for tomographic scanner systems dependent on detector size and voxel resolution. Additionally, ways for improving spatial resolution and sensitivity are identified such as motion correction or time-of-flight technology. The second part of the talk will highlight developments for high-resolution PET imaging based on multi-wire proportional chamber-based gas detectors. These detectors provide a large field-of-view in combination with sub-millimeter spatial resolution. Examples for high-resolution imaging will be given and future developments for improving the detector technology and quantification discussed.

Notes

QUANTIFICATION OF PRESYNAPTIC CARDIAC SYMPATHETIC FUNCTION USING ^{11}C -HED AND PET: ANALYSIS AND INTERPRETATION OF SIMPLIFIED APPROACHESGonçalves Antunes, S.^{1,2}, Rizzo, G.¹, Gämperli, O.³, Gebhard, C.³, Cerutti, S.², Camici, P. G.⁴, Rimoldi, O.^{1,3}¹Istituto di Bioimmagini Segrade, Italy; ²Politecnico di Milano, Milan, Italy; ³Clinical Sciences Centre, London, UK; ⁴Vita-Salute University, Milan, Italy (sofigantunes@gmail.com)

Introduction: Positron Emission Tomography (PET) with the nor-epinephrine analogue ^{11}C -Hydroxyephedrine (HED) allows the non invasive measurement of the re-uptake1 mechanism *in vivo*. Quantification of the HED distribution volume (V_d ref) was proposed based on a single compartment model and continuous sampling of arterialized blood during a PET dynamic scan lasting 60 minutes¹. The clinical use of this approach, although accurate, is hampered by the substantial amount of blood sampling and long scanning duration, we sought to test the accuracy of a simplified method of HED quantification which could be more easily applied in the clinical settings^{2,3}.

Methods: We studied a group of 11 normal volunteers (age 51 ± 10 yrs). After the injection of ^{11}C -HED, arterialized venous continuous blood sampling was monitored using a BGO detection system. The model input function (IF) was obtained from the combination of BGO counting system and ROIs in the left atrium¹. Different parameters were modified for V_d quantification with one compartment model: acquisition time duration from 60 (t_{60}) to 40 (t_{40}) minutes and input function non corrected for metabolites (IF_{nm}). A semi quantitative approach, calculating a retention index (RI) by normalizing mean myocardial tracer activity from 30 to 40 min (t_{30-40}) and from 30 to 60 (t_{30-60}) to the integral of the arterial input function without (IF_{nm}) and with metabolite correction (IF) was also investigated. Statistical comparisons were carried out by means of linear regression, Deming regression and Bland-Altman plot.

Results: Comparison between V_d ref and the simplified methods:

| Simplifications vs. V_d ref | R^2 | Deming Reg. | | Bland-Altman(mean difference; Limits of agreement) |
|---------------------------------------|-------|---|------------------------|--|
| | | Slope (mean; CI) Intercept (mean; CI) | | |
| $V_d(\text{IF}_{t_{40}})$ | 0.77* | 0.91; (0.82)-(1.00) | -4.97; (-9.28)-(-0.66) | 9.7; (-6.7)-(26.1) |
| $V_d(\text{IF}_{nm-t_{60}})$ | 0.27* | 0.12; (0.09)-(0.16) | 4.66; (2.82)-(6.50) | 42.9; (10.9)-(74.9) |
| $\text{RI}(\text{IF}_{nm-t_{30,40}})$ | 0.36* | 0.17; (0.14)-(0.20) | 8.38; (6.38)-(10.37) | |
| $\text{RI}(\text{IF}_{nm-t_{30,60}})$ | 0.32* | 0.11; (0.09)-(0.13) | 6.51; (5.11)-(7.91) | |
| $\text{RI}(\text{IF}_{t_{30,40}})$ | 0.73* | 0.35; (0.32)-(0.38) | 11.72;(10.01)-(13.43) | |
| $\text{RI}(\text{IF}_{t_{30,60}})$ | 0.80* | 0.36; (0.34)-(0.38) | 9.11; (7.63)-(10.6) | |

All V_d values are expressed in ml/g; RI values in %/min. * $P < 0.0001$
Deming regression and Bland-Altman plots show a positive bias in all comparisons. Non correction for metabolites introduces a proportional error to the measurements. RI always underestimates V_d value, even if 60 minutes PET acquisition and metabolite correction are applied.

Conclusions: Our results suggest that simplification of the model generate non negligible errors in the V_d quantification, with major discrepancies if metabolite correction is not applied.

Acknowledgement/References: 1. Schafers M, Lerch H, Wichter T, Rhodes CG, Lammertsma AA, Borggrefe M, Hermansen F, Schober O, Breithardt G, Camici PG. Cardiac sympathetic innervation in patients with idiopathic right ventricular outflow tract tachycardia. *J Am Coll Cardiol* 1998;32(1):181-6. 2. Bengel FM, Ueberfuhr P, Schiepel N, Nekolla SG, Reichart B, Schwaiger M. Effect of sympathetic reinnervation on cardiac performance after heart transplantation. *N Engl J Med* 2001;345:731-73 3. Schwaiger M, Hutchins GD, Kalif V, Rosenspire K, Haka MS, Mallette S, Deep GM, Abrams GD, Wieland D. "Evidence for regional catecholamine uptake and storage sites in the transplanted human heart by positron emission tomography". *Journal of Clinical Investigation*. 1991; 87(5): 1681-1690

MODELLING IN DCE-MRI

Tofts, P.

Brighton and Sussex Medical School, University of Sussex

(P.S.Tofts@bsms.ac.uk)

Modelling of DCE (Dynamic Contrast-Enhanced) image data in MRI has enabled physiological characteristics of tumours and other lesions to be measured, as an aid to monitoring disease progress and treatment response. A contrast agent (CA; e.g. Gd-DTPA) is injected intravenously as a short bolus, and the subsequent enhancement in tissue signal in a T1-weighted imaging sequence is measured. The widely-used one-compartment 'Tofts model' was first used in Multiple Sclerosis[1], was extended to include a vascular compartment[2], taken up by the cancer imaging community[3,4], and analysed in some detail to find its limits of validity[5,6].

The extracted (fitted) tissue parameters (transfer coefficient K_{trans} , extra-vascular extracellular space EES_{ve} , rate constant k_{ep} ($k_{ep}=K_{trans}/ve$) and plasma volume vp) are sensitive to some of the fixed parameters (tissue native T1, called T10, and relaxivity $r1$ (change in $1/T1$ per unit volume of CA)[3].

Quantification in medical imaging represents a paradigm shift[7]. Complex equipment can be used as a scientific instrument to make measurements (rather than to visualise in a qualitative way). To be an effective biomarker, a quantity should be i) biologically relevant ii) accurate (i.e. true) iii) reproducible (measured from repeated within-subject imaging). A perfect imager is one which contributes insignificant variance compared to the biological variance.

Recently these principles of modelling and quantification have been applied to the measurement of kidney function and vascularity[8]. The model takes account of the large vascular bed, and PC spreadsheet implementation is convenient. In healthy volunteers, values agree with those published using other methods. Reproducibility is acceptable (8-17%).

A crucial constraint to the model is to restrict time to the uptake portion, which in a large ROI lasts at least 90s. By avoiding efflux, the simplified model with a reduced number of free parameters has improved variance. ROI's larger than the nominal kidney outline enabled total filtration to be measured, unaffected by partial volume errors (the Object Strength approach[9].

Sensitivity analysis shows how fitted parameters are affected by the values of fixed parameters. T10, $r1$, MRI flip angle and haematocrit Hct are influential. Small vessels have reduced Hct compared to arteries (~24% vs. 42%) (the Fahraeus effect[10]). Thus measurements of blood volume and perfusion are uncertain, whilst plasma measurements are unaffected (since the CA resides in plasma; also in CT).

From these experiences in DCE-MRI a number of principles for modelling in a quantification procedure are clear:

1. relate the model to the known tissue physiology
2. use the simplest possible model that fits the data
3. ensure the fit is independent of starting values (use constraints)
4. identify the influential fixed parameters (related to the instrument, CA and tissue) and measure the sensitivity of the fitted parameters to these.

5. use repeated imaging (if possible) to estimate measurement variance

6. use phantoms (if possible) to measure accuracy[11]

7. output goodness-of-fit parameters (e.g. rms residual) and exclude fit failures

8. estimate (if possible) fitted parameter variance from Hessian (beware parameter covariance).

More material is on the websites www.qmri.org and www.paul-tofts-phd.org.uk (including pdf's of references)

References: 1. Tofts PS, Kermode AG. Measurement of the blood-brain barrier permeability and leakage space using dynamic MR imaging. 1. Fundamental concepts. *Magn Reson Med* 1991; 17(2):357-367. 2. Tofts PS. Modeling tracer kinetics in dynamic Gd-DTPA MR imaging. *J Magn Reson Imaging* 1997; 7(1):91-101. 3. Tofts PS, Berkowitz B, Schnall MD. Quantitative analysis of dynamic Gd-DTPA enhancement in breast tumors using a permeability model. *Magn Reson Med* 1995; 33(4):564-568. 4. Leach MO, Brindle KM, Evelhoch JL, Griffiths JR, Horsman MR, Jackson A, Jayson GC, Judson IR, Knopp MV, Maxwell RJ, McIntyre D, Padhani AR, Price P, Rathbone R, Rustin GJ, Tofts PS, Tozer GM, Vennart W, Waterton JC, Williams SR, Workman P. The assessment of antiangiogenic and antivascular therapies in early-stage clinical trials using magnetic resonance imaging: issues and recommendations. *Br J Cancer* 2005; 92(9):1599-1610. 5. Sourbron SP, Buckley DL. On the scope and interpretation of the Tofts models for DCE-MRI. *Magn Reson Med* 2011; 66(3):735-745. 6. Sourbron SP, Buckley DL. Tracer kinetic modelling in MRI: estimating perfusion and capillary permeability. *Phys Med Biol* 2012; 57(2):R1-R33. 7. Tofts PS. Quantitative MRI of the brain: measuring changes caused by disease. New York: Wiley, 2003. 8. Tofts PS, Cutajar M, Mendichovszky IA, Peters AM, Gordon I. Precise measurement of renal filtration and vascular parameters using a two-compartment model for dynamic contrast-enhanced MRI of the kidney gives realistic normal values. *European Radiology* 2012; (in press 2012). 9. Tofts PS, Silver NC, Barker GJ, Gass A. Object strength - an accurate measure for small objects that is insensitive to partial volume effects. *MAGMA* 2005; 18(3):162-169. 10. Goldsmith HL, Cokelet GR, Gaehtgens P, Robin Fahraeus: evolution of his concepts in cardiovascular physiology. *Am J Physiol* 1989; 257(3 Pt 2):H1005-H1015. 11. Tofts PS, Collins DJ. Multicentre imaging measurements for oncology and in the brain. *British Journal Cancer* 2012.

keynote lecture

THE PAST ACHIEVEMENTS OF BRAIN PET AND THE ROLE OF QUANTIFICATION

Jones, T.

PET Research Advisory Company*

(terry.jones40@googlemail.com)

Introduction: In order to foresee the future of Brain PET, it is necessary to document the achievements of this field thereby defining its strengths and weaknesses upon which future strategies can be based. Achievements fall into two categories. The first is methodological developments which provide for improved specificity and sensitivity enabling more advanced clinical research questions to be addressed. The second is the outcomes, impacts and consensus changes that have come about through Brain PET based research i.e. what relevant new information on the human brain in health and disease has been produced. Examples are given of these outcomes and reference given to the corresponding methodology emphasising, within the theme of the 2012 ESMI Winter Conference, the quantitative procedures used.

Methods: A review has been written on the future of Brain PET co-authored by Ilan Rabiner of IMANOVA UK to be published in the forthcoming 30th anniversary issue of the Journal of Cerebral Blood Flow and Metabolism. This review needed to cover past achievements and for this an authoritative treatise was required on past clinical achievements. Hence 13 experts in specific clinical applications of brain PET were invited to contribute by summarizing what had been achieved in their respective areas of the human application of brain PET.

Results: Methodological developments are briefly summarized. These cover cyclotron and target chemistry, radiochemistry, automation, tracer and ligand discovery and development, PET scanner technology, PET data processing/reconstruction and analysis. The outcomes from PET brain research are presented by showing examples of the new information derived in a range of specific brain disorders and in normal subjects as well as for supporting drug development. In doing so the corresponding quantitative methodologies used to derive this information are presented. The disorders covered include stroke, dementia, schizophrenia, epilepsy, addiction, depression, anxiety, movement disorders and brain tumours. In addition, the new information on the normal brain is illustrated and the role played in supporting drug development.

Conclusion: There have been major methodological developments over the last 30 years in radio chemistry, PET scanners, data processing and analysis with a range of quantitative methods deriving fundamental parameters of brain function such as blood flow, metabolism and neuro receptor density. Strikingly some 40 specific tracers and ligands have been characterized and validated in humans and at least a further 7 have been validated in humans ready for clinical research. In recent years, carbon-11 labeled tracers and ligands dominate. All of the identified clinical achievements have required quantification to analyze and communicate the data, often in a form of defined neuro chemical and functional parameters. There have been a significant number of achievements in the form of new information on the diseased and normal human brain. However, these are not increasing over time as one would expect given the accumulation of a significant number of methodological advances. Few have translated into clinical health care practice. Lack of wide spread access to these specific imaging biomarkers for brain studies is seen as being the reason for the lack of growth of this field.

The contribution made by a number of international experts in the specific application of brain PET who provided summaries on what has been achieved is acknowledged. References: The Development, Past Achievements and Future Directions of Brain PET Terry Jones and Eugenii A Rabiner: an invited review in the Journal of Cerebral Blood Flow and Metabolism's 30th anniversary year edition in 2012-in press. Oxygen Metabolism, Oxygen Extraction and Positron Emission Tomography: Historical Perspective and Impact on Basic and Clinical Neuroscience. Jean-Claude Baron and Terry Jones: an invited review in the Journal Neurolmage's 20th anniversary year edition in 2012-in press; *<http://www.the-pra.co.uk/>

THE GATE MONTE CARLO SIMULATION PLATFORM: AN OPENSOURCE TOOL FOR MEDICAL IMAGING AND RADIATION THERAPY APPLICATIONS

Jan, S.

CEA, Orsay, France

(sebastien.jan@cea.fr)

Introduction: Monte Carlo simulations are essential for many medical applications, especially for imaging and radiotherapy. Numerical approaches for imaging applications are used to design new devices, to optimize and study the effect of acquisition parameters on the image quality. They are also extremely useful to validate and assess compensation methods and image reconstruction techniques. For radiotherapy applications, Monte Carlo simulations are used to develop planning treatments so as to optimize the dose distribution in tumor and organs at risk. In this research context, the GATE [1][2] simulation platform has been developed and used since 2002 by the international OpenGATE collaboration.

Material and method: After a complete presentation of the GATE platform with a focus on different highlight results from pre-clinical to clinical imaging, we will present a study based on the relation between cancer therapy by ionizing radiation and imaging devices to characterize the quality of treatment. Actually, the GATE Monte Carlo simulation platform is the only numerical tool to study this kind of research activities. In the field of hadrontherapy combined with imaging, we propose to use GATE to study the relationship between deposited dose and Positron Emission Tomography (PET) image quality used as therapy control. We will present the first results of hyperrealistic GATE simulations including a carbon ions (12C) pencil beam scanning, a numerical patient including lung tumor and a PET scanner to perform the post radiation acquisition. These simulations were performed on a supercomputer of 1000 CPUs. The results of this kind of studies are intended to provide informations to guide the design of dedicated PET detectors for therapeutic control, to identify the best protocols to control and follow the deposited dose and finally to estimate the efficiency by using PET imaging for therapeutic control in the case of hadrontherapy treatment.

Results: First results of a full scale simulation including 12C beams with a multi-energy definition (to model a Bragg peak modulated beam) are presented. A commercial PET scanner (Siemens HR +) was specifically modeled to obtain a PET image with a post-radiation acquisition of 10 minutes. This allows to have the distribution of radio-isotopes 11C and 15O produced by nuclear reactions of 12C. The results of the dose deposited versus the quality control by PET imaging will be presented and discussed.

Conclusions and perspectives: Beyond the initial results of these full scale simulations that allow defining the areas for which a therapeutic control by PET imaging will be possible, we will discuss the future challenges associated to the GATE developments. These focus firstly on immootherapy applications and are also related to the optimization of computing time related to the use of a Monte Carlo approach.

References: [1] Jan S. et al. "GATE: a simulation toolkit for PET and SPECT" Physics in Medicine and Biology, 2004, 49 4543–61; [2] Jan S. et al. "GATEV6: a major enhancement of the GATE simulation platform enabling modelling of CT and radiotherapy" Phys Med Biol. 2011 Feb 21;56(4):881-901

OPTIMAL SELECTION OF IMAGING WAVELENGTHS FOR SPECTRAL UNMIXING

van de Giessen, M.^{1,2}, Mezzanotte, L.³, Dijkstra, J.¹, Lelieveldt, B.^{1,2}

¹Leiden University Medical Center Division of Image Processing, Leiden, Netherlands; ²Delft University of Technology Department of Intelligent Systems, Delft, Netherlands; ³Leiden University Medical Center Endocrinology, Leiden, Netherlands (m.vandegiessen@lumc.nl)

Introduction: Real-time multispectral intra-operative imaging of fluorescent probes imposes constraints on the imaging hardware that are not present in pre-clinical imaging. One constraint is that, to be real-time, all spectral bands must be imaged simultaneously. This constraint, together with the form factor of a camera that can be easily handled limits the number of wavelengths that can be imaged. The absolute minimum number of acquired spectral bands is the number of probes (and tissue auto-fluorescence) that need to be separated. For probes with peaks that are far apart, one can select imaging bands centered around the peak wavelengths. However, for peaks that lie close together or for probe responses with a broad spectrum measurements at other wavelengths may give better unmixing results. In this work a method is proposed to determine the optimal measurement wavelengths based on measured spectra.

Methods: Assuming a linear mixing model, the measured light intensity in a single spectral band to a mix of probes can be described by a row in a mixing matrix. Similar rows (i.e. measurements) add little information about the ratio between imaged probes, contrary to very different rows. Mathematically, in the latter case, rows are linearly independent, while in the former case they are (almost) linear dependent. The condition number of a matrix [1] is small for spectra that are linearly independent (the desired situation) and large for linear dependent spectra. Here we propose to select the minimum wavelengths such that they minimize the condition number. The unmixing results using the 'optimal' wavelengths are compared to unmixing results using the 'peak' wavelengths of the probes for simulated multi-spectral images with increasing noise levels. The probe spectra are based on an acquisition with the Maestro system between 630nm and 850nm (interval 20nm). The experiment is repeated for all combinations of 2 to 5 probes: AF680, QD700, AF750, QD800 and skin auto-fluorescence. For real multi-spectral luminescence data from the IVIS Spectrum system, the unmixing results using optimized and peak wavelengths are compared to unmixing based on all acquired wavelengths (500nm to 700nm, interval 20nm) in in-vitro experiments with wells of two mixed probes: CBG99 (540nm) and PpYRE8 (620nm).

Results: In simulations the 'peak' unmixing errors were on average 2.86 times larger than the 'optimal' unmixing errors. This number varied from comparable errors for peaks far apart (e.g. AF680 and AF750) to a 9.01 times larger error for peaks close together (AF680 and QD700). Selecting the optimal wavelengths was especially beneficial for unmixing 3 or more probes. The IVIS in-vitro measurements showed that unmixing with the 'optimal' wavelengths was 8.9% more precise than using the 'peak' wavelengths.

Conclusions: The results clearly showed that selecting the optimal wavelengths as proposed gives almost 3 times more precise unmixing estimates than measuring at the spectral peaks of the imaged probes, both in simulations as in real measurements.

Acknowledgement/References: This research was supported by the Center for Translational Molecular Medicine (MUSiS); [1] Silvan-Cardenas and Wang, Fully Constrained Linear Spectral Unmixing: Analytic Solution Using Fuzzy Sets, IEEE Trans. Geoscience and Remote Sensing, 2010

IMAGE RECONSTRUCTION FROM PROJECTIONS IN SPECT, PET AND TOF-PET.

Nuyts, J.

KU Leuven Nuclear Medicine, Herestraat 49, 3000 Leuven, Belgium

(Johan.Nuyts@uz.kuleuven.be)

Introduction: The image reconstruction problem in PET and SPECT can be represented as follows: given a sinogram Y and a system sensitivity matrix A , compute the image X which "best" satisfies the equation $AX = Y$. This seemingly simple problem is complicated by two issues. First, due to noise and other physical effects, there is no image X that exactly satisfies the equation. Second, the sizes of the matrix A , the image X and the sinogram Y are huge. Analytical and iterative reconstruction algorithms proposed to solve this problem are discussed. Similar methods can be applied in transmission tomography.

Methods: One approach is to derive solutions that minimize the unweighted sum of squared differences, i.e. to minimize the function $(AX-Y)^T(AX-Y)$. It will be shown that in idealized situations, finding the solution of this least squares problem is (nearly) equivalent to the well known filtered backprojection algorithm. However, in other cases, the least squares solution cannot be found analytically, and one needs to use iterative reconstruction algorithms. Similarly, no practical general analytical (i.e. non-iterative) reconstruction algorithm exists for the more appropriate weighted least squares solution. The most popular iterative reconstruction algorithm in emission tomography is the MLEM algorithm (maximum-likelihood expectation-maximization). The algorithm takes into account the Poisson noise that always affects the measured data in emission tomography. MLEM is designed to find the image that is most likely, given the measured sinogram, and assuming no prior knowledge about the image. An intuitive explanation of the algorithm will be given. We show that MLEM often yields images of superior quality, when compared to FBP. In transmission tomography (e.g. CT), the acquired sinogram depends in a non-linear way on the attenuation values that must be estimated by the reconstruction algorithm. Similar (but different) maximum-likelihood algorithms can be developed for this reconstruction problem. Finally, in some cases one wishes to jointly estimate the activity distribution and the attenuation coefficients in the object. This problem occurs in quantitative PET imaging, when for some reason no reliable attenuation can be obtained. An ML algorithm for this joint estimation problem is discussed. This joint estimation problem has multiple solutions in SPECT and non-TOF PET. However, we show that application of this algorithm to TOF-PET data yields quantitatively accurate PET images. Mathematical analysis confirms that TOF-PET data uniquely determine the attenuation correction factors up to a single constant. This result is of interest for imaging with current TOF-PET/CT and future TOF-PET/MR systems.

Results: MLEM reconstruction has become the main reconstruction algorithm in PET and SPECT. Also for transmission tomography iterative algorithms exist and are being studied. Joint estimation of attenuation and activity is possible in TOF-PET.

Conclusions: An introduction to iterative reconstruction in nuclear medicine imaging is presented.

day three: wednesday april 18, 2012



IMPLEMENTATION AND ANALYSIS OF A LIST-MODE ALGORITHM USING TUBES OF RESPONSE ON A DEDICATED BREAST PET.

Moliner, L.¹, González, A.¹, Correcher, C.², Benlloch, J. M.¹

¹Instituto de Instrumentación para Imagen Molecular (I3M) Detectors for Molecular Imaging (DMI), Valencia, Spain; ²Oncovision (GEM Imaging SA) I+D, Valencia, Spain (lmoliner@i3m.upv.es)

Introduction: Breast cancer is the most common non-skin cancer and the second leading cause of death in women [1]. The success of breast cancer treatment strongly depends on early detection, the ability to define the extent of disease, the proper monitor response and to accurately predict the tumor behavior. Positron Emission Tomography (PET) devices, including state-of-the-art dedicated systems [2], are routinely used for diagnosis and therapy assessment of these lesions. High quality and efficiency PET images are essential to reach these objectives. PET designs using continuous crystals [3] have the potential to allow one to define very small virtual pixels in their geometry. This ability is especially useful for List-Mode (LM) reconstruction algorithms [4], since they do not need a pre-calculated system matrix. We have developed and proved an LM algorithm for the dedicated breast PET called MAMMI [2]. Such an algorithm instead of using the typical line of response, incorporates an innovative calculation of tubes of response, resulting on an image quality improvement.

Methods: The MAMMI PET is composed by twelve detector containing a single continuous LYSO crystal and a position sensitive photo-multiplier. In the reconstruction process, only coincidences between one module and its seven opposite are considered. The transaxial and axial FoVs are 170 mm and 40 mm, respectively. The first evaluation of reconstructed images concerned about the uniformity and spatial system resolution. The uniformity study was carried out with a polyethylene cylinder of 100 mm in diameter and 40 mm height filled with 370 uCi of FDG. To study the spatial resolution, we used an array of 81 point sources of Na-22 equally spaced (5 mm). Data with the uniformity phantom was taken for 10 min, whereas the acquisition with the array lasted 20 minutes. Several combinations of virtual pixel sizes varying from 0.4 to 2 mm and voxel dimensions ranging from 0.25 to 1 mm have been evaluated.

Results: The data reconstructed using the LM algorithm has been compared with the currently used MLEM [5]. The analysis of the cylinder data showed that the new algorithm reduces about 4% the detector uniformity. However, we found that the spatial resolution (FWHM) improved on average about 15%. In particular, FWHM values ranged from 1.4 mm at the center of FoV to around 2 mm at the edges.

Conclusions: The initial results of the implemented LM algorithm on continuous crystals, allows one to significantly reduce the virtual pixel sizes and thus, to especially improve the image quality. We found an image quality improvement along the three spatial axes. The uniformity worseness is most likely due to the event by event type of reconstruction method. Common filters could be applied to relatively easy correct for such quality losses.

Acknowledgement/References: [1] R.T. Greenle, *Cancer J. Clin.* 50 (2000) p7. [2] A. Soriano, *Nucl. Instr. Meth. A* 648 (2011) p575. [3] J.M. Benlloch, *Nucl. Instr. Meth. A* 571 (2007) p4273. [4] A.J. Reader, *IEEE Trans. Nucl. Sci.* 49 (2002) p42. [5] L.A. Sheep, *IEEE Trans. Med. Imag.* 11 (1982) p165.

3D INVERSION RECOVERY MEMRI USING SUPER-RESOLUTION RECONSTRUCTION

Plenge, E.¹, Poole, D. S.², Poot, D.¹, Niessen, W.^{1,3}, van der Weerd, L.², Meijering, E.¹

¹Biomedical Imaging Group, Erasmus MC, Depts. of Medical Informatics & Radiology, Rotterdam, Netherlands; ²Molecular Imaging Group, University Medical Center, Leiden, Netherlands; ³Quantitative Imaging Group, University Delft, Netherlands (e.plenge@erasmusmc.nl)

Introduction: Manganese-enhanced MRI (MEMRI) is increasingly used in small animal imaging studies for the unique T1-contrast it provides. Often, due to time limitations, but not only, T1-weighted gradient-echo (GE) sequences are used to monitor the manganese uptake, but spin-echo (SE) sequences offer the advantage of being less susceptible to field inhomogeneities. Also, a better contrast between the regions with high and low manganese uptake is obtainable with inversion recovery spin-echo (IR-SE) sequences [1], but high-resolution 3D imaging in this mode is unfeasible in-vivo due to extensive acquisition times. Such images would, however, be of great value for visualization and analysis purposes. Here we investigate whether super-resolution reconstruction (SRR) methods may provide for this. Such methods allow to create a high-resolution 3D image from a set of low-resolution 2D slice-stacks that each sample the field-of-view in a distinct fashion [2]. For sequences such as IR-SE, which cannot practically be acquired in 3D, SRR can be a useful alternative.

Methods: We constructed a 2% agar phantom with compartments containing manganese concentrations characterized by T1 values of 650, 720, 900, and 1000 ms. A set of 12 IR-SE slice-stacks (TE/TI/TR = 8/650/2700 ms, 1 excitation, 30 slices of 1mm thickness, in-plane isotropic resolution of 0.2mm, acquisition time per stack = 6 min) of the phantom was acquired, rotating the stacks in increments of 180/12 degrees around the frequency encoding axis. From these, an image was reconstructed on an isotropic 0.2mm resolution grid using SRR. For comparison, a 3D GE T1W image (RARE 3D T1W-GE: TE/TR = 3.2/30 ms, flip angle = 30, 4 excitations, isotropic resolution = 0.2mm, acquisition time = 78 min) was acquired. All images were obtained with a 7T Bruker Pharmascan horizontal bore system. SRR was performed on the IR-SE data-set using a Tikhonov-regularized reconstruction scheme minimizing aliasing and spectral distortions [3].

Results: Contrast and contrast-to-noise ratio (CNR) between two compartments with manganese concentrations characterized by T1-values of 650 and 900 ms, respectively, was measured in the SRR IR-SE and GE images. In the GE image the contrast was 1.43, the CNR was 20.13, and the acquisition time was 78 minutes. In the SRR IR-SE image the contrast was 1.87, the CNR was 21.97, and the total acquisition time for 12 slice-stacks was 72 minutes, a time compatible with in-vivo mouse experiments. A 3D IR-SE acquisition with equivalent contrast and resolution settings was estimated to take ~18 hours. On visual inspection the resolution of the SRR IR-SE image was comparable to that of the GE image.

Conclusions: We have shown that SRR can be applied to obtain high-resolution isotropic 3D MEMRI images from 2D slice-stacks, in a time-frame compatible with in-vivo experiments, and that such images offer better contrast than the widely used GE images.

Acknowledgement/References: Supported by Medical Delta, NWO-VENI, and the 7th European Framework Programme. [1] Tindemans et al. *NMR Biomed.* 2006 Feb;19(1):18-29. [2] Greenspan et al. *Magn Reson Imaging*, 20(5):437-446, 2002. [3] Poot et al. *Proc. of MICCAI 2010*, 615-622, Berlin 2010. Springer-Verlag.

ITERATIVE RECONSTRUCTION TECHNIQUES FOR FASTER SCAN SPEED IN MAGNETIC RESONANCE IMAGING

Block, K.T.¹, Uecker, M.², Zhang, S.³, Feng, L.¹, Chandarana, H.¹, Otazo, R.¹

¹NYU Langone Medical Center Center for Biomedical Imaging, New York, US; ²University of California Berkeley Department of Electrical Engineering and Computer Science, Berkeley, US; ³Biomedizinische NMR Forschungs GmbH, Goettingen, Germany (tobias.block@nyumc.org)

Introduction: Magnetic resonance imaging (MRI) is a fascinating technique to image the human body non-invasively without use of ionizing radiation. However, a major limitation is the relatively long acquisition time compared to other imaging modalities, which has been a main research focus in the MRI community for many years. Currently, iterative reconstruction techniques are receiving strong interest because they enable image reconstructions from highly incomplete data, which can be exploited to skip time-consuming acquisition steps and, thus, to reduce the measurement time. This talk will first revise the conventional methods for reconstruction of MRI data, covering Cartesian and radial sampling schemes. In the second part, the iterative reconstruction concept is explained step-by-step and it is demonstrated how the concept can be applied for MRI acquisitions. The technique is based on formulating the reconstruction mathematically as an inverse problem and solving it with a numerical optimization method, which allows for incorporation of additional prior knowledge. Thus, if acquisition steps are skipped during the measurement so that the recorded data is incomplete, the algorithm can be driven to select the solution that is most probable based on the incorporated prior knowledge. If the data is additionally skipped in a way that the resulting undersampling artifacts are inconsistent with the prior knowledge, images can be recovered from a surprisingly small number of samples. This concept recently became popular under the name “compressed sensing”. The following parts of the talk will discuss practical applications of the technique to illustrate its advantage over the conventional reconstruction methods. In the first example, it is shown that the higher sampling requirement for radial k-space sampling compared to Cartesian sampling can be ameliorated using iterative reconstruction with a constraint on the solution's total variation (TV), based on the assumption that many objects are piecewise constant to some degree. Because radial undersampling creates streaking artifacts that increase the TV value relative to the true object, artifacts are suppressed by penalizing the TV in addition to enforcing consistency with the sampled data. Further, by extending the signal model to include locally varying sensitivities of receive RF coils, all coil elements can be processed simultaneously in a parallel-imaging manner, which enables reconstructions from very limited data. Example 2 extends the concept to the temporal dimension in order to obtain highest possible temporal resolution for serially acquired images. The approach uses a continuous radial k-space measurement with a slice-selective FLASH sequence, which creates strongly flickering artifacts at high undersampling rates. By exploiting redundancies among successive time frames, artifacts can be suppressed during the reconstruction. In this way, the technique achieves temporal resolutions of up to 20 ms and yields novel cinematic insight into the human body. Finally, example 3 demonstrates that the temporally-constrained reconstruction can be also applied for 3D acquisitions. Combined with a 3D stack-of-stars FLASH sequence, the approach enables high-resolution volumetric perfusion imaging of the abdomen during free breathing with 2.8 sec temporal resolution, which cannot be achieved using conventional MRI approaches.

Acknowledgement/References: [1] Block KT, MRM 57:1086–1098; [2] Uecker M, NMRBiomed 23:986–994; [3] Feng L, ISMRM 20:1117

IMAGE RECONSTRUCTION: WHAT MAKES OPTICAL IMAGING AN ILL-POSED PROBLEM?

Ripoll, J.^{1,2}

¹University of Fribourg Department of Physics, Fribourg, Switzerland; ²Foundation for Research and Technology-Hellas Institute for Electronic Structure and Laser, Heraklion, Greece (jripoll@iesl.forth.gr)

Introduction: In this talk we will tackle the main reason behind the ill-posed nature of optical imaging, and how it is affected by the presence of scattering. We shall cover the main governing principles of light propagation and concentrate on one main aspect: the transfer function. The transfer function relates an image at a certain plane z (which could be the collection of fluorophores we intend to image) to the image we measure at a certain plane z' (which could be our CCD measurement, or our eye). We shall see that this transfer function contains all the information related to our ability to recover the original image, or rather, that it is responsible for the loss of information on propagation. We shall see, first of all what limits the amount of information that can travel from plane z to plane z' , and secondly how this transfer function reduces even further the amount of information that can be recovered depending on the amount of scattering present in the medium. Direct examples of how this relates to microscopy, whole animal fluorescence imaging and whole animal bioluminescence imaging will be presented, with image reconstruction as the main application in mind.

Once we understand the basics of image propagation we will cover the different approaches that can be used to reduce the ill-posed nature of optical imaging and discuss what are the main differences between bioluminescence and fluorescence imaging.

In particular we shall cover the following topics:

- The basics of light propagation: what is the wavenumber and what does it relate to in a material
- How does light travel from plane z to plane z' : the transfer function
- How does the transfer function depend on scattering and what effect does this have on our image reconstruction
- What renders optical imaging in scattering media an highly ill-posed problem?
- What are the approaches we can use to reduced this ill-posedness: multispectral imaging, introducing a spatial dependence on the excitation, etc.

FAST EDGE-PRESERVING ITERATIVE IMAGE RECONSTRUCTION METHOD FOR FLUORESCENCE DIFFUSE OPTICAL TOMOGRAPHY USING ANATOMICAL PRIOR INFORMATION

Correia, T., Arridge, S.

University College London Department of Computer Science, Gower Street, UK
(tcorreia@cs.ucl.ac.uk)

Introduction: Fluorescence diffuse optical tomography (fDOT) is a powerful research tool, mostly used for small animal imaging and preclinical studies, which uses near infrared (NIR) light to monitor functional and metabolic activity of tissues. In fDOT, fluorescent markers, which are administered to the tissue, bind to specific targets and emit light when excited by a light source. The emission, and possibly, excitation light intensities are collected by charged-coupled device (CCD) cameras. The image reconstruction problem involves finding the spatial distribution of fluorescence activity from multiple projection measurements. However, this is an ill-posed inverse problem, hence, regularisation methods need to be used to stabilise the solution. This can be achieved by incorporating prior information about the smoothness of the solution and, if available, anatomy.

Methods: A nonlinear anisotropic diffusion regularisation term that incorporates anatomical information is used. However, most existing nonlinear reconstruction methods are slow and computationally expensive. We introduce a fast and efficient split operator method, which reduces the nonlinear inverse problem into a Levenberg-Marquardt minimisation step that alternates with a nonlinear anisotropic diffusion filtering step [1]. We test our method using simulated, phantom and *ex-vivo* mouse data. Prior anatomical information is obtained from X-ray computed tomography (XCT) images.

Results: The images reconstructed using this novel image reconstruction method show better spatial localisation and size of fluorescent inclusions than images obtained using standard reconstruction techniques. The reconstructed images reflect both information present in the anatomical image and also that present in the fluorescence images. This method can provide reconstructions within less than 1 min.

Conclusions: We proposed a split operator method for solving the fDOT inverse problem using nonlinear anisotropic diffusion regularisation and anatomical prior information. This method produces images with high quality and accuracy. It has the ability to smooth image noise whilst preserving/enhancing edges, whereas other methods tend to smooth edges, thus providing blurred images. Furthermore, it is straightforward to implement and solve.

Acknowledgement/References: This work has been supported by ECs seventh framework programme FMT-XCT under grant agreement No. 201792. We thank V. Ntziachristos, A. Ale, M. Koch, from Technische Universität München (Germany) for the experimental data. We also thank J. Aguirre, A. Sisniega, J. Abascal, J. Servent, J. Vaquero and M. Desco, from Universidad Carlos III de Madrid (Spain), for the experimental data and for useful discussions.
[1] Correia *et al* (2011) *Biomed Opt Express*, 2(9): 2632-2649.

IMPROVING FMT RECONSTRUCTION ACCURACY USING CT-BASED SHAPE AND NUMERICALLY DETERMINED OPTICAL TISSUE PROPERTIES

Gremse, F.¹, Kinkeldey, A.², Lederle, W.¹, Lammers, T.¹, Jähnen-Dechent, W.², Kiessling, F.¹

¹RWTH-Aachen Experimental Molecular Imaging, Aachen, Germany ; ²RWTH-Aachen Biointerface Laboratory, Aachen, Germany
(fgremse@ukaachen.de)

Introduction: FMT and CT are often used to combine anatomical and molecular imaging capabilities. The CT data can be used to incorporate shape information for an improved FMT reconstruction (1). Since mouse bodies have inhomogeneous optical properties, organ segmentation and specific optical parameters can be included into the forward model. This requires automated segmentation, which is difficult for native CT images and restricted to a few organs (2). To overcome this limitation, we determine the optical tissue properties numerically as suggested in (3). To evaluate improvements in reconstruction accuracy, single small inclusions can be implanted (1). However, this may generate results that are not representative for whole body scans or are biased by reconstruction priors. We propose to use a well known probe (OsteoSense) that binds to bones, compute a smoothed calcium map from the dual energy CT data set and use this as ground-truth FMT reconstruction. Using this approach, we evaluated the improvement of our FMT reconstruction in an automated and user independent way.

Methods: In 12 ApoE mice, FMT-CT scans were acquired 24 hours after injection of OsteoSense. This was repeated after 6 weeks to acquire a total number of 24 scans. Automated marker detection was used for image fusion. The residual error of a hold out marker was determined to estimate the fusion accuracy. The shape of the mouse body was automatically segmented based on the CT data. From this shape and the excitation boundary values, absorption and diffusion coefficients were computed using nonlinear optimization and automated differentiation of the inverse diffusion problem (3). Subsequently, the fluorescence concentration was reconstructed using the normalized born ratio. To generate ground truth reconstruction data sets, the calcium map was computed from the dual-energy CT and smoothed with the estimated point spread function of the FMT. FMT reconstructions with and without shape information and with and without predetermined tissue properties were evaluated against the ground-truth reconstructions using normalized cross-correlation.

Results: More than 6 markers were determined in all images, enabling robust automated registration with average residual error of 0.16 mm. The mouse shape was robustly segmented in all data sets. Shape information and predetermined tissue properties significantly increased the cross-correlation with the ground-truth reconstructions.

Conclusions: Robust automated marker detection and surface extraction enables routine use of FMT-CT imaging. Shape information and predetermined tissue parameters improve the FMT reconstruction accuracy of in-vivo whole body scans.

Acknowledgement/References: 1. Schulz RB, Ale A, Sarantopoulos A, et al. Hybrid system for simultaneous fluorescence and x-ray computed tomography. *IEEE Trans Med Imaging* 2010;29(2):465-473; 2. Freyer M, Ale A, Schulz RB, et al. Fast automatic segmentation of anatomical structures in x-ray computed tomography images to improve fluorescence molecular tomography reconstruction. *J Biomed Opt* 2010;15(3); 3. Davies AJ, Christianson DB, Dixon LCW, Roy R, van der Zee P. Reverse differentiation and the inverse diffusion problem. *Advances in Engineering Software* 1997;28(4):217-221

BIOIMAGE ANALYSIS OF CELLULAR AND MOLECULAR DYNAMICS

Meijering, E.

Erasmus University Medical Center Medical Informatics and Radiology, Rotterdam, Netherlands

(meijering@imagescience.org)

Introduction: Molecular imaging holds the promise of revolutionizing medicine by enabling in-vivo visualization, quantification, and characterization of (sub)cellular biological processes. Optical microscopy plays a pivotal role toward fulfilling this promise, as it is currently the only imaging modality with sufficient spatial and temporal resolution to visualize life at the single-cell and even single-molecule level [1]. For the precise quantification, and ultimately the characterization and modeling of cellular and molecular dynamic processes from microscopic image data, powerful computational tools are needed to ensure efficiency, consistency, and completeness in processing and analyzing these data.

Methods: An essential aspect of the study of biological dynamic processes is the ability to automatically track large numbers of individual objects and their interactions in time-lapse microscopy images [2]. The classical approach to object tracking is to divide the problem into a detection (or segmentation) stage and a linking (or association) stage and to solve these separately. However, methods following this approach usually show rather limited performance, and are beaten by expert human observers. One of the key observations explaining the difference is that the human visual system integrates to a high degree spatial and temporal information. Recently, new methods have been investigated that mimic this property, and that also allow to more easily exploit prior knowledge. Generally these methods are based on (deterministic or probabilistic) model-evolution approaches.

Results: First attempts to automate the tracking task in bioimaging applications date back at least thirty years, but the development of more advanced methods, and their public release in the form of open-source software implementations, really soared in the past decade. At present there exist several dozens of readily available software tools for cell and particle tracking [3]. The results of preliminary evaluation studies seem to indicate that integrative tracking methods, which aim to solve the problem in a global fashion by using all available (image and prior) information, are more powerful than classical two-stage tracking approaches. A careful screening of the literature, however, reveals that many studies of biological dynamic processes are still based on manual tracking.

Conclusions: Automated bioimage analysis solutions for object tracking are essential for the study of cellular and molecular dynamic processes. The field is developing rapidly, and major steps forward have already been made, with dozens of software tools currently being available, but further improvements in terms of accuracy, robustness, and general applicability are still very much needed. Ultimately, however, tracking is only the first step toward characterization and modeling biological dynamics. A major challenge for future research will be to develop tools for automatically mining biologically relevant phenomena from tracking results.

Acknowledgement/References: [1] R. Y. Tsien. Imagining imaging's future. *Nature Reviews Molecular Cell Biology* 4:S16-S21, September 2003. [2] E. Meijering, O. Dzyubachyk, I. Smal, W. A. van Cappellen. Tracking in cell and developmental biology. *Seminars in Cell and Developmental Biology* 20:894-902, October 2009. [3] E. Meijering, O. Dzyubachyk, I. Smal. *Methods for Cell and Particle Tracking*. *Methods in Enzymology* 504:183-200, February 2012.

MULTI-PARAMETRIC PHENOTYPE PROFILING OF 3D CELL CULTURES FOR THE CLASSIFICATION OF BIOLOGICALLY ACTIVE MOLECULESDi, Z.¹, Verbeek, F.², Meerman, J.¹, Price, L.¹¹Toxicology LACDR, Leiden, Netherlands; ²Liacs Leiden University, Netherlands (zid@chem.leidenuniv.nl)

Introduction: 3D cell cultures are gradually replacing the animal model and 2D cell cultures, to study cellular processes, especially for the study of tissue development where the 3D culture environment allows for the spatial organization of the cells. 3D cultures better simulate in vivo conditions compared to 2D cultures and allow cells to self-associate into complex tubular structures – a process known as tubulogenesis. This process cannot occur in a conventional two-dimensional tissue culture environment[1]. The phenotype of 3D epithelial tissues was markedly changed after addition of molecules with known effects on cellular signalling pathways. To be able to characterize the phenotypic influence induced by different molecules, we developed a 3D screening platform which can automatically identify biologically active molecules that influence cellular morphogenesis. Pattern recognition methods were then used to classify molecules according to the phenotype they induced and establish a phenotypic pattern for each class.

Methods: An automated image analysis pipeline was developed to profile the morphogenesis phenotype with multiple parameters. We first applied a Watershed Masked Clustering algorithm[2] and Local Niblack algorithm[3] on the Hoechst stained nuclei channel and Rodamine-phalloidin-stained cytoskeleton channel separately, in order to segment the nuclear and cellular regions. In the second step, 598 parameters were measured including morphological parameters and intensity parameters. In addition to classical intensity parameters such as the mean intensity of the nuclei, moments[4] and wavelets[5] were calculated on both whole image and each defined cellular segment. We also defined many subpopulation-related parameters after classifying each cellular segment, using a pre-trained classifier with user defined training data set.

Results: With the multi-parametric phenotype profile that we obtained, we were able to identify biologically active molecules using multi-parametric statistical comparison between treated and non-treated conditions. For each biologically active molecule, a dose response trajectory was obtained in the principle components space that was compound specific. In addition, we were able to cluster molecules that inhibit the same target into similar phenotypic classes.

Conclusions: In the present study, we developed a 3D screen platform that is able to profile cellular morphogenesis with 598 parameters. By comparing the phenotype profiles from different biologically active molecules, distinct phenotypes were identified specific for certain biological effects. More importantly, our multi-parametric profiling enables us to classify molecules according to biological activity. This offers the potential to develop our methodology into a high throughput compound screen for biological activity.

Acknowledgement/References: [1] Zegers MM, O'Brien LE, Yu W, Datta A, Mostov KE (2003) Epithelial polarity and tubulogenesis in vitro. *Trends Cell Biol* 13: 169-176. [2] Yan, K. & F.J., V. Watershed Masked Clustering Segmentation in High-throughput Image Analysis. On the processing of Pattern Recognition (2010). [3] Niblack, W. An introduction to digital image processing. (Prentice-Hall International, 1986). [4] Zernike, C. F. A. Beugungstheorie des Schneidenverfahrens und seiner verbesserten Form, der Phasenkontrastmethode For a detailed description: . *Physica*(1), pp. 689-704 (1934). [5] Manjunath, B. S. & Ma, W. Y. Texture features for browsing and retrieval of image data. *IEEE T Pattern Anal* 18, 837-842 (1996).

AUTOMATED SEGMENTATION AND TRACKING OF *CAENORHABDITIS ELEGANS* – EMBRYOGENESIS IN FLUORESCENCE MICROSCOPY

Dzyubachyk, O.^{1,2}, Jelier, R.³, Krüger, A.³, Lehner, B.³, Meijering, E.¹

¹ErasmusMC-UniversityMedicalCenterRotterdamDepartments of Medical Informatics and Radiology, Netherlands; ²Leiden University Medical Center Department of Radiology, Netherlands; ³EMBL-CRG Systems Biology Unit Centre for Genomic Regulation, Barcelona, Spain (O.Dzyubachyk@lumc.nl)

Introduction: The nematode *Caenorhabditis elegans* is a widely used model organism in biology for its relative simplicity (the adult organism consists of only 959 cells), known genome, ease of genetic manipulation, invariant lineage tree, fast reproduction, and its transparency. Modern fluorescence microscopy techniques enable imaging of *C. elegans* embryogenesis with good spatial and temporal resolution (3D+t). However, a single data set typically contains thousands of images, showing hundreds of cell divisions, and on the order of 10,000 cell nuclei over the different time points, precluding manual analysis. Previous tools for computerized analysis of such data show limited performance for screening applications. Here we present an improved tool for automated segmentation and tracking of *C. elegans* embryogenesis in fluorescence microscopy.

Methods: The state of the art software tool for tracking *C. elegans* nuclei [1] does not yield their segmentation, but only detection (assuming spherical shape). Precise segmentation of the cell nuclei at every stage of development may provide a more detailed picture of the processes underlying embryogenesis. Continuing our previous work [2], we developed a new method that can perform both segmentation and tracking of *C. elegans* embryogenesis in fluorescence microscopy data. Based on a model evolution approach, it allows incorporation of information about the status of the system at the current time step for segmentation of next time step. Afterwards, a large set of shape and intensity related features is automatically computed for every segmented nucleus. To monitor each of these features throughout the embryogenesis, we also developed a visualization scheme that represents their distribution by a color map overlaid on the reconstructed lineage tree.

Results: The performance of our new method was evaluated on four image sequences from two different labs. Two data sets were acquired on a Leica TCS SP5 microscope (stack size: 712x512x20 voxels, xy-resolution: 0.13 µm, z-resolution: 1 µm, t-resolution: 1 min), and the other two on a Zeiss LSM510 microscope (stack sizes: 708x512x35 and 736x512x31 voxels, xy-resolution: 0.13 µm, z-resolution: 1 µm, t-resolutions: 1 min and 1.5 min). Reconstructed lineages were compared to the corresponding manually built reference lineage using four measures: false positives and negatives, mismatch, and error rate per division. In all cases, the results were comparable to or better than [1].

Conclusions: The method presented here improves on previous state of the art tools for *C. elegans* embryogenesis cell lineage tracking by (1) providing precise segmentation of every cell nucleus, (2) showing better tracking (lineaging) performance, and (3) offering a visualization scheme for analyzing a large number of extracted features. This opens the door to high-throughput screening of *C. elegans* embryogenesis by means of fluorescence microscopy.

Acknowledgement/References: 1. Bao Z, Murray JI, Boyle T, Ooi SL, Sandel MJ, Waterston RH. Automated cell lineage tracing in *Caenorhabditis elegans*. *Proceedings of the National Academy of Sciences of the United States of America* 103(8):2707–2712, February 2006. 2. Dzyubachyk O, Jelier R, Lehner B, Niessen WJ, Meijering E. Model-based approach for tracking embryogenesis in *Caenorhabditis elegans* fluorescence microscopy data. In *Annual Conference of the IEEE Engineering in Medicine and Biology Society*, 2009, pp. 5356–5359.

beyond one's nose lecture

A SYSTEMS MICROSCOPY RESEARCH PLATFORM FOR ANALYSIS OF SYSTEM FORM AND FUNCTION IN CELL MIGRATION

Strömblad, S.

Karolinska Institutet, Department of Biosciences and Nutrition, Huddinge, Sweden (Staffan.Stromblad@ki.se)

Cell migration is a complex behavior that emerges at the cellular scale from interactions between innumerable individual actors at the molecular scale. A quantitative exploration of how this migratory “function” arises from the underlying organizational “form” of the cellular system remains to be achieved. We present a Systems Microscopy research platform that is designed to address this challenge by employing live cell fluorescence imaging, quantitative image analysis and automated statistical interrogation techniques. This platform generates highly dimensioned quantitative data defining cell migration system form and function on a time-resolved, per cell basis with all spatial scales mathematically integrated. We leverage both induced and natural heterogeneity across the derived multi-scale data to capture mathematical relationships within the cell migration system. Ultimately, we employ statistical analyses of causality to define features of system form, such as adhesion complex dynamics, that potentially regulate cell migration function. We thus begin to elucidate fundamental linkages between cell migration system form and function.

SEEING THE INVISIBLE; PREDICTING THE UNEXPECTED

Irani, M.

Dept. of Computer Science and Applied Mathematics, The Weizmann Institute of Science

(michal.irani@weizmann.ac.il)

In this talk I will show how internal redundancy within visual data can be exploited to solve complex visual inference tasks (such as classification, reconstruction, enhancement, super-resolution, detection of irregularities, and more). Comparing and integrating local pieces of visual information gives rise to complex notions of visual similarity and to a general “Inference by Composition” approach, even without any prior examples or training.

I will demonstrate the power of this approach to several problems (as time permits):

1. Detection of objects and dynamic behaviors of interest.
2. Prediction of missing visual information.
3. Detecting the “irregular” and “unexpected”
4. Space/time Super-resolution (even from a single image/video)
5. Summarization of visual data.

SETUP FOR SIMULTANEOUS MEASUREMENT OF LASER SPECKLE FLOWMETRY, RGB REFLECTOMETRY AND POSITRON EMISSION TOMOGRAPHY: VALIDATION AND IN VIVO APPLICATIONGramer, M.¹, Steimers, A.², Takagaki, M.¹, Feuerstein, D.¹, Backes, H.¹, Kohl-Bareis, M.², Graf, R.¹¹Max-Planck-Institute of Neurological Research, Cologne, Germany; ²University of Applied Science Koblenz Mathematics and Technology, Remagen, Germany

(mgramer@nf.mpg.de)

Introduction: Spreading depolarizations (SDs), waves of local depolarization that propagate slowly through the cortex, are believed to play a major role in the secondary deterioration of cortical tissue in the immediate vicinity of the initial lesion. However, their underlying mechanisms of neurometabolic and neurovascular coupling are still unclear. Employing *in vivo* multi-modal imaging, we aimed to investigate metabolic and hemodynamic effects during the passage of SDs. For this purpose, we developed a setup that combines [18F]-fluoro-2-deoxyglucose (FDG) positron emission tomography (PET), a static method to measure glucose consumption, with the real-time optical imaging methods RGB reflectometry (RGR) and laser speckle flowmetry (LSF) to investigate spatiotemporal tissue oxygenation and blood flow patterns, respectively.

Methods: To allow simultaneous acquisition of optical and positron emission data, an animal holder equipped with sensors for the regulation of basic systemic parameters (anesthesia, body temperature, breathing rate) was modified to minimize attenuation of gamma rays by the optical equipment. Optical imaging was performed with double illumination consisting of a laser diode in the near-infrared range for LSF and high power white light LEDs in the visible spectrum for RGR. The obtained signals reflected from within the PET gantry were mirrored outside onto a CCD camera in which they were spectrally separated by a prism and directed onto two CCD chips [1]. Sensitivity and interference of each modality were determined with the help of phantoms. In male Wistar rats, the temporoparietal cortex was exposed through thinned skull and a burr hole was drilled to be able to place a stainless steel hook below the medial cerebral artery (MCA). In the PET scanner, the MCA was lifted using a high precision piezo-electric motor, occluding the artery and eliciting SDs [2]. To co-register the 2D optical images and the 3D PET maps, we developed a spatially well-defined fiducial marker visible in all modalities. It includes small light reflecting spheres detectable in the optical images and a ring-shaped radiotracer tubing visible in the PET data. Based on a computer aided design drawing of the marker, the optical and PET data were aligned in an image analysis software.

Results: In a set of validation experiments we showed that there is minimal interference between the different modalities with no visible artefacts and with preserved sensitivities. The combination of LSF and RGR showed that the spatiotemporal patterns of tissue oxygenation matched the haemodynamic response. During the first SD event following MCA occlusion we observed an oligemic wave that was time-locked with a congruent wave of decreased oxygenated haemoglobin and increased deoxygenated haemoglobin. With the FDG-PET images we distinguished between different types of metabolic tissue conditions and compared them to their co-registered haemodynamic and oxygenation response.

Conclusions: This setup allows for the examination of dynamic vascular and metabolic disturbances in the rodent brain with high spatiotemporal accuracy.

Acknowledgement/References: [1] Steimers et al., Proc. SPIE 2009;7368-30; [2] Takeda et al., JCBFM 2011; 31:1863-1873

discussion

THE FUTURE OF PET: A DISCUSSION

led by Jones, T.

PET Research Advisory Company*

(terry.jones40@gmail.com)

Notes

The starting point for this discussion is to define what is the un-met need for PET based molecular imaging in experimental medicine and clinical health care? This will be defined and developed in the discussion for brain and cancer studies, as well as across a wide range of internal medicine.

In the face of these needs and despite major methodological advances, it will be seen that PET is not addressing this potential.

The thesis developed is that this underachieving is due to the lack of access to short lived, positron emitting radio nuclides and efficient low cost, GMP compatible, means for producing labelled imaging biomarkers for human administration. Access is required at the "point of contact" within the various clinical specialities. Additionally, for many areas of potential clinical application, there is an absence of suitable PET based imaging biomarkers, the development of which requires top level biology and chemistry expertise which also require access to short lived, positron emitting radio nuclides.

To focus the discussion on how to address these challenges, the prospect is introduced of improving access through the introduction of low powered, low cost, low radiation emitting, easy to operate micro-cyclotrons along with single use, micro-fluidics based, radio chemistry units.

*<http://www.the-pra.co.uk/>

day four: thursday april 19, 2012



DATA STORAGE & ANALYSIS: “OPPORTUNITIES AND CHALLENGES IN BIOMEDICAL IMAGING RESEARCH”

Niessen W.J.

Departments of Radiology & Medical Informatics, Erasmus MC ; Faculty of Applied Sciences, TU Delft

(w.niessen@erasmusmc.nl)

In both clinical and biomedical research, there is a sheer data explosion. Both data heterogeneity and volume pose enormous challenges, and the storage, access, processing, and sharing of data have become serious challenges. Several European initiatives are addressing these challenges.

For dealing with biomedical imaging data, the ESFRI project EuroBioImaging is working towards a roadmap to construct a “European Biomedical Imaging Data Storage and Analysis Infrastructure”. Three key objectives of this infrastructure are:

To support efficient and standardized storage for and access to curated biomedical image data.

To support open-source software for biomedical image analysis through coordination of community efforts, provision of an actively maintained repository of state-of-the-art validated algorithms for quantitative image analysis and thorough training.

To interface with high performance computing facilities for high-throughput and/or computation-intensive image analysis.

In this presentation we will discuss these three issues. Examples will be given from multiple application areas, ranging from biological imaging, to population imaging studies.

FULLY AUTOMATED IMAGE POST-PROCESSING OF (F)MRI DATA DURING AN IMAGING SESSION USING A REMOTE CLUSTERPracht, E.¹, Kalthoff, D.¹, Wiedermann, D.¹, Vollmar, S.², Hoehn, M.¹¹MPI for Neurological Research In Vivo NMR, Cologne, Germany ; ²IT & Electronics Development, Cologne, Germany

(epracht@nf.mpg.de)

Introduction: Usually, fully processed MR images (including motion correction, coregistration and further analysis) are only available after the imaging session. Online reconstruction is often impossible due to computational intensive reconstruction pipelines. Such a workflow would lead to high CPU/memory load and extensive processing times, which is unacceptable on scanner hosts. To overcome this limitation we propose a different, fully automatic post-processing approach using a remote server. Immediately after completion of each scan the data is sent to a remote cluster and the whole post-processing pipeline is applied. Meantime the imaging session continues and further scans are acquired. After completion of each post-processing workflow on the remote cluster the results are sent back to the scanner database and are ready for inspection during the imaging session, using the standard scanner software. Additionally, an html-report is generated including the whole reconstruction pipeline, all final images, and additional results of the analysis. In this work a typical rat fMRI session is presented as an example.

Methods: MRI datasets were acquired on an 11.7 T scanner (Bruker BioSpin, Ettlingen, Germany) using a standard fMRI protocol for rats [1]. Before the imaging session a macro was started on the scanner host in the background, monitoring the current scanner status. After completion of each scan the macro sent a “scan finished” message to the remote server. Afterwards the server grabbed the acquired raw images from the scanner and started a single Python script, containing a post-processing pipeline based on NiPype [2]. Uniform access to FSL tools (<http://www.fmrib.ox.ac.uk/fsl>) is provided by NiPype, enabling robust post-processing, such as motion correction and brain extraction. Furthermore, custom-made reconstruction extensions were included in the NiPype framework allowing further analysis of the pre-processed data. To speed-up processing time, parts of more complex workflows were executed in parallel using the distributed computing capabilities of NiPype.

Results: Processing on the remote cluster involved brain extraction and co-registration to a rat brain template. Additionally, the fMRI data was slice-wise motion corrected and statistical analysis was performed. After the reconstruction, the processed images were converted back to the scanner image format by the NiPype pipeline and put back into the session database on the scanner host. Moreover, an html report was automatically generated, including the most important images and imaging parameters, as well as results of the statistical analysis. Due to the fast processing times it was possible to investigate the imaging results “online” during the imaging session. Hence, it was possible to change imaging parameters on the fly to guarantee optimal imaging results.

Conclusions: A versatile automatic, online data processing framework is presented. Once a study specific, standardized reconstruction workflow is created, no further user interaction is necessary, before, during or after the imaging sessions. Due to the modularity of NiPype, this framework is extensible and applicable to various types of MRI studies and other imaging modalities as well. Furthermore, offline execution of the reconstruction pipelines without a scanner host is possible.

Acknowledgement/References: [1] Seehafer et al, J Neurosci. 2010 Apr 14;30(15):5234-41.[2] Gorgolewski et al, Front Neuroinform. 2011;5:13

THE OPEN MICROSCOPY ENVIRONMENT: OPEN IMAGE INFORMATICS FOR THE BIOLOGICAL SCIENCES

Allan, C.^{1,2}, Burel, J.-M.^{1,2}, Moore, J.², Blackburn, C.¹, Linkert, M.², Loranger, B.¹, Loynton, S.¹, Moore, W.J.¹, Neves, C.², Patterson, A.¹, MacDonald, D.¹, Rueden, C.³, Tarkowska, A.¹, Wells, S.¹, Eliceiri, K.W.³, Swedlow, J.A.^{1,2}

¹Wellcome Trust Centre for Gene Regulation & Expression, University of Dundee, UK.

²Glencoe Software, Seattle, USA. ³Lab. for Optical and Computational Instrumentation, University of Wisconsin at Madison, Madison, WI, USA (j.r.swedlow@dundee.ac.uk)

Despite significant advances in cell and tissue imaging instrumentation and analysis algorithms, major informatics challenges remain unsolved: file formats are proprietary, facilities to store, analyze and query numerical data or analysis results are not routinely available, integration of new algorithms into proprietary packages is difficult at best, and standards for sharing image data and results are lacking. We have developed an open-source software framework to address these limitations called the Open Microscopy Environment (<http://openmicroscopy.org>). OME has three components—an open data model for biological imaging, standardised file formats and software libraries for data file conversion and software tools for image data management and analysis.

The OME Data Model (<http://ome-xml.org>) provides a common specification for scientific image data and has recently been updated to more fully support fluorescence filter sets, the requirement for unique identifiers, screening experiments using multi-well plates.

The OME-TIFF file format (<http://www.loci.wisc.edu/ome/ome-tiff.html>) and the Bio-Formats file format library (<http://www.loci.wisc.edu/ome/formats.html>) provide an easy-to-use set of tools for converting data from proprietary file formats. These resources enable access to data by different processing and visualization applications, sharing of data between scientific collaborators and interoperability in third party tools like Fiji/ImageJ.

The Java-based OMERO platform (<http://openmicroscopy.org/site/documents/data-management/omero>) includes server and client applications that combine an image metadata database, a binary image data repository and high performance visualization and analysis. The current release of OMERO (Beta4.3; <http://openmicroscopy.org/site/support/omero4/downloads>) includes a single mechanism for accessing image data of all types-- regardless of original file format-- via Java, C/C++ and Python and a variety of applications and environments (e.g., ImageJ, Matlab and CellProfiler). Support for large images from digital pathology is now included. This version of OMERO includes a number of new functions, including SSL-based secure access, distributed compute facility, filesystem access for OMERO clients, and a scripting facility for image processing. Demos of OMERO are available at <http://openmicroscopy.org/site/products/feature-list>.

THE OPEN MICROSCOPY ENVIRONMENT: OPEN IMAGE INFORMATICS FOR THE BIOLOGICAL SCIENCES

Allan, C.^{1,2}, Burel, J.-M.^{1,2}, Moore, J.², Blackburn, C.¹, Hill, E.^{1,2}, Linkert, M.², Littlewood, S.¹, Loynton, S.¹, Moore, W.¹, Neves, C.², Patterson, A.¹, Rueden, C.³, Tarkowska, A.¹, Wells, S.¹, Eliceiri, K.³, Swedlow, J.^{1,2}

¹Wellcome Trust Centre for Gene Regulation & Expression, University of Dundee, UK.

²Glencoe Software, Seattle, USA. ³Lab. for Optical and Computational Instrumentation, University of Wisconsin at Madison, Madison, WI, USA (j.burel@dundee.ac.uk)

Introduction: Despite significant advances in cell and tissue imaging instrumentation and analysis algorithms, major informatics challenges remain unsolved: file formats are proprietary, facilities to store, analyze and query numerical data or analysis results are not routinely available, integration of new algorithms into proprietary packages is difficult at best, and standards for sharing image data and results are lacking.

Methods: We have developed an open-source software framework to address these limitations called the Open Microscopy Environment (<http://openmicroscopy.org>). OME has three components—an open data model for biological imaging, standardised file formats and software libraries for data file conversion and software tools for image data management and analysis.

Results: The OME Data Model (<http://ome-xml.org>) provides a common specification for scientific image data and has recently been updated to more fully support fluorescence filter sets, the requirement for unique identifiers, screening experiments using multi-well plates. The OME-TIFF file format (<http://www.loci.wisc.edu/ome/ome-tiff.html>) and the Bio-Formats file format library (<http://www.loci.wisc.edu/ome/formats.html>) provide an easy-to-use set of tools for converting data from proprietary file formats. These resources enable access to data by different processing and visualization applications, sharing of data between scientific collaborators and interoperability in third party tools like Fiji/ImageJ. The Java-based OMERO platform (<http://openmicroscopy.org/site/documents/data-management/omero>) includes server and client applications that combine an image metadata database, a binary image data repository and high performance visualization and analysis.

Conclusions: The current release of OMERO (Beta4.3; <http://openmicroscopy.org/site/support/omero4/downloads>) includes a single mechanism for accessing image data of all types-- regardless of original file format-- via Java, C/C++ and Python and a variety of applications and environments (e.g., ImageJ, Matlab and CellProfiler). Support for large images from digital pathology is now included. This version of OMERO includes a number of new functions, including SSL-based secure access, distributed compute facility, filesystem access for OMERO clients, and a scripting facility for image processing. Demos of OMERO are available at <http://openmicroscopy.org/site/products/feature-list>.

IMAGE ANALYSIS CHALLENGES IN MULTI-MODAL PRE-CLINICAL IMAGING STUDIES

Lelieveldt, B.^{1,2}

¹Leiden University Medical Center Division of Image Processing, dept of Radiology, Albinusdreef 2, 2300RC 2300RC, Netherlands; ²Delft University of Technology Intelligent Systems, Mekelweg 4, Delft, Netherlands

(b.lelieveldt@lumc.nl)

Introduction: The rapid developments in in-vivo molecular imaging modalities such as fluorescence and bioluminescence imaging enable the live imaging of gene expression, cell fate and protein interactions. Combined with detailed structural imaging modalities such as magnetic resonance (MR), the biochemical onset of disease and therapy can be monitored in combination with structural and functional consequences over time. However, the heterogeneity and sheer bulk of imaging data make it difficult for a human observer to interpret and quantify the relationships between molecular processes and the structural and functional changes they cause. Differences in imaging geometry, subject posture, and information content occur between modalities, but also between time points in follow-up studies using the same modality. The lack of automated techniques to interrelate imaging data and to keep track of dynamic phenomena occurring in these data is rapidly becoming the bottleneck for effective data interpretation.

Methods: This presentation discusses a number of techniques to address the image analysis challenges emerging from longitudinal pre-clinical molecular imaging studies. Three steps towards a quantitative 3D analysis of follow-up small animal imaging are presented: whole-body registration, change visualization and quantification in follow-up data, and fusion of optical and 3D structural imaging data.

Results: Application examples and quantitative study results are presented in the context of cell tracking and translational cancer research, in particular:

- study of micrometastasis formation in breast cancer
- development and validation of novel tracers for fluorescence guided surgery
- tracking of stem cell migration and differentiation

Conclusions: Automated integration and quantification algorithms can greatly facilitate and enhance pre-clinical imaging studies.

Acknowledgement/References: This work was partially supported by EU FP7 project ENCITE and the Medical Delta consortium.

OPTICAL TRACKING SYSTEM FOR IMAGING FREELY MOVING MICE WITH THE QUADHIDAC SMALL ANIMAL PET SCANNER

Schmid, S.^{1,2}, Dawood, M.¹, Frohwein, L.¹, Jiang, X.², Schäfers, K.¹

¹European Institute for Molecular Imaging, Münster, Germany ; ²University of Münster Dept. of Mathematics and Computer Science, Münster, Germany

(soenke.schmid@uni-muenster.de)

Introduction: Small animal PET scanners are widely used to study molecular processes inside living animals offering high spatial resolution. Animals are usually anesthetized to avoid image blurring effects due to motion. Anesthesia, however, heavily influences the tracer uptake in various organs and should thus be avoided. We are developing a new imaging technology to study freely moving animals within a high-resolution PET scanner. The aim of this study is to build an optical tracking system inside the quadHIDAC small animal scanner to determine the motion of a conscious mouse. A prototype of the tracking system was build and tested for its applicability.

Methods: The quadHIDAC is a dedicated small animal PET scanner offering very high spatial resolution of about 1 mm within a large field-of-view of 16x16x28cm³. For accurate motion correction, a tracking accuracy of 0.5 mm was defined as our final goal to utilize this high spatial resolution of the scanner. A small animal chamber was constructed with a size of 10x10x20cm made of acrylic glass. Four optical cameras were placed around this chamber, a pair of stereo cameras on each small side. Based on simulations using ray tracing techniques for estimating the hardware requirements, cameras with a resolution of 659x494 pixels, wide angle lenses, and a frame rate of 100 fps were used. This frame rate is required to provide the necessary temporal resolution. For optimal ambient illumination a grid of LED's emitting infrared light at 850 nm was build into the ceiling of the chamber, shining through a diffusial layer. This wavelength ensures that the cameras operate at high sensitivity and, at the same time, making the infrared light almost invisible to the mouse eye. A first experimental validation of the tracking system was conducted using only one pair of stereo cameras estimating the position of a marker at 60 positions inside the chamber. A thin plate splines correction for lense distortion was applied and the light refraction at the chamber walls was included into the calibration and triangulation methods.

Results: The analysis of the 60 tracked markers showed an average triangulation accuracy of 0.76 mm with a minimum and maximum value of 0.3 mm and 1.3 mm respectively. The simulations based on ray tracing showed that light refraction at the chamber walls may lead to triangulation errors of up to 1 mm in certain areas of the chamber. Thus, this effect is not neglectable and has to be taken into account.

Conclusions: The presented system provides high accuracy to track a freely moving, non-anesthetized mouse inside the quadHIDAC scanner. The LED's provide excellent ambient light for accurate tracking while not disturbing the mouse. Further work needs to be done to improve the tracking accuracy by using more sophisticated calibration methods. The motion and position information could then be incorporated in the image reconstruction step leading to a motion-free PET image of a conscious and freely moving mouse.

Acknowledgement/References: Kyme A et al.: "Motion tracking of fully conscious small animals in PET" Nuclear Science Symposium Conference Record (NSS/MIC), 2009 IEEE 2009; 2561-2566

CONSTRUCTION OF A STATISTICAL MOUSE ATLAS FOR PRECLINICAL IMAGE ANALYSIS

Wang, H., Stout, D., Chatziioannou, A.

Crump Institute for Molecular Imaging, UCLA, Los Angeles, California USA

(wang.hongkai@gmail.com)

Introduction: Over the past decade, several clinical imaging modalities including PET, SPECT, CT and MRI have been adapted for preclinical imaging using mice, which has created the need for automated image analysis of mouse metabolic and anatomical images. We are constructing a statistical mouse atlas based on multiple training subjects, and developing methods to register the atlas with individual mouse images to assist automated preclinical image analysis of organ region definition and uptake quantification.

Methods: The statistical mouse atlas was constructed based on 83 segmented contrast enhanced micro-CT images, including different strains, ages, and sexes. Major trunk organs (skin, skeleton, heart, lungs, liver, spleen and kidneys) and detailed brain structures were included into the atlas. To minimize the posture variations, a standardized mouse chamber was used for imaging, and the articulated mouse skeleton atlas [1] was used to achieve whole body alignment align between the training subjects. For trunk organs, the statistical shape model (SSM) technique was used to describe inter-subject anatomical deformations, and conditional Gaussian models (CGM) were built to describe the inter-organ anatomical correlations [2]. The brain structures of the Digimouse atlas [3] were included in the atlas. To register the atlas with a certain imaging modality, the SSM of the high-contrast organs of that modality was fitted to the image, and then the low-contrast organs were estimated via the high-contrast organs using the CGM.

Results: Preliminary tests have been performed to register this atlas to 45 micro-CT images and 9 micro-PET images. The micro-CT registration results showed that the statistical atlas obtained good match for larger organs like the liver (mean value of Surface Distance (SD)=0.45 mm), and suboptimal accuracy for smaller organs like the spleen (SD=0.72mm). For micro-PET images, the organ regions of the registered atlas were used for quantification of organ uptakes. The recovery coefficient (RC=A/G) was calculated as a metric of quantification accuracy, where A is the organ uptake quantified with the atlas, and G is the gamma counter measurements of the dissected organs. Similar to micro-CT results, the atlas-based quantifications matched well with gamma counter measurements for larger organs (RC=0.89 for the liver) and were suboptimal for smaller organs (RC=0.48 for spleen).

Conclusions: The statistical mouse atlas has demonstrated the potential of assisting preclinical mice image analysis. Currently the atlas is still being improved. More organs are being added into the atlas and better statistical training methods are being developed for modeling inter-subject anatomical variations.

Acknowledgement/References: [1]. Khmelinskii et al. (2011). Articulated whole-body atlases for small animal image analysis: construction and applications. *Mol. Imag. Biol* 13(5), 898-910.[2]. Wang et al (2012). Estimation of Mouse Organ Locations through Registration of a Statistical Mouse Atlas with Micro-CT Images. *IEEE Trans Med Imaging*. 31(1), 88-102.[3]. Dogdas et al. (2007). Digimouse: a 3D whole body mouse atlas from CT and cryosection data. *Phys. Med. Biol.* 52(3), 577-87.

CHANCES AND CHALLENGES OF PET/MR IMAGING

Wehrl, H.

University of Tuebingen Department for Preclinical Imaging and Radiopharmacy, Tuebingen, Germany

(hans.wehrl@med.uni-tuebingen.de)

Introduction: The combination of Positron-Emission-Tomography (PET) and Magnetic Resonance (MR) imaging offers the possibility to combine molecular information with the strengths of anatomical and functional imaging. In contrast to PET/CT where a sequential acquisition is applied, the majority of PET/MR devices aim to acquire the data from both modalities simultaneously. This isochronous acquisition scheme offers unique chances in studying functional processes, but also poses challenges in experimental design and evaluation. Examples of cross calibration between PET and MR perfusion as well as monitoring multiple stages of brain activation are presented.

Methods: An overview about the current state of PET/MR technology is given. Simultaneous comparison measurements between PET [^{15}O]H₂O perfusion imaging and MR arterial spin labeling (ASL) have been performed. Approximately 48 MBq of [^{15}O]H₂O have been injected in BALB/c mice (n=5) during oxygen and carbogen breathing and an simultaneous ASL acquisition. Quantitative perfusion values were obtained by means of kinetic modeling (one tissue compartment model for [^{15}O]H₂O PET) and by solving a simplified Bloch equation (for MR ASL). In a second experiment brain activation in rats (n=8) during whisker stimulation was compared using a simultaneous measurement of [^{18}F]FDG accumulation and fMRI blood oxygen level dependent (BOLD) effect. fMRI and BOLD data were analyzed using statistical parametric mapping. Besides these activation comparisons also the resting state brain activity was studied by an independent component analysis of fMRI as well as PET uptake time courses.

Results: Many of the initial technological challenges of combined PET/MR systems have been solved by the use of semiconductor detector devices, allowing to operate these PET/MR scanners with a performance on par with stand alone systems. The simultaneous perfusion measurements comparing [^{15}O]H₂O with ASL indicate, that many physiological variations such as temperature, compared to sequential measurements, could be minimized. PET and MR perfusion show a mismatch in the high flow regime. The PET-fMRI comparison allowed depicting multiple brain networks during activation. Where more activation areas are observed using the PET method compared to the fMRI technique. Resting state measurements combining PET and MR seem to offer new possibilities to study brain function.

Conclusions: The ability to simultaneously image PET and MR data, allows minimizing many confounding parameters such as subject motion, fluctuations in physiology or image co registration. However care must be taken with the interpretation of the data. The mismatch between PET and MR perfusion measurements can be possibly attributed to limited BBB permeability for radioactive water – but could also stem from differences in PET and MR data modeling. Brain activation measurements reveal different networks, when visualized with PET and MR methods. Here the two techniques are complimentary, with [^{18}F]FDG depicting the glucose consumption changes and BOLD revealing oxygenation alterations. Some limitations are given by tracer kinetics for the state of simultaneity that can be achieved. The mentioned examples indicate a big potential for combined PET/MR technology. With a more widespread use of this technology it is likely that a new domain of functional imaging is opened potentiating the capabilities of the individual modalities.

VINCI - CO-REGISTRATION OF RAT BRAINS (PET-MR)

Vollmar, S., Sué, M., Hüsken, A., Endepols, H., Backes, H.

Max Planck Institut für Neurologische Research, Cologne, Germany

(vollmar@nf.mpg.de)

Introduction: Fully automatic co-registration of PET and MR images of human brain [1] has been a central feature of VINCI [2], our package for visualization and analysis of tomographical data, for several years. Recent improvements and adaptations now allow us to also use the same registration engine for a number of registration tasks in rat brains, in particular FDG- and FDOPA-PET studies with T2-MRI scans of the same animal.

Methods: A difficulty with typical data from our animal scanners is that MR images comprise mainly brain while PET images include the animal's whole head: as a result, our previous attempts already failed at the coarse-grain stage, i.e. to bring the two studies within the core algorithm's [1] capturing range, except when pre-registered manually. We replaced this manual step by a new and automated preprocessing method: (1) we co-register the MRI data to a common template which we have generated from one of our MRI studies by multiplying with a blurred brain mask (1 mm Gauss filter). (2) We then match the PET image to the same MRI template. As an intermediate step, the PET data is registered to a common "head mask" (using thresholding, border detection and rigid-body registration with mutual information). This head mask is already aligned to the MRI template. Now both images should be within capturing range and we can expect our usual method to work.

Results: We have compared our new fully-automatic co-registration approach using manual co-registration and found very similar results when matching T2-scans (Bruker 11.7 T) of the same animals. Results for matching FDG- and FDOPA-PET studies (Siemens microPET Focus 220) with T2-MRI scans were very encouraging, H₂O-PET did work well in some cases.

Conclusions: Fully automatic co-registration of PET studies with MRI data for rat brains seems to be feasible for certain cases. Apart from eliminating or easing a difficult manual task, we see a potential for improved "Good Scientific Practice" when combined with extended logging of the associated workflows [3]-[5].

Acknowledgement/References: [1] J. Cizek, K. Herholz, S. Vollmar, R. Schrader, J. Klein, W. D. Heiss. Fast and robust registration of PET and MR images of human brain, *NeuroImage* 1 (22) (2004) 434-42. [2] VINCI, <http://www.nf.mpg.de/vinci> [3] S. Vollmar, M. Sué, A. Hüsken, J. Nock, R. Krais. VHIST/VINCI – New Concepts for typical Problems in Multi-Modality Imaging. 4th European Molecular Imaging Meeting, Barcelona, May 2009. [4] S. Vollmar, M. Sué, A. Hüsken, J. Nock, R. Krais. VHISTdiff - comparing workflow histories (VHIST/VINCI), 5th European Molecular Imaging Meeting, Warsaw, May 2010. [5] A. Hüsken, M. Sué, M. Gramer, D. Feuerstein, H. Backes & S. Vollmar. VHIST/VINCI - Scripting with Meta-Information, 6th European Molecular Imaging Meeting, Leiden, June 2011

ATTENUATION CORRECTION OF PRECLINICAL PET IMAGES BASED ON MRI SCOUT PAIR SEGMENTATION

Papp, L.¹, Bandi, P.¹, Egri, G.¹, Babos, M.², Mathe, D.³, Hobor, S.²

¹Mediso Medical Imaging Systems Software R&D, Budapest, Hungary ; ²Mediso Medical Imaging Systems PET-MRI Development, Budapest, Hungary ; ³CROMed Research, Budapest, Hungary

(laszlo.papp@mediso.hu)

Introduction: PET-CT multi-modal systems play an important role in the field of preclinical imaging. Usually, several CT image acquisitions are performed on the same animal during the study period. The absorbed dose can thus interfere with the living organism, e.g. it may effect tumor healing. Furthermore, CT provides poor soft tissue contrast which makes the perfect PET lesion localization difficult. MRI is an excellent alternative of CT, since it dramatically decreases the total absorbed radiation dose (35-40%), and provides a well-detailed soft tissue contrast as well. Nevertheless, MRI based body-air segmentation is challenging. To generate an attenuation map, fast MRI scout scans are required. These scans usually contain ghost artifacts – perpendicular to the frequency direction – originated from organ and internal fluid motions. In order to overcome this issue and provide a valid attenuation map for PET reconstruction, our approach built on dual information analysis by the processing of two MRI scout pair scans having perpendicular frequency directions.

Methods: Five rat PET/MRI studies with 18F-FDG PET were performed, all cases had two MRI fast scout scans (with a 3D steady-state gradient echo sequence) having perpendicular frequency directions over axial slices. The images were acquired with a nanoScan® PM PET/MRI camera manufactured by Mediso. The MRI scout pairs were filtered with a Gaussian disc to reduce background noise. Region growing from both images was independently performed from background regions automatically to create two binary masks. These masks included not only the body but also outside-of-body regions due to ghost artifacts. The two masks involved artifacts having perpendicular directions, hence the masks were merged by a logical AND operator to acquire the final mask representing only the body of the animal. Two 3D EM PET reconstructions were performed by the Mediso Tera-Tomo™ reconstruction engine representing with and without AC cases. The PET images were compared by visual inspection and by 3D isocount VOI statistical analysis as well.

Results: Difference between the AC and non-AC PET is significant even on a visual level. Statistical VOI analyses shown that the average standard deviation is 8% less in case of AC PET in particular over hot spots than in corresponding non-AC images.

Conclusions: We have proposed a novel approach to eliminate ghost artifact based issues of MRI scout images for a successful body-air mask segmentation. Statistical analyses have shown that PET AC makes sense even in the field of preclinical imaging. As the next step of our work, we will focus on lung segmentation of MRI scout images to further increase the accuracy of the PET reconstruction.

FAST, ROBUST AND ACCURATE EXTRACTION OF TIME ACTIVITY CURVES IN RODENT PET WHOLE-BODY IMAGESMaroy, R.¹, Boisdard, R.^{1,2}, Comtat, C.¹, Tavitian, B.^{1,2}, Jan, S.¹¹CEA SHFJ, Orsay, France ; ²INSERM U1023, Orsay, France

(renaud.maroy@yahoo.fr)

Introduction: Numerous new drug candidates fail because of inadequate pharmacokinetics. Positron Emission Tomography (PET) enables the non-invasive characterization of the drug in humans and animals. In this work, a fast, robust and accurate method is proposed for the extraction of organ time activity curves from rodent PET images without requiring resort to anatomical information.

Methods: The rodent organs were segmented using the Local Means Analysis (LMA) method [1]. The Time Activity Curves (TACs) were extracted using an improvement of the Geometric Transfer Matrix (GTM) method [2]. This improvement consists in defining the GTM Regions of Interest (ROI), for the extraction of the segmented region mean TACs, through a selection of voxels in the segmented region, rather than using all its voxels. For this selection, the voxels are ordered (i) by decreasing Region Spread Function, result of one step of the GTM process, and by (ii) increasing Local Variance, result of one step of the LMA segmentation process, using the PROMETHEE [3] information fusion method. The GTM ROIs were then defined using the $p\%$ (here $p=20\%$) best ranked voxels of the region voxels, and the GTM correction was performed. Our method, called LMA-GTM p was compared to the LMA segmentation followed by either the mean computation or by GTM, in terms of error (e) expressed as percentage of the true value.

Results: For phantom simulations, our LMA-GTM p correction (mean $e=4.8\%$) method performed much better on phantom images than the GTM method (mean $e=14.8\%$), enhancing considerably (mean $e=26.9\%$ without correction) the TAC despite physiological movements and segmentation errors. For the experimental datasets, similar results were obtained: LMA-GTM p (mean $e=3.2\%$) outperformed GTM (mean $e=9.7\%$) and the mean computation (mean $e=12\%$).

Conclusions: Combining the LMA segmentation method with the proposed PVE correction method allows, within few minutes (including the manual naming of the segmented regions), the robust extraction of accurate TACs using PET in rodents. These results suggest that systematic use of both LMA and LMA-GTM could efficiently enhance the quality of the information extracted during the drug development preclinical phase.

Acknowledgement/References: 1. R. Maroy et al., "Segmentation of Rodent Whole-Body Dynamic PET Images: An Unsupervised Method Based on Voxel Dynamics," *IEEE Trans. Med. Imaging*, 27(3), 2008, 342-354. 2. V. Frouin, et al., "Correction of Partial-Volume Effect for PET Striatal Imaging: Fast Implementation and Study of Robustness," *J. Nucl. Med.* vol. 43, no. 12, 2002, pp. 1715-1726. 3. J.P. Brans and P. Vincke, A preference ranking organisation method. The PROMETHEE method for MCDM, *Management Science*, 31, 1985, 647-656. 4. W. P. Segars et al., "Development of a 4D Digital Mouse Phantom for Molecular Imaging Research," *Mol. Imaging Biol.*, 6(3), 2004, pp. 149-159.



day five: friday april 20, 2012

DEVELOPMENT OF IMAGING BIOMARKERS FOR NEURODEGENERATIVE DISEASES

Ourselin, S.

University College London Centre for Medical Image Computing, London, UK

(s.ourselin@ucl.ac.uk)

Introduction: The last decade witnessed a huge interest from society into the understanding of neurodegenerative diseases such as Alzheimer's disease (AD), and the prospect of an early diagnosis. While the cure for AD is not yet on the horizon, Phase III clinical trials are emerging testing potential new drugs.

Methods: Some of the Trial outcomes are judged based on longitudinal analysis of the brain changes, measured from diagnostic images such as magnetic resonance images (MRI) and positron emission tomography (PET). In our current research program between the Centre for Medical Image Computing (CMIC) and the Dementia Research Centre (DRC), we are aiming at developing novel imaging biomarkers to support such trials.

Results: A panel of biomarkers are currently under development, extracting from MRI and PET diverse anatomical and molecular information, such as the rate of brain atrophy, hippocampal atrophy, the abnormal cortical thinning, or the deposition of beta amyloid plaques.

Conclusions: In this talk, we will present current and future imaging biomarkers under development, which could potentially lead to an early diagnosis of neurodegenerative diseases such as AD.

Acknowledgement/References: This work was undertaken at UCLH/UCL with funding from the Department of Health's National Institute of Health Research Centres funding scheme, EPSRC, MRC, and Alzheimer's Research UK. The Dementia Research Centre is an Alzheimer's Research UK Co-ordinating Centre and has also received equipment funded by the Alzheimer's Research UK.

CALIBRATED BOLD FMRI AND MEASURING OXYGEN METABOLISM

Bulte, D.

University of Oxford FMRI Centre, John Radcliffe Hospital, Oxford, UK

(bulte@fmrib.ox.ac.uk)

Introduction: BOLD FMRI is the number one imaging technique for brain imaging research. One of the key reasons it has not been widely adopted into clinical settings is the difficulty in using the images diagnostically. The activation maps are very difficult to interpret in terms of physiology or pathology because the BOLD signal change is an amalgam of several distinct physiological parameters. Several methods to calibrate BOLD FMRI have been developed. These try to separate vascular and metabolic contributions to the signal changes. The calibration techniques attempt to alter individual elements of the BOLD signal in isolation, combined with simultaneous perfusion imaging using arterial spin labelling (ASL). Recently, imaging methods have been developed that use mathematical models linking resting physiology to MRI signals. These models enable the production of quantitative images of cerebrovascular physiology.

Methods: MRI scanning sequences that combine traditional BOLD imaging with ASL, either by interleaving or with a dual echo, can be used to obtain images during a functional task or stimulus. If a respiratory challenge such as hypercapnia¹ or hyperoxia² is added to the paradigm, the resultant data can be used in mathematical models of the BOLD signal change to calculate changes in cerebral blood flow, and cerebral rate of oxygen metabolism during the functional activation. Respiratory gas challenges can also be used to measure cerebral blood volume³ and cerebrovascular reactivity. If the ASL sequence used employs multiple inversion times, then it is also possible to obtain quantitative measures of cerebral blood flow and arterial arrival times. Newly developed techniques combine both hyperoxia and hypercapnia during advanced ASL sequences to produce quantitative images of all of these parameters at rest, including oxygen extraction fraction⁴. The end-tidal levels of both carbon dioxide and oxygen need to be measured. The calibration methods require ~10 minutes of extra scanning on top of the functional experiment. Full measurement of cerebral physiology requires a separate 18-minute scan.

Results: Calibrated BOLD imaging is useful for disentangling vascular and metabolic effects, and so is particularly valuable in longitudinal treatment, recovery, development and learning studies. They also provide more physiological information, which is useful for clinical and diagnostic applications. Quantitative physiological imaging enables the production of clinical information previously only available from oxygen-15 PET.

Conclusions: Newly developed, sophisticated MRI pulse sequences based on ASL can provide substantially more information about brain functional brain. Combining these sequences with respiratory gas challenges and mathematical models of the BOLD signal can produce a multitude of quantitative physiological information about the brain.

Acknowledgement/References: Funding: EPSRC UK. 1. Davis TL, et al. Proc Natl Acad Sci U S A. 1998;95:1834-1839 2. Chiarelli PA, et al. A calibration method for quantitative bold fmri based on hyperoxia. Neuroimage. 2007;37:808-820 3. Bulte DP, et al. Measurement of cerebral blood volume in humans using hyperoxic mri contrast. J Magn Reson Imaging. 2007;26:894-899 4. Bulte DP, et al. Quantitative measurement of cerebral physiology using respiratory-calibrated mri. Neuroimage. 2012;60:582-591

AUTOMATIC SPECTRAL CLUSTERING FOR SEGMENTATION OF DYNAMIC PET IMAGES

Zbib, H.¹, Mouysset, S.², Stute, S.³, Girault, J. - M.¹, Charara, J.⁴, Chalon, S.¹, Galineau, L.¹, Buvat, I.⁵, Tauber, C.¹

¹UMRS INSERM U930 - Université de Tours Hôpital Bretonneau, France ; ²CNRS UMR 5055 - Université de Toulouse, France; ³CEA, Service Hospitalier Frédéric Joliot, France; ⁴Lebanese University, Lebanon; ⁵IMNC, Universités Paris 7 & Paris 11, Orsay, France (hiba.zbib@etu.univ-tours.fr)

Introduction: The definition of regions of interest is often required for quantification of dynamic PET images. While clustering methods can identify functional regions, they are generally either sensitive to initialization, favoring convex-shaped clusters, or requiring manual setting of parameters. To address these limitations, we propose an Automatic Spectral Clustering (ASC) that yields deterministic segmentation of dynamic PET images with arbitrary shaped clusters. We tailor an unsupervised criterion and use it to automatically estimate the scale parameter involved in ASC.

Methods: In ASC, a fully connected graph is used as a high-dimensional representation of the data. Affinity between voxels is based on their time activity curves (TAC), accounting for the duration and number of events of each frame. The dominant eigenvectors of the kernel matrix span a lower dimensional space wherein data are clustered with global k-means (GKM) to avoid any random step in the method. The scale parameter of the affinity measure is chosen using a two stage hierarchical subdivision, so as to maximize an unsupervised normalized minimal distance (NMD). NMD is the ratio of the minimal inter-cluster distance that decreases when voxels representing similar time courses are assigned to different clusters, over the average of maximal intra-cluster distances, which increases when voxels with distinct kinetics are grouped into the same cluster. We performed GATE Monte Carlo simulations of Gemini GXL PET 4D acquisitions. The Zubal brain phantom was used with TAC based on a 3-compartment model. Two PET images were reconstructed with 2.2×2.2×2.8 mm³ voxels and 20 frames of 1 minute each, using fully 3D OSEM (5 iterations, 8 subsets). Two supervised criteria were calculated: Pratt's figure of merit (PFOM) measuring identification of edges and Adjusted Rand Index (ARI) measuring quality of clustering. For ten 2D+t slices of each image we manually determined the maximal ARI (ARI_{max}) and PFOM (PFOM_{max}) scores that could be obtained with the proposed spectral clustering method without using the automatic scale parameter. ASC results were compared to these maximal scores and to those obtained by a GKM approach [Likas *et al* 2003].

Results: ASC significantly improved the segmentation results compared to GKM. The ARI scores averaged over the 20 2D+t studied slices were respectively 0.73±0.10 with ASC and 0.54±0.23 with GKM, while the average ARI_{max} score was 0.79±0.05. In average, the ARI score obtained with ASC was 96%±3.2 of the ARI_{max} score for the same slice, indicating accurate estimation of the scale parameter, while it was 70%±27 with GKM. The average PFOM scores were respectively 0.75±0.08 with ASC and 0.48±0.19 with GKM, while the average PFOM_{max} score was 0.80±0.05. In average, the PFOM score obtained with ASC was 94%±7.0 of the PFOM_{max} score while it was 61%±25 with GKM.

Conclusions: In these simulations, ASC objectively and automatically identified functional regions without anatomical prior or knowledge on the kinetic model.

Acknowledgement/References: Likas A *et al*. The global k-means clustering algorithm. *Pattern Recognition* 36 (2003) 451-461

CONTRAST-ENHANCED 3-D ULTRASOUND SKELETONIZATION FOR THE QUANTITATIVE IMAGING OF TUMOR VASCULAR PATTERN

Molinari, F.¹, Meiburger, K. M.¹, Giustetto, P.^{2,3}, Boffa, C.^{2,3}, Terreno, E.^{2,3}, Castano, M.⁴

¹Politecnico di Torino Dep. of Electronics & Telecommunications, Italy; ²Univ. of Torino Dep. of Chemistry, Italy; ³Mol. & Preclin. Imaging Center, Torino, Italy; ⁴Bracco Research Center, Italy (filippo.molinari@polito.it)

Introduction: Contrast-enhanced ultrasound imaging (CEUS) can be used to assess in-vivo the vascularization of tumors. Perfusion studies only provide information about the overall blood uptake of the tumor, but the accurate reconstruction of the vascular pattern could be required in follow-up therapeutic protocols. The aim of this work was to develop an image processing procedure for the 3-D characterization and reconstruction of the tumor vascular pattern.

Methods: We used C57Bl6 mouse models (10 weeks old, weight 23 ± 4 gr). Singeneic tumor cells (melanoma B16) were subcutaneously grafted in the rear paw's thigh. We used a VisualSonics VEVO2100 equipped with a 24-MHz probe. Traditional high-resolution US images were acquired, along with 3-D CEUS images of the tumor. CEUS images were acquired after the injection of 50 ml of non-targeted Vevo MicroMarker (Bracco, Geneva) optimized for use on the Visualsonics High-Resolution Micro-Ultrasound System. The bolus of contrast agent was followed by the injection of 40 ml of saline solution. The 3-D CEUS images were first intensity normalized and low-pass filtered, then we segmented the bright microbubbles by using Otsu's thresholding. The obtained mask was reduced by a combination of distance transform and morphological skeletons. This operation reduced the blooming due to the contrast agent interaction with ultrasounds while maintaining the correctness of the spatial distribution of the vascular tree. Once skeletonized, the resulting 3-D representation was analyzed in order to extract 7 descriptors of the vascular pattern: number of vascular trees, number of branches, vessel radius, vascular density, 2-D tortuosity, 3-D tortuosity, number of vascular flexes.

Results: Our procedure allowed for the 3-D representation of the tumor vascularization. Unlike other proprietary CEUS-based algorithms, our technique preserved the tridimensional vessel connectivity, thus improving the overall quality of the reconstruction. Preserving connectivity also avoided biases in the quantification of the vascular parameters. In repeated controls on mice models (3 to 7 days), we measured an increase of the vascular density and of the number of vascular trees of about 10%.

Conclusions: CEUS 3-D skeletonization allows the visualization and numerical characterization of tumor vascular patterns. This technique could be useful in follow-up studies or in evaluating the effect of anti-tumoral procedures/drugs.

Acknowledgement/References: [1] Molinari F, Mantovani A, Deandrea M, Limone P, Garberoglio R, Suri JS. Characterization of single thyroid nodules by contrast-enhanced 3-D ultrasound. *Ultrasound Med Biol.* 2010;36:1616-25.

WHEN ELECTROPHYSIOLOGY MEETS NEUROIMAGING: MAGNETOENCEPHALOGRAPHY.

Mattout, J.

INSERM U1028 - CNRS UMR5292; Lyon Neuroscience Research Center, Lyon, France

(jeremie.mattoutinserm.fr)

Magnetoencephalography (MEG) is a recent non-invasive technique that enables the observation of brain activity in humans, *in vivo*. Importantly, it benefits from the very high temporal resolution of electrophysiology and offers at the same time a much higher spatial precision than Electroencephalography (EEG). In the last decade, MEG has grown mature. Great advances have been achieved in terms of methods to extract fine information out of those signals, in the temporal, spatial and frequency domains. Outstanding results have been obtained in cognitive neuroscience using MEG. Finally, MEG has been used in clinical research, to shed light onto many different pathological brain processes. In particular, MEG has begun to be used routinely as part of the surgical planning of severe epilepsies. In this talk, I will briefly introduce the MEG technique and its short history. I will try to propose a comprehensive coverage of the main aspects and latest advances in the methods used to analyze MEG data. Finally, I will illustrate the current and possible future usefulness of MEG with emblematic examples borrowed from both basic and clinical research studies.

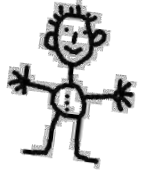
the EMIM 2012 will take place in the scope of the WMIC in
Dublin 5-8 Sep. '12
abstract submitted?
deadline 17 April

ESMI PhD Award - interested?

WWW.E-SMI.EU



My Notes

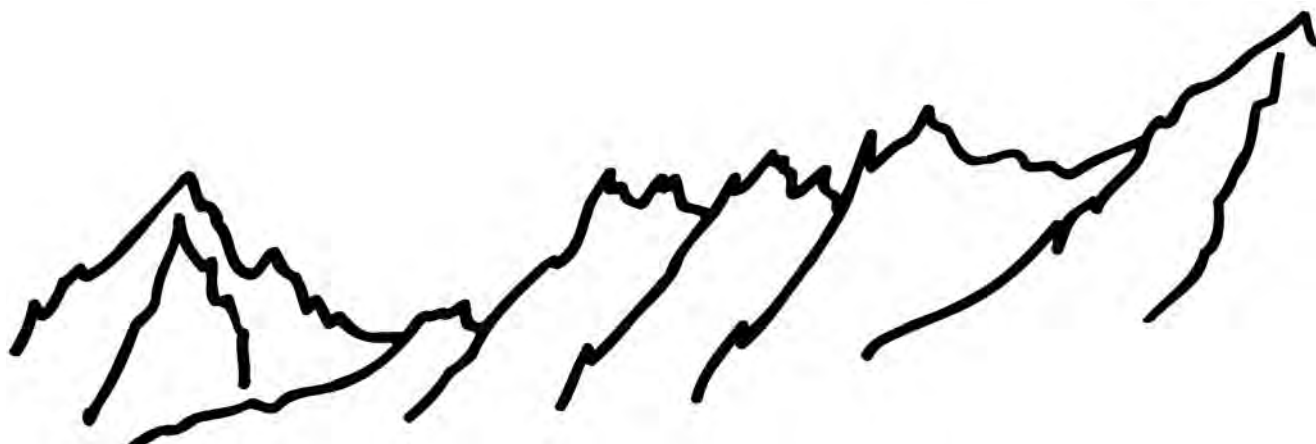


Quantitative Image Analysis and Application Specific Imaging

- PRIMA IV in Dublin Sep. 10-14 right after the WMIC 2012

WWW.PRIMA-CURRICULUM.EU

POSTER



poster #1

INTEGRATED VISUALIZATION OF MULTI-MODAL MULTI-TIMEPOINT SMALL ANIMAL IMAGING DATA WITH THE CVPKok, P.^{1,2}, Dijkstra, J.², Lelieveldt, B.^{2,1}, Botha, C. P.^{1,2}¹Delft University of Technology Intelligent Systems, Delft, Netherlands; ²Leiden University Medical Center Radiology, Netherlands

(P.Kok@tudelft.nl)

Introduction: The use of appropriate visualization techniques is essential for properly exploring and understanding of imaging data. In small-animal imaging, research frequently involves multiple, heterogeneous imaging modalities being applied in longitudinal studies. Although scanners are usually equipped with software for image processing and visualization, the possibilities for combining data across modalities and over time are often limited. We have developed a toolkit that integrates techniques for the registration and visualization of multi-modality multi-timepoint data, and is specifically aimed at small-animal imaging.

Methods: We implemented a system as an extension to the Cyttron Visualization Platform [1], which is a visualization framework aimed at the integration and visualization of multi-scale, multi-timepoint data. It mainly uses the VTK libraries [2] for processing and visualization. Our small-animal extension features the following highlights:

For multi-angle BLI/FLI-image acquisition: a carousel visualization, including semi-automatic registration to 3D structural modalities. (CT/MRI) [3]

Employing an articulated hierarchical registration approach, we can automatically select and visualize volumes of interest corresponding to the main bones. We named this Articulated Planar Reformation (APR) [4]. When applied to multi-timepoint, multi-subject or multi-modality data, progression or differences can be studied using synchronized side-by-side or overlay visualizations.

Combining the above APR method with the Super Resolution Reconstruction (SRR) algorithm described in [5], we are able to rapidly apply SRR to a volume of interest. Acquiring low-resolution whole-body MR images, and subsequently limiting the reconstruction to smaller subvolumes of interest drastically reduces the time required for scanning and processing.

We implemented a method for semi-automatic 2D-3D landmark-based registration to enable registration of 2D BLI/FLI-images to a 3D image of a structural modality. After this, we can easily create a combined visualization, for instance a signal overlay on CT-data.

Results: Our system has been evaluated by a number of experts in, among others, case evaluation studies [4] and is currently in active use in support of several running small animal imaging studies. Feedback of the evaluations was positive and showed that the software can indeed be effectively applied in small-animal research.

Conclusions: We have developed an extension to an existing visualization platform that enables the flexible exploration and study of small-animal imaging data through a number of integrated processing and visualization tools. Enabling the combined visualization of multi-modality and multi-timepoint data leads to magnified insight and understanding of the data.

Acknowledgement/References: 1. Kallergi A, et al, "Cyttron: A virtualized microscope supporting image integration and knowledge discovery", Cell Death and Disease Series: Proteins Killing Tumour Cells, ResearchSignPost, 2009; 2. Visualization Toolkit, <http://www.vtk.org>; 3. Kok P, et al, "Integrated visualization of multi-angle bioluminescence imaging and micro CT", Proceedings of SPIE, Vol 6509, 2007; 4. Kok P, et al, "Articulated planar reformation for change visualization in small animal imaging", IEEE transactions on visualization and computer graphics, 2010; 5. Poot DHJ, et al, "General and efficient super-resolution method for multi-slice MRI", MICCAI, 2010

poster #2

AUTOMATED CELL QUANTIFICATION IN MRI WITH A CRYOPROBE: FEASIBILITY IN AN VITRO STUDYBalvay, D.^{1,2}, Kolosnjaj-Tabi, J.^{1,3}, Autret, G.^{1,2}, Alfaraj, A.^{3,1}, Gazeau, F.³, Wilhelm, C.³, Clément, O.^{1,2}¹INSERM - Université Paris Descartes, France; ²Plate Forme d'Imagerie du Petit Animal, Université Paris Descartes, Sorbonne, France; ³CNRS - Université Denis Diderot UMR 7057, Paris, France

(daniel.balvay@inserm.fr)

Introduction: Cell quantification is an unsolved issue in MR imaging. Indeed, iron-labeled cells are visible as signal losses in images, which depends on the amount of cells but also the amount of their internalized iron and on the MRI sequence sensitivity. By using a cryoprobe, labeled cells are visible as new patterns: focused and saturated black holes. Theoretically, saturation should allow a more specific quantification of number of cells. The aim of this preliminary work was to demonstrate in tubes the feasibility of an automated cell quantification.

Methods: Cell labeling was performed by incubating a suspension of anionic magnetic nanoparticles and cells were suspended in agarose. MRI sequence was a FISP-FID 3D with the following parameters: TR/TE = 20/5 ms, $\alpha = 25^\circ$, FOV 1.5x1.5x0.65 cm, spatial resolution 50x50x50 μm . The steps for quantification were as follows: 1) suppression of air around the liquid portion, by automated thresholding performed on a smoothed MRI volume. 2) Identification of dark patterns in tubes, by an automated gray thresholding processed on the difference between original and smoothed volumes. 3) Calibration of corresponding objects by size analysis. It resulted in a histogram of black objects sorted by size. Finally the software provided a number of detected objects, the total corresponding volume (in pixels) to take into account possible aggregation of cells, and tools for visual control: a synthetic image showing air, tube and cell objects in 3D view, in arbitrary colors and a multi 2D navigator interface showing fusion between original volume and cell-objects. We evaluated the sensitivity to intracellular iron concentration with a first set of tubes, corresponding to different duration of cell incubation. Also, we evaluated the relation between quantification of black-hole objects and original amounts of cells in tubes, for zero, 10000 and 20000 cells in tubes.

Results: The count of black-objects, for various times of incubation, (10000 cells; 2h,3h,3h) gave 273/280/293, indicating a low sensitivity of the automated counting to iron labeling. Conversely, the second test indicated a linear relationship between cell counting and amount of cells in tubes, both by counting number of cell-objects ($R^2=98.9$) and corresponding volume ($R^2=99.0$). Mean time for cell counting and control imaging was around 30 s per tube (300x300x100 pixels).

Conclusions: We demonstrated that it was possible to quantify automatically the amount of iron labeled cells in vitro using a cryoprobe. This preliminary study, in a small population, showed a linear relationship between quantification and amount of cells. These results have to be confirmed in a more extensive study. It indicated that it should be possible to count marked cells in vivo, if black hole patterns of cells can be separated from other black patterns in tissues.

Acknowledgement/References: the European Commission FP7 Health Encite for supporting this work.

poster #3

SPM FOR ACTIVATION STUDIES IN RATS ON STRESS CONDITIONS

Gallivanone, F.¹, Di Grigoli, G.², Salvatore, C.³, Valtorta, S.², Grosso, E.⁴, Gilardi, M. C.^{1,5}, Moresco, R. M.³, Castiglioni, I.¹

¹IBFM - CNR, Milan, Italy ; ²Tecnomed Foundation, University of Milan, Italy ; ³University of Milan-Bicocca, Italy ; ⁴LATO HSR Giglio, Milan, Italy ; ⁵Scientific Institute H. San Raffaele, Milan, Italy
(gallivanone.francesca@hsr.it)

Introduction: SPM has been widely used for the operator independent assessment of functional and molecular differences in human PET or MRI brain images using between group or condition paradigms. Despite the large diffusion of dedicated images system and protocols, its preclinical use have been described in a limited number of studies, particularly for PET. Aim of this work was to assess the feasibility of the SPM methodology for the identification of patterns of altered metabolism in the rats brain using PET ¹⁸F-FDG and an acute stress stimulus based on Foot-shock (FS) paradigm.

Methods: 16 male CD rats, randomly assigned into two groups (8 rats for control group and 8 rats for stressed group), were injected with ¹⁸F-FDG in a lateral tail vein. Following the FS protocol, the group of stressed animals was exposed, just after radiotracer injection, to a 50 minutes of shock session. Both control and stressed rats were acquired for 30 minutes, 1 hour after injection. A statistical SPM based model was adapted to rodents brain in order to evaluate patterns of hyper-metabolism and hypo-metabolism involving brain areas, comparing the control rats with respect to the stressed rats.

Results: A specific SPM design model was evaluated and designed for the analysis of rat PET images. A rat template was created using a control rat, outside of the two groups, who performed both PET and MRI study. The PET study for this rat, co-registered to his MRI, was used as ¹⁸F-FDG template. Both control and stressed rat brains were normalized to the rat template. Normalized images were smoothed with an isotropic Gaussian kernel (2 mm FWHM). A compare-populations model (1 scan/subject, two sample t-test) was used to evaluate statistical differences between control and stressed rats. A value of 28 mol/100 g/min cerebral glucose utilization in whole rat brain [1] was used for global normalization. The statistical threshold was set at $p = 0.05$ with an extent threshold of 100 contiguous voxels. T-value maps of statistical significant SPM blobs were superimposed on the MRI template. The signal of SPM analysis showed a relative reduction of regional brain metabolism at the level of thalamus, hypothalamus, entorhinal and piriform cortex, in hippocampus and cerebellum, while motor cortex and somatosensory cortex resulted in a relative increase of the signal. The patterns of altered metabolism was found compatible with areas involved in stress conditions.

Conclusions: We adapted SPM for the voxel-based assessment of changes in glucose metabolism during an acute stress paradigm. Correlation analysis between brain function and stress markers (blood glucose or cortisol) are under evaluation.

Acknowledgement/References: [1] Shimoji K et al., Measurement of cerebral glucose metabolic rates in the anesthetized rat by dynamic scanning with ¹⁸F-FDG, the ATLAS small animal PET scanner, and arterial blood sampling, J Nucl Med. 2004; 45(4):665-72. The study was in collaboration with Dr. S. Corna and Prof. G. Racagni (Pharmacology Department - University of Milan) and with Dr. L.S. Politi (MRI studies – San Raffaele Institute) and supported by the Young Research Project of the Minister of Health.

poster #4

COMPARISON OF DISPLACEMENT FIELDS AND SPLINE TRANSFORMATIONS FOR MASS-PRESERVING MOTION CORRECTION OF PET

Gigengack, F.^{1,2}, Ruthotto, L.³, Burger, M.⁴, Wolters, C. H.⁵, Jiang, X.², Schäfers, K.¹

¹EIMI, WWU Münster, Germany; ²WWU Münster Dep of Mathematics & Computer Science, Germany; ³Institute for Computational and Applied Mathematics, Germany; ⁴Institute for Biomagnetism and Biosignalanalysis, Germany ⁵Univ of Lübeck Institute of Mathematics and Image Computing (MIC), Germany; (fabian.gigengack@uni-muenster.de)

Introduction: In Positron Emission Tomography (PET), motion due to the cardiac and respiratory cycle causes blurred images. In this context, we proposed the incorporation of prior knowledge (preservation of mass) into the registration process with the Variational Algorithm for Mass-Preserving Image REgistration (VAMPIRE) [1]. Given our Mass-Preserving (MP) transformation model, we evaluate in this work different motion models: dense displacement field (compute for each voxel an individual displacement) vs. spline transformation (i.e. free-form deformation). Based on the ground-truth motion vectors, provided by the established XCAT software phantom, we make a quantitative comparison of the motion estimates of the different motion models.

Methods: Two realistic (simulation of Poisson noise and the PVE) PET images with varying cardiac and respiratory phase are generated with the XCAT software phantom: one template image, showing the systolic heart phase at maximum inspiration, and a reference image in the diastolic heart phase at mid-expiration. In our MP transformation model VAMPIRE, the template image is transformed by interpolation on the deformed grid y with an additional multiplication by the volumetric change. The implementation is based on the FAIR registration toolbox (see [1]). For the Displacement Field (DF) registration we performed a parameter search for the hyperelastic regularizer parameters by minimizing the error measure $e(y, y_{GT}) := 1/|\Omega| \int_{\Omega} |y(x) - y_{GT}(x)| dx$, where y_{GT} is the ground-truth transformation (provided by XCAT) and Ω the field of view. For the Spline Transformation (ST) we varied the regularization between hyperelastic and the internal FAIR regularization for splines (penalizing the norm of the coefficients). In addition, the optimal number of spline coefficients was part of the optimization.

Results: For both motion models (DF and ST) the registration results are evaluated by 1) the total processing time and 2) the error measure $e(y, y_{GT})$. For the DF an accuracy of 1.96mm could be achieved. The VAMPIRE algorithm terminated after 326 seconds. For ST we found an optimal spacing for the spline coefficients of 3.375cm. Hence, we present only results for this spacing in the following. The accuracy for hyperelastic regularization is 1.47mm with a processing time of 79 seconds. With the internal FAIR regularization we could achieve an accuracy of 1.59mm with a processing time of 28 seconds.

Conclusions: Comparing the different regularization methods for ST, the processing time of hyperelastic regularization (79 seconds) is longer compared to internal FAIR regularization (28 seconds) with comparable accuracies. Hence, the internal FAIR regularization should be given preference. Comparing the ST results with the DF results reveals that the spline transformation model is superior to the displacement field strategy in terms of processing time (ST: 28 seconds vs. DF: 326 seconds) and accuracy (ST: 1.59mm vs. DF: 1.96mm). Note that all results represent a subvoxel accuracy, given a voxel size of 3.375mm.

Acknowledgement/References: [1] <http://vampire.uni-muenster.de>

A VARIATIONAL FRAMEWORK FOR REGION-BASED SEGMENTATION INCORPORATING PHYSICAL NOISE MODELS

Sawatzky, A.¹, Tenbrinck, D.², Jiang, X.², Burger, M.¹

¹University of Münster Institute for Computational and Applied Mathematics, Germany ; ²University of Münster Department of Computer Science, Germany (alex.sawatzky@wwu.de)

Introduction: This work describes a region-based segmentation framework which is able to incorporate different physical noise models, in particular non-Gaussian ones. Motivated by applications in biomedical imaging, the cases of Poisson and multiplicative speckle noise are discussed, occurring e.g. in positron emission tomography (PET) and medical ultrasound (US) imaging, respectively. Different regularization functionals are investigated in order to provide a-priori knowledge regarding the expected solution. The performance of the framework is illustrated by experimental results on synthetic and real data from PET and medical US imaging.

Methods: A Bayesian modeling approach via maximum a-posteriori probability estimation is used to compute the partition of the image domain and an approximation of the original noise free image. The resulting region-based segmentation framework is able to handle the information (i.e. the occurring type of noise and the desired smoothness conditions) in each subregion of the image domain, separately. The Fisher information [1] as regularization functional (incorporating a-priori knowledge) is investigated, in particular with respect to the desired functions representing densities or intensity information which occur typically in applications with data corrupted by Poisson or multiplicative speckle noise. The Fisher information seems to be more appropriate for density functions than the squared H^1 -seminorm, which is usually used in the segmentation community (e.g. in the popular Mumford-Shah model [2]). Using a two-phase formulation of the segmentation framework and an alternating minimization scheme (similar to the Chan-Vese model [3]), efficient numerical schemes are proposed in the cases of Poisson and multiplicative speckle noise models. The segmentation step in the minimization scheme is solved using globally convex segmentation models [4] in order to avoid the deficiencies (e.g. existence of local minima) of active contour models such as snakes and level set methods.

Results: Different experimental settings on synthetic data illustrate the importance of a correct chosen physical noise model for the accuracy of segmentation results. The impact of the Fisher information and the squared H^1 -seminorm regularization functional on a synthetic density image is investigated. The performance of the proposed segmentation framework is illustrated on real data from cardiac $H_2^{15}O$ PET measurements and blood vessel data in medical US imaging.

Conclusions: The proposed region-based variational segmentation approach provides a flexible basic framework for biomedical real life applications incorporating different physical noise models. In particular, different noise models and smoothing functionals can be chosen in each subregion, in case subregions of different characteristics are expected. Compared with the popular Mumford-Shah and Chan-Vese model, the proposed framework describes a direct generalization of these segmentation models to non-Gaussian noise problems.

Acknowledgement/References: This study has been supported by the German Research Foundation DFG, SFB 656 MoBiI (project B2, B3, C3). [1] C. Villani, Topics in Optimal Transportation, 2003. [2] D. Mumford and J. Shah, Optimal approximations by piecewise smooth functions and associated variational problems, 1989. [3] T. F. Chan and L. A. Vese, Active contours without edges, 2001. [4] T. F. Chan et al., Algorithms for finding global minimizers of image segmentation and denoising models, 2006.

REAL-TIME CONSTRAINED SPECTRAL UNMIXING

van de Giessen, M.^{1,2}, Dijkstra, J.¹, Lelieveldt, B.^{1,2}

¹Leiden University Medical Center Division of Image Processing, Leiden, Netherlands; ²Delft University of Technology Department of Intelligent Systems, Delft, Netherlands

(m.vandegiessen@lumc.nl)

Introduction: Multispectral imaging enables the separation of signals coming from different (fluorescent) sources through spectral unmixing. In a clinical setting, tumor visualization using fluorescence has proven to be of great help during surgical procedures, but mainly using a single near-infrared channel due to technical constraints, one of them being real-time spectral unmixing of the acquired spectra that is robust to varying lighting conditions. Unconstrained spectral unmixing as in [1] can lead to false positive identification of probes under varying light conditions. In [2] it was proposed to constrain the unmixed signals to be nonnegative, thereby suppressing these false positives, but the proposed algorithm was not applicable in a real-time setting. In this abstract we present an algorithm that enables real-time unmixing including nonnegativity constraints.

Methods: Similar to [2] we constrain the linear unmixing problem with non-negativity constraints (i.e. light intensities are not permitted). However, to solve this problem we adapt the Active Set algorithm, which takes a finite number of steps to the global optimum. Hereby we use that the mixing matrix only contains nonnegative elements and that therefore constraints only need to be applied directly to the unmixed values themselves. The implementation also makes use of the fact that unmixing of each pixel in the multispectral image can be processed in parallel. The effectiveness of the non-negative constrained unmixing was validated using multispectral data of AF680, AF750 and QD800 imaged with the Maestro camera. From the 22 wavelengths imaged by the Maestro camera, 3 wavelengths were selected manually, to mimic a real intraoperative system. Before unmixing, the system was calibrated by imaging the used probes outside of tissue.

Results: Simulations showed that especially for low signal to noise ratios (SNR) the constrained unmixing performed much better. SNR ~10: unconstrained error 9.9%, constrained error 9.6% of signal values. SNR ~4: unconstrained error 33%, constrained error 28%. In real measurements constraints were active for on average 27% of the foreground pixels, showing their necessity. The times needed for spectral unmixing were measured on a computer with an Intel Xeon 4 core CPU at 2.67 GHz using images with a resolution of 640x480. The computation times were 2.4 ms per frame (parallelized) and 9.2 ms per frame (non parallelized). For our intra-operative camera in development, this comes down to 416 frames/s, much faster than the acquisition rate of 30 frames/s.

Conclusions: Under varying lighting conditions and in the presence of unknown signals, e.g. tissue auto-fluorescence, non-negativity constraints help to suppress false positive signals. The algorithm that is implemented in this work allows for real-time spectral unmixing with frame-rates up to 416 frames/second. Therefore the pure unmixing time can be considered negligible and the unmixing can be added easily in intra-operative multi-spectral camera systems.

Acknowledgement/References: This research was supported by the Center for Translational Molecular Medicine (MUSiS). [1] G. Themelis, et al. Real-time intraoperative fluorescence imaging system using light-absorption correction. J Biomed Opt, 14(6):064012, 2009. [2] H. Xu and B. W. Rice. In-vivo fluorescence imaging with a multivariate curve resolution spectral unmixing technique. J Biomed Opt, 14(6):064011, 2009.

poster #8

MRI – ASSISTED FMT OF GLIOMA GROWTH

Arranz, A.^{1,2}, Zacharopoulos, A.³, Grandjean, J.¹, Rudin, M.^{1,2}, Ripoll, J.^{3,1}

¹ETH Zurich Institute for Biomedical Engineering, Zurich, Switzerland; ²University of Zurich Institute of Pharmacology and Toxicology, Zurich, Switzerland; ³Foundation for Research and Technology-Hellas (FORTH) Heraklion, Greece

(arranz@biomed.ee.ethz.ch)

Introduction: Methods for the in vivo follow-up of tumor progression represent a useful tool in the study of tumor biology and an essential element in the analysis of new potential therapeutic approaches. Fluorescent molecular tomography (FMT) is a simple-to-use and cost-effective technology that has been applied to the analysis of tumor vascularity and several tumor-associated enzymatic activities (1). A main drawback of FMT, however, is the lack of anatomical information. This hurdle is primarily overcome with the combination of FMT with other imaging technologies such as X-ray-CT (X-CT) (2) or MRI (3).

Methods: GL261 glioma cells were transfected with a TurboFP635-expressing vector (Evrogen). Single-cell clones were obtained and one was chosen for its high fluorescent intensity (high levels of TurboFP635 expression). 2x10⁵ cells of this clone were implanted in the right frontal lobe of 7 weeks old female Balb/c nude mice. Tumor growth was followed up over the time using an FMT setup adapted specifically for brain imaging. After each FMT measurement, an Gd-enhanced MRI was taken in order to assess the accuracy of the method in retrieving the size and position of the glioma.

Results: The reconstructed FMT can be accurately combined with an anatomical reference provided by MRI. In this first implementation only the surface of the mouse is taken into consideration and no additional priors have been used. However, comparison of the results for glioma growth with the corresponding MRI data show very good agreement.

Conclusions: FMT reconstructions obtained with surface information show very good comparison with MRI data measured on the same mouse. Future work consists on including anatomical priors in the FMT reconstruction.

Acknowledgement/References: E.U. FP7 Collaborative Project “FMT-XCT”. AA acknowledges support from a Marie Curie Fellowship (FP7-PEOPLE-2010-IEF). (1) Ntziachristos, V., C. H. Tung, et al. (2002), *Nat Med* 8(7): 757-60. (2) Hyde, D. et al (2009), *Neuroimage* 44(4): 1304-1311. (3) Stuker, F. et al (2011) *IEEE Trans Med Imaging* 30(6):1265-73.

poster #9

SEGMENTATION OF WHOLE-BODY MICROPECT MOUSE DATA

Khmelninskii, A.¹, Groen, H.², de Jong, M.², Lelieveldt, B.^{1,3}

¹LUMC Dept. of Radiology, Leiden, Netherlands; ²ErasmusMC Dept. of Nuclear Medicine, Rotterdam, Netherlands; ³Delft University Dept. of Intelligent Systems, Delft, Netherlands

(H.C.Groen@ErasmusMC.nl)

Introduction: Whole-body SPECT/CT small animal imaging is widely used in pre-clinical research. Comparing and exploring whole-body datasets can be a difficult and time-consuming task due to the inherent heterogeneity of the data. The goal of this study is to provide a method to align and compare side-by-side multiple whole-body SPECT datasets in a common reference, eliminating any postural and positioning variability that exists between the subjects in cross-sectional and follow-up studies.

Methods: The first step of the proposed approach is to extract the skeleton from the SPECT data. Subsequently, the articulated MOBY mouse atlas [1] is registered to the data following a hierarchical anatomical tree: first, the atlas is coarsely registered to the entire skeleton. Then, starting with the skull, each atlas bone is accurately registered to the correspondent bone in the data using the Iterative Closest Point approach. After the atlas is registered to the data, we apply the APR algorithm [2] to reformat the segmented data into segments corresponding to a mouse atlas and thus mapping the data to a standardized atlas space. The presented method is validated using 3 Balb/c mice injected with the ^{99m}Tc-HDP and 3 others injected with the ^{99m}Tc-MDP tracers which are taken up by the bones.

Results: To validate the registration accuracy quantitatively and enable comparison with the registration error achieved in μ CT data as reported in [2], we used the same error metric to quantitatively evaluate the SPECT segmentation: the Euclidean point to surface distance. For each SPECT dataset, we calculated this distance between the registered atlas skeleton and the correspondent co-registered CT skeleton, before and after articulated registration. The obtained results indicate that after registration, the mean Euclidean distance decreased from 11.5 ± 12.1 to 2.6 ± 2.1 voxels and is of the same order as the previously published results for μ CT, 1.8 ± 0.1 voxels [2]. The entire articulated registration process was implemented in MATLAB R2008b™ and took approximately 2 minutes of run-time on a standard desktop PC. Applying the APR algorithm to multi-modal cross-sectional data proved to be useful to provide proper referencing and visualization for an intuitive exploration and comparison of μ CT, SPECT data.

Conclusions: An articulated atlas-base skeleton segmentation method for SPECT whole-body small animal data was presented. The evaluation of the method demonstrated it to be accurate and robust for intuitive, side-by-side, whole-body, cross-sectional, longitudinal and multi-modal data exploration. When a tracer that doesn't concentrate in the bone is used and a complementary μ CT is available the same approach holds true. In those cases, due to the robustness of the CT data, one can use the automatically segmented bones as masks for SPECT signal quantification. The approach presented here can be applied to other animals, provided an atlas.

Acknowledgement/References: [1]-Khmelninskii et al. “Articulated whole-body atlases for small animal image analysis: construction and applications”, MIB, 2011 [2]-Baiker et al. “Atlas-based whole-body segmentation of mice from low-contrast micro-CT data”, MEDIA, 2010 [3]-Kok et al. “Articulated planar reformation for change visualization in small animal imaging”, IEEE TVCG, 2010

poster #10

COMPUTER VISION TOOLS FOR THE QUANTIFICATION OF IRON OXIDE NANOPARTICLES IN THE BRAIN

Frindel, C., David, R., Marlène, W.

Université de Lyon Laboratoire CREATIS-INSa LYON, Villeurbanne, France

(carole.frindel@creatis.insa-lyon.fr)

Introduction: Linking physiological or anatomical informations at the living cell scale with information accessible at larger scales by multimodal imaging is a current hot topic in life science (see for instance correlative imaging [1]). This approach raises new applications for computer vision depending on the physical imaging systems used and the information extracted at each scale. We here present such image processing considerations for an on going biomedical research program on cerebral ischemia [2].

Methods: Synchrotron radiation micro computed tomography (μ CT) is used to produce 3D ex vivo images of mouse brains with cerebral ischemia. The spatial resolution of 8 micrometers allows to visualize iron oxide nanoparticles phagocytosed by macrophages. Magnetic Resonance Imaging (MRI) acquisition of these mouse brains has been performed in vivo at a 100 times lower resolution.

Results: We analyze the different image processing steps required to perform computer assisted counting and localization of these nanoparticles in μ CT for similarity analysis with the signal abnormalities observed in MRI. This include the 3D segmentation of the ischemic lesion. A denoising algorithm for the spatial circular noise typical of reconstruction artefacts in μ CT is introduced. A review of multiscale blob detection algorithm is then presented [3,4,5]. This is followed by a reslicing of the micro computed tomography images which are coarse grained for comparison with MRI. This quantitative comparison is based on statistical information theory metrics [6].

Conclusions: A full pipeline of state of the art computer vision tools for the counting of iron oxide nanoparticles in mouse brain is proposed. Preliminary results are presented and opened to discussion.

Acknowledgement/References: [1] J. Robinson, T. Takizawa, A. Pombo, P. Cook. Correlative fluorescence and electron microscopy on ultrathin cryosections: Bridging the resolution gap. *Journal of Histochem Cytochem* vol. 49: 803–808, 2001. [2] V. Desetret, J. C. Brisset, E. Devillard, S. Moucharrafie, S. Nataf, J. Honnorat, N. Nighoghossian, Y. Berthezène, M. Wiart, Early stage investigation of USPIO-induced signal changes after focal cerebral ischemia in mice, *Stroke*, vol. 40, pp. 1834–1841, 2009. [3] T. Lindeberg. Detecting salient blob-like image structures and their scales with a scale space primal sketch: a method for focus-of attention. *International Journal of Computer Vision*, vol. 11:283–318, 1993. [4] J. Byun, M. R. Verardo, B. Sumengen, G. P. Lewis, B. S. Manjunath and S. K. Fisher. Automated tool for the detection of cell nuclei in digital microscopic images: application to retinal images. *Molecular Vision*, 12: 949–960, 2006. [5] C. Damerval and S. Meignen. Blob detection with wavelet maxima lines. *IEEE Signal Processing Letters*, 14(1): 39–42, 2007. [6] E. Ruiz, S. Pérez, P. Bonev, B. Ivanov, *Information Theory in Computer Vision and Pattern Recognition*, 2009, Springer.

poster #11

QUALITY CONTROL OF PROSPECTIVE PHASE BASED GATING METHOD IN PETDidierlaurent, D.¹, Jaudet, C.², Dierickx, L. O.², Zerdoud, S.², Ribes, S.¹, Caselles, O.¹, Courbon, F.³¹Institut Claudius Regaud, Toulouse, France ; ²Institut Claudius Regaud Toulouse, France ; ³Médecine Toulouse Rangueil, Toulouse, France

(didierlaurent.david@claudiusregaud.fr)

Introduction: Prospective phase based gating PET/CT is one of the method to limit motion of tumors induced by breathing. Some clinical studies have shown the interest of 4D respiratory gated PET/CT by a SUVmax increase and a decrease of the BTV [1-2]. The aim of this study is to evaluate the performance of the most used gating device (RPM) to synchronize PET/CT with breathing. Then a retrospective phase based method has been implemented and used as a reference to observe quantization differences on SUVmax and BTV.

Methods: Respiratory data of 17 patients underwent a 4D PET/CT were analyzed to evaluate temporal reproducibility of triggers used for PET binning. Triggers are normally emitted at each maximal inspiratory amplitude for each breathing cycle. To assess the performance of gating device, the mean and standard deviation of delta time between trigger and maximal inspiratory amplitude was computed for each cycle. Triggers were also counted and compared to breathing cycle number for each patient. Retrospective binning method based on maximal inspiratory amplitude has been carried out. SUVmax, BTV and centroid position was assessed after prospective and retrospective reconstruction on a clinical case.

Results: Our study shows a significant loss of 15% of breathing cycles with a prospective binning and a high temporal dispersion of triggers compared to maximal inspiratory amplitude over time acquisition, depending on respiratory signal of patient. These findings suppose an inconsistency of data binning along time acquisition for the prospective gating method. On a clinical case, SUVmax has been improved by 26,5% in average after retrospective binning and was always superior to the SUVmax measured after prospective binning. BTV was smaller after retrospective binning (1,83 times smaller than after prospective method). After prospective binning, the position of tumor was clearly inconsistent to the breathing pattern and binning, with a limited amplitude motion (maximum amplitude 4 mm). A higher amplitude of motion (8,27 mm) with a high consistency to breathing pattern was observed after the retrospective binning.

Conclusions: In conclusion, this study showed inaccuracies of respiratory gating device to detect prospectively cycles and emit triggers temporally reproducible for the breathing signal of patients. These defects had an impact on image quantization of prospective respiratory phase gated exam. Quality control of 4D PET/CT is necessary and retrospective phase gated method could improve significantly 4D PET/CT image quantization.

Acknowledgement/References: 1- Nehmeh SA, Erdi, Y. E., Rosenzweig, K. E., Schoder, H., Larson, S. M., Squire, O. D., and Humm, J. L. Reduction of respiratory motion artifacts in PET imaging of lung cancer by respiratory correlated dynamic PET: methodology and comparison with respiratory gated PET. *J Nucl. Med.* 2003; 44(10):1644-1648. 2 -Garcia Vicente AM, Castrejon, A. S., Leon Martin, A. A., Garcia, B. G., Pilkington Woll, J. P., and Munoz, A. P. Value of 4-Dimensional 18F-FDG PET/CT in the Classification of Pulmonary Lesions. *J Nucl. Med Technol* 2011; 39(2):91-99.

poster #12

INFLUENCE ON THE IMAGE QUALITY BY THE AMOUNT OF OVERLAP OF THE PROJECTIONS IN HELICAL SPECT

de Swart, J., Groen, H., Konijnenberg, M., Koppe, J., de Jong, M.

Erasmus MC Nuclear Medicine, Rotterdam, Netherlands

(j.deswart@erasmusmc.nl)

Introduction: In helical SPECT the amount of overlap between the projection data plays a role in image quality, besides the time per projection and the number of projections. The aim of this study was to describe the influence of the amount of overlap in respect to spatial resolution, uniformity and quantification accuracy.

Methods: A hot rod phantom was filled with 43 MBq In-111 to measure the spatial resolution. Various SPECT acquisitions were made. Time per projection was 60 s/projection on all acquisitions, the number of projections ranged from 8 to 32 and the Quality Factor (QF, the acquisition parameter for the amount of overlap) ranged from 0.5 to 1. Smaller QF values indicate higher overlap. Uniformity and quantification accuracy were measured by making SPECT acquisitions of a 3 mL syringe which was filled with 15 MBq In-111. The syringe was put into an attenuator filled with water to mimic the attenuation of a mouse. Time per projection was 15 s/projection, the number of projections ranged from 12 to 24 and the QF ranged from 0.3 to 1. SPECT was made using a four head NanoSPECT/CT (Bioscan Inc.). Nine pinhole apertures with a pinhole diameter of 1.0 mm were used for the hot rod phantom SPECT scans, and the pinhole diameter was 1.4 mm for the SPECT scans of the syringe. All data sets were reconstructed using the OSEM algorithm. The number of iterations was nine. The resolution was determined by measuring the FWHM of the rods in the resulting images. VOI's were drawn to measure the uniformity and to quantify the images of the syringe.

Results: The spatial resolution improved by an increasing number of projections, but smaller QF values did not improve spatial resolution. Quantification accuracy was high in all SPECT images. The mean recovery was 98.1% (SD 0.4%). There was no difference in quantification accuracy at the various QF settings. Uniformity improved when the QF decreased. The best uniformity results were achieved when the number of projections were set to 16, the uniformity was less when the number of projections was set to 20 or 24.

Conclusions: In this study, spatial resolution and quantification accuracy were not influenced by changing the QF value. From a previous study we learned that increasing the QF to a value above 1 will introduce artifacts in the resulting images having, of course, a negative effect on the resolution. Higher overlap between the projection data increases the uniformity. The number of projections also influences the uniformity and, surprisingly, best uniformity was achieved at 16 projections. It is our hypothesis that this may be due to the number of subsets in the iterative reconstruction. Further research to the influence of the reconstruction settings in regard to the number of projections is needed to optimize image quality.

poster #13

SPARSE RECOVERY IN MYOCARDIAL BLOOD FLOW QUANTIFICATION VIA PETEngbers, R.¹, Benning, M.¹, Heins, P.¹, Schäfers, K.², Burger, M.¹¹University of Muenster Institute for Computational and Applied Mathematics, Germany ; ²University of Muenster European Institute for Molecular Imaging, Muenster, Germany

(ralf.engbers@uni-muenster.de)

Introduction: Dynamic PET (positron emission tomography) can be used to analyze physiological processes over time, e.g., myocardial blood flow. Therefore, the PET data need to be separated into temporal bins. A simple way reconstructing dynamic PET data is to compute a standard EM reconstruction for each temporal bin, with the obvious drawback of neglecting the temporal correlation between the bins. One way to overcome this problem is to incorporate mathematical models for the analysis of the tracer activity over time into the reconstruction process. The aim of our work is to show how sparsity methods can be used in the framework of kinetic modeling to improve dynamic PET reconstructions.

Methods: We are using a linear model operator developed by Reader et al., which is based on a one-compartment model. The operator consists of the input curve, exponential basis functions and their associated coefficients. The basis functions depend on a set of possible perfusion values, which is assumed to be large. Assuming the input curve to be known, we are interested in recovering the coefficients via a variational formulation. Furthermore, we assume the „true“ perfusion value to be contained in the set of possible perfusion values, so we are interested in only one coefficient corresponding to the true perfusion value, which gives rise to use sparsity methods. In a general variational formulation we have several possibilities of choosing the fidelity and regularization term. One reasonable choice for the fidelity term is, of course, to use the Kullback-Leibler divergence, to use the information that the radioactive decay follows a Poisson process. Another possibility is to use a weighed l^2 fidelity term, that can be derived by approximating the Kullback-Leibler fidelity. For the regularization we are actually interested in finding a sparse solution for each pixel (we want to recover the one basis function that corresponds to the perfusion for that pixel), so we want to have a regularization like $l^{1,\infty}$. But one could also use an EM-TV regularization on the coefficients to identify the largest coefficient.

Results: The ideas above have been tested on both synthetic and real data. The real data are from a dynamic PET scan with radioactive water being the tracer, thus, showing a low signal-to-noise ratio. The synthetic data have been simulated to show a similar behavior. In both cases, the quality of the reconstructions are higher (i.e. less noise, more details) than by reconstructing each temporal bin independently.

Conclusions: The proposed method improves dynamic PET reconstructions by including the temporal correlation between the datasets through a mathematical model.

Acknowledgement/References: M. Benning et al., A Nonlinear Variational Method for Improved Quantification of Myocardial Blood Flow Using Dynamic H2150 PET, 2008. G.T. Badinger et al., Dynamic single photon emission computed tomography --- basic principles and cardiac applications, 2010. A.J. Reader et al., Fully 4D image reconstruction by estimation of an input function and spectral coefficients, 2007. A. Sawatzky et al., Accurate EM-TV Algorithm in PET with low SNR, 2008. M.N. Wernick et al., Emission Tomography: The Fundamentals of PET and SPECT, 2004.

poster #14

SUPER-RESOLUTION RECONSTRUCTION OF WHOLE-BODY MRI MOUSE DATAKhmelninskii, A.¹, Plenge, E.², Kok, P.^{1,3}, Dzyubachyk, O.¹, Poot, D.², Suidgeest, E.¹, Botha, C. P.³, Niessen, W.^{2,4}, van der Weerd, L.^{1,5}, Meijering, E.², Lelieveldt, B.^{1,3}¹LUMC Dept. of Radiology, Netherlands; ²ErasmusMC Rotterdam, Netherlands; ³Delft University of Technology, Netherlands; ⁴Delft University of Technology Dept. of Imaging Science, Netherlands; ⁵LUMC Depts. of Anatomy & Embryology, Netherlands (e.plenge@erasmusmc.nl)

Introduction: Super-Resolution Reconstruction (SRR) is the process of producing a high-resolution (HR) image from a sequence of low-resolution (LR) images, where each LR image transforms and samples the HR scene in a distinct fashion. However, visualization of HR data is often computationally heavy and the time necessary to reconstruct large volumes can be large. To overcome this disadvantage, we make use of recent progress in the areas of articulated atlas-based segmentation of whole-body small animal data[1,2] and MRI SRR[3]. We present a novel approach for producing HR, localized isotropic volumes-of-interest (VOIs) in whole-body mouse MRI which enables interactive HR visualization and exploration of anatomical structures.

Methods: One post-mortem C57BL6, 6 month old, male mouse was scanned on a 7T Bruker Pharmascan using a fast recovery FSE sequence. TR=6648ms, TE=33ms, Navg=1, NSP=1. The 2D slice stack consisted of 64 slices, with a FOV of 50x32mm, and a resulting resolution of 0.125x0.125x0.5mm³. The scan time per stack was 213s. The slice stack was rotated 23 times in uniform increments of 180/24 degrees. To segment the mouse, the semi-automated atlas-based bone approximation method[1] was applied on one of the LR datasets. Next, the Articulated Planar Reformation[2] was applied to reformat the data into segments specified by the atlas, thus mapping it to the standardized atlas space. Now, the user can interactively select any VOI for a subsequent SRR. The data needed to reconstruct the VOI at the requested level of resolution is collected from a database of LR images. For the purpose of both effective and efficient reconstruction, the method developed in [3] was chosen. This method employs Tikhonov regularization using the L2-norm of the second order derivative of the reconstruction as the regularization term, together with an affine transformation scheme that minimizes aliasing and spectral distortions.

Results: The proposed local SRR approach was tested for each segmented bone, using an increasing number of LR images. The SRR times for each bone experiment were compared with SRR times for the whole-body. SRR time scale approximately linearly with the size of the LR dataset. Where the entire mouse requires hours to reconstruct, the VOI can be reconstructed within minutes. The sample axial slices demonstrate that the quality of the reconstructions clearly improves when an increasing number of LR images is used. In agreement with the results of the quantitative experiments, it can be observed that the quality improvement is substantial going from 2-to-8 LR images, while a smaller effect is seen when going from 12-to-23 LR images.

Conclusions: This method allows overcoming the time and memory limitations of the SRR technique. However, the mean time for the best quality SRR result, using 12 LR images, is still in the order of minutes. Since the results presented here were acquired on a MATLAB™ implementation, the computation times will considerably decrease with a re-implementation in a C/C++ and GPU programming environment combination.

Acknowledgement/References: [1]-Khmelninskii, IEEE ISBI, 2010 [2]-Kok, IEEE TVCG, 2010 [3]-Poot, MICCAI, 2010

poster #15

DEPTH SOURCE ESTIMATION FROM A SINGLE, MULTISPECTRAL ACQUISITIONvan de Giessen, M.^{1,2}, Lelieveldt, B.^{1,2}, Dijkstra, J.¹¹Leiden University Medical Center Division of Image Processing, Netherlands;²Delft University of Technology Department of Intelligent Systems, Netherlands (m.vandegiessen@lumc.nl)

Introduction: Fluorescent light sources close to the surface of tissue can easily be located accurately. However, due to the absorption and mainly scattering properties of biological tissue, deeper sources do not produce a clearly delineated signal at the surface, but a wavelength dependent blurred blob. Using the wavelength dependent scattering and absorption properties, Kuo et al. [1] have been able to reconstruct the locations and intensities of deeper lying sources. However, due to the limited resolution of the imaged surface, estimates of source locations in the large underlying 3D volume are by definition inaccurate. In mathematical terms: the problem is ill-defined. In this abstract we show that by adding extra knowledge about the reconstruction problem, the accuracy of the reconstructions can be improved.

Methods: In this work we assume that only a small part of the imaged volume contains fluorescent sources. We use this knowledge to iteratively estimate potential source locations, essentially repeating the procedure in [1] on an increasingly constrained volume. Locations that are very unlikely to contain sources are declared 'forbidden' and the remaining volume is regridded at a higher resolution. This procedure is repeated until the potential volume with sources does not decrease anymore.

Results: As validation of the algorithm, 20 simulations were performed with 1 to 5 sources in a bar-shaped volume of 20x20x08 (depth) mm with known tissue properties. The sources were randomly positioned according to a uniform distribution and had random intensities, also according to a normal distribution. After a single iteration (this is the same as in [1]) source locations were estimated with an accuracy of 0.9 mm close to the surface and 1.7 mm at 0.7 mm depth. After convergence (on average 3 iterations) these values improved to 0.5 mm and 0.8 mm, respectively.

Conclusions: The addition of the knowledge that only a small subvolume contains fluorescent sources can be used to iteratively increase the precision of the estimated sources. Further evaluations will take place in pre-clinical multispectral data.

Acknowledgement/References: This research was supported by the Center for Translational Molecular Medicine (MUSiS). [1] C. Kuo, O. Coquoz, et al. Three-dimensional reconstruction of in vivo bioluminescent sources based on multispectral imaging, J Biomed Opt, 2007

poster #16

VALIDATION OF THE GATE MONTE CARLO SIMULATION PLATFORM FOR MODELING A NEW SEMI-CONDUCTOR GAMMA CAMERA DEDICATED TO NUCLEAR CARDIOLOGYImbert, L.^{1,2}, Galbrun, E.³, Karcher, G.², Wolf, D.³, Noel, A.³, Poussier, S.²¹Centre Alexis Vautrin, Nancy, France ; ²GIE Nancyclotep CHU de Nancy, France ; ³Université de Nancy – CNRS, France

(sylvain.poussier@univ-lorraine.fr)

Introduction: Recently, significant improvements have been proposed for cameras dedicated to myocardial perfusion imaging including the use of the new cadmium-zinc-telluride (CZT) detectors and/or collimation systems. Monte Carlo simulations are widely used in scintigraphic imaging to model imaging systems, to develop acquisition process and to assess tomographic reconstruction algorithms. GATE (Geant4 Application for Emission Tomography) is the most common tool of Monte Carlo simulations used for medical imaging in both SPECT and PET [1]. It includes the description of the detector design, the modelling of the detector response and the physical interactions. The objective of this work is to develop a new simulation platform for modeling the first CZT gamma-camera in order to optimize the acquisition and reconstruction clinical protocols.

Methods: The DSPECT gamma-camera involved 9 mobile blocks of pixelated Cadmium Zinc Telluride (CZT) detectors with a wide-angle square-hole tungsten collimator system. Placements and movements of each detector were simulated. Each block recorded a total of 120 projections by means of a 'region-centric' acquisition. The simulation model included Monte Carlo modeling of the detector response in terms of intrinsic spatial resolution and energy resolution [2]. This simulation platform was evaluated by comparing simulated Tc99m point source, detection sensitivity, energy resolution and spatial resolution with the corresponding experimental measurements. A specific algorithm of iterative reconstruction was used to compensate for the collimator-related loss in spatial resolution.

Results: Results showed an excellent agreement between simulated and experimental data : detection sensitivity determined with a Tc99m point source located in air was predicted with an error less than 1%. The difference between experimental and simulated spatial resolution expressed as FWHM with the same source was inferior to 0.5 mm in the two directions. In the X direction, the simulated and experimental spatial resolutions were 16.4 mm and 16.0 mm, in the Y direction, they were respectively 16.3 mm and 15.8 mm. Finally, simulated and experimental energy resolutions were within 1%. These results allow validating this new simulation platform.

Conclusions: The modeling of the DSPECT gamma-camera has been performed with the GATE code. The simulation platform was validated by comparing the simulated and experimental results. It is now possible to use this simulator to optimize acquisition and reconstruction protocols (including dual-isotope studies) and to develop the use of the DSPECT camera for other clinical applications (neurology or endocrinology). Our future work will be to integrate the XCAT phantom and the voxelized sources in the simulation.

Acknowledgement/References: Thank to the Spectrum Dynamics company (M. ROTH Nathaniel) for his help on the geometry and operation of the camera Dspectrum.[1] Jan S., Santin G., Strul D., Staelens S., Assié K, "GATE: a simulation toolkit for PET and SPECT," Phys. Med. Biol., vol. 49, pp4543-4561, 2004.[2] Assié K, Gardin I, Véra P, Buvat I, "Validation of the Monte Carlo simulator GATE for indium-111 imaging", Phys Med Biol. 2005 Jul 7;50(13):3113-25. Epub 2005 Jun 22.

poster #17

TRACER KINETIC MODEL FOR [¹¹C]LANIQUIDAR: A NOVEL TRACER OF P-GP EXPRESSIONPostnov, A.¹, Froklage, F.², Reijneveld, J. C.², Boellaard, R.¹, Schuit, R. C.¹, Eriksson, J.¹, Windhorst, A. D.¹, Hendrikse, N.³, van Berckel, B. N. M.¹, Lammertsma, A.A.¹¹VU University Medical Center Nuclear Medicine Amsterdam, Netherlands; ²VU University Medical Center Neurology, Amsterdam, Netherlands; ³VU University Medical Center, Amsterdam, Netherlands (a.postnov@vumc.nl)

Introduction: Overexpression of P-glycoprotein (P-gp) is thought to play a role in drug resistance, affecting some 30% of patients with epilepsy. A substrate tracer, such as (R)- [¹¹C]verapamil, is not ideal for measuring overexpression of P-gp, as an already small brain signal even becomes smaller, leading to significant noise problems. Laniquidar is an inhibitor of P-gp and, as such, overexpression of P-gp should lead to an increased signal. The aims of the present first-in-man study were to characterize [¹¹C]laniquidar kinetics human subjects and to develop a tracer kinetic model for analyzing [¹¹C]laniquidar data.

Methods: Dynamic 60 minutes [¹¹C]laniquidar PET scans (24 frames) were performed in 11 healthy volunteers using an HR+ scanner (CTI/Siemens). T1-weighted MRI scans were acquired on a SONATA 1.5T scanner (Siemens) and used for co-registration and volume of interest delineation. Plasma input functions were obtained using an on-line sampling device, with metabolite correction based on up to 7 manual HPLC processed samples. Regional time activity curves were fitted to various one and two tissue compartment models in order to identify the best model describing [¹¹C]laniquidar kinetics.

Results: Modeling was complicated by the low first-pass extraction fraction of [¹¹C]laniquidar, which was estimated to be 2-3%. Metabolism of [¹¹C]laniquidar in plasma was fast (only 50% of parent tracer remaining after 10 minutes, 20% after 60 minutes). In all subjects, cerebral [¹¹C]laniquidar concentrations started to increase after 5-10 minutes, suggesting a second tissue compartment. Nevertheless, k_2 values were too small to be determined reliably. At the same time, however, a single tissue compartment model did not fit the data well. The quality of the fits improved significantly by adding a second parallel (single tissue) compartment with one of the labeled plasma metabolites as input function, suggesting that metabolites do indeed enter the brain. The most robust model was found to be an irreversible single tissue compartment model providing estimates for K_1 and V_b and using only the first 3 minutes of PET data in order to prevent the contribution of metabolites entering the brain. The mean value (\pm SD) for K_1 was 0.020 ± 0.004 .

Conclusions: [¹¹C]laniquidar kinetics suggest that labeled metabolites enter the brain. Taking this into account a dual input model, with both parent tracer and metabolite input functions, is preferred for 60 minutes scans. If only parent plasma is used as input function, robust estimates of K_1 can still be obtained by fitting only the first 3 minutes of PET data.

Acknowledgement/References: J&J pharmaceuticals, Euripides (FP7)

poster #18

MODELING 3D REALISTIC ORGANIC TISSUES FROM 2D DIGITAL MICROSCOPY IMAGESPrieto, J. C.¹, Revol-Muller, C.¹, Camelliti, P.², Odet, C.¹¹CREATIS, Insa-Lyon, Villeurbanne, France ; ²NHLL, Imperial College London, UK

(prieto@creatis.insa-lyon.fr)

Introduction: In this paper, we propose a method that is able to reproduce complex 3D objects by using 2D textured samples. Our method is able to create a 3D texture that resembles the 2D image in every slice. We choose as 2D reference images, some highly textured images provided by light or confocal microscopy. A major advantage of our method is to extend 2D histological information to a 3D representation.

Methods: Our approach is based on an energy proposed by [kwatra05]. It is based on a distance metric that compares the neighborhoods of a texel in the object and neighborhoods taken in the sample texture. When minimized, the result is an increase of similarity between the sample and the synthetic object. The procedure begins at a coarse resolution assigning random values from the sample to the synthetic object. Then, it alternates between a search phase where the closest neighborhoods are found and an optimization phase where the weighted average of every texel is calculated. When the optimization converges, it changes to a finer resolution level using linear interpolation. Following the optimization phase, an histogram matching is done to preserve the global statistics of the object relative to the exemplar.

Results: Synthetic 3D images were generated using different type of textures from histology images acquired with light or confocal microscopy.

Isotropic texture We get 3D isotropic texture when the same exemplar is used to perform the optimization in each direction. We illustrate our method with the 3D synthesis of the striated cardiac muscle tissue and the liver cell tissue from only one histology slice. Let us note that any axial, longitudinal or transversal slice of the volume is similar to the reference texture without being, however, identical.

Anisotropic texture We show the result of selecting two different textures to constrain the optimization. Selecting a zebra texture for the longitudinal and transversal planes with a dot pattern for the axial plane generated cylinder like structures. When rendering the surface of the object, we can see that the generated structure is very complex and consists of tubes that join and separate at arbitrary slices.

Anisotropic texture constrained by additional masks We show synthesis results using different exemplar textures obtained from confocal images and extra channels provided by signed Euclidean distance maps computed from binary masks. The 3D texture representing a myocyte cell tissue are quite representative of cells organisation (myocytes in red and fibroblasts in blue). The anisotropy of the cells is conspicuous and the contrast of staining is well preserved thanks to the use of the binary masks.

Conclusions: One main advantage of our method is to generate a 3D tissue from 2D information. Up to now, it was impossible for the biologist or the physician to have a 3D representation of the cell tissue, since it is technically very difficult or even impossible to have an axial resolution as good as those in the slice. Thanks to our approach, the experts can get a virtual 3D representation of the tissues that is close to reality without being it.

poster #19

A BIOPHYSICAL TRANSPORT MODEL FOR PREDICTING THE ENHANCED PERMEABILITY AND RETENTION EFFECT FOR LIPOSOME TRANSPORT IN SOLID TUMOURSStapleton, S.¹, Milosevic, M.², Allen, C.³, Jaffray, D.^{1,2}¹University of Toronto Canada ; ²Ontario Cancer Institute Radiation Medicine, Canada ; ³University of Toronto Pharmaceutical Sciences, Canada

(shawn.stapleton@rmp.uhn.on.ca)

Introduction: Solid tumors contain hyper-permeable vasculature and lack lymphatic vessels. The combined effect causes passive retention of nanoparticle drug delivery systems in tumours, termed the enhanced permeability and retention (EPR) effect [1]. A CT contrast agent comprised of iohexol encapsulated in a liposome has been developed to noninvasively image the EPR effect [2]. We have developed a biophysical EPR transport model based on fluid convection to predict liposome retention in solid tumors. The goal of this study was to use the imaging data to validate the EPR transport model.

Methods: The liposome retention kinetics were made in 5 mice bearing subcutaneous non-small lung cell (H520) tumors and 4 mice bearing orthotopic cervix tumors (ME180) for up to 6 days using microCT. The measured time intensity curves were fit to the EPR transport model using least squares minimization. The coefficient of determination (R^2) was used as a goodness of fit metric. There were 4 free parameters which reflect tissue transport properties: vascular and interstitial permeability, microvascular pressure and interstitial volume fraction. The free parameters obtained were compared to accepted values obtained from the literature.

Results: The H520 tumors had a faster accumulation, peak concentration and clearance of liposomes compared the the ME180 tumor bearing mice. The EPR transport model fit the liposome retention curves in both tumor types with an $R^2 > 0.90$. The EPR transport model identified that tumor size was a contributing factor to the different liposome retention kinetics observed between the two tumor types. The free parameters obtained from the fitting process had large variabilities, but were within the range of previously published values.

Conclusions: The EPR transport model was able to fit the measurements of liposome retention in two mouse tumor models. Therefore our work has shown that the biophysical model provides a foundation to mathematically describe the EPR effect. The long term goal is to have mathematical model which can predict liposome drug delivery and provide a quantitative, image-based approach to non-invasively estimate transport properties in solid tumors.

Acknowledgement/References: 1. Maeda H., The enhanced permeability and Retention (EPR) effect in tumor vasculature: the key role of tumor-selective macromolecular drug targeting. *Advan. Enzyme Regul.*, 41:189–207 (2001). 2. Zheng J., Liu J., Dunne M., Jaffray D.A. & Allen C., In vivo performance of a liposomal vascular contrast agent for CT and MR-based image guidance applications. *Pharmaceutical research*, 24(6):1193-1201 (2007). The authors would like to thank Dr. Naz Chaudary and Dr. Richard Hill for providing the ME180 tumor bearing mice and Mr. Michael Dunne for providing the H520 tumor bearing mice.

poster #20

MORPHOLOGY QUANTIFICATION: ELLIPTICAL 2D FOURIER ANALYSIS FOR CRANIOFACIAL PHENOTYPING IN MOUSE BASED ON MCT ACQUISITIONSBornert, F.^{1,2}, Schmittbuhl, M.^{1,2}, Gros, C. - I.¹, Constantinesco, A.^{3,4}, Choquet, P.^{3,4}¹INSERM-UMR 977, Strasbourg, France ; ²Faculty of Dentistry Strasbourg ³Faculty of Medicine Strasbourg ⁴UF 6237 Preclinical Imaging, Nuclear Medicine Strasbourg (fabienbornert@free.fr)

Introduction: Extracting measurements or values from acquired medical images is highly desirable and nowadays a common goal. However for morphology, it is very challenging as studies in this field are essentially qualitative. Up to now, morphological quantitative analysis is mainly based on landmarks approaches which require the unbiased recognition of some singular points common in model and control individuals. A main drawback relies on the limited number of points used, reducing the accuracy of the form description. 2D Elliptical Fourier analysis (EFA) applied on outlines is another way to quantify differences in organs form (1) and had the advantage of working on the shape in a global manner. We present here an example of EFA application on μ CT images of mouse heads to characterize mandibular dysmorphoses in Tabby's mice, an animal model of the X-linked hypohidrotic ectodermal dysplasia (XLHED) (2).

Methods: 74 adults specimens, 15 hemizygous males (Eda^{Ta^y}), 24 heterozygous females (Eda^{Ta^y/+}), and 35 control WT mice (19 males, 16 females) were used. Ex vivo imaging of full heads was performed using a micro-CT (eXplore CT 120, GE Healthcare, Waukesha, USA). After reconstruction, left hemimandibles were segmented manually by using region and volume of interest functions (MicroView®, GE Healthcare, Waukesha, USA). 2D mandibular outlines were extracted from lateral views of a 3D isosurface rendering of each mandible (Visilog 5.4®, Noesis, Gif sur Yvette, France). The curve contained a series of 512 points expressed by their 2D Cartesian coordinates. Elliptical Fourier analysis was used to describe the mandibular outline based on an already published method (1). The degree of distinction among mouse strains was assessed using a discriminant analysis (Statistica 7.1 software package, Statsoft Inc., Tulsa, USA), which was performed on the first 10 harmonics.

Results: Discriminant analysis reveals that significant distances separate the Eda^{Ta^y} specimens from the other groups of mice (3). A difference in shape is especially highlighted between hemizygous males and WT males based on Fourier analysis and reconstructions on the 1st ten harmonics. Hemizygous males have a more rostro-caudal mandibular development in comparison with WT males.

Conclusions: 2D EFA enables the characterization of the shape as a whole, unlike other morphometric approaches based on anatomical landmarks and their associated measurements. 2D EFA is especially pertinent for structures with a thin 3rd dimension eg nearly planar like mandibles, but of course extension to the third dimension is possible. EFA is a very sensible biomedical image processing tool for comparison between different phenotypes based on shape's quantification and adequate statistical analysis.

Acknowledgement/References: 1. Schmittbuhl, M., Allenbach, B., Le Minor, J. M., and Schaaf, A. (2003). *Math. Geol.* 35, 853-872. 2. Clauss, F., Maniere, M. C., Obry, F., Waltmann, E., Hadj-Rabia, S., Bodemer, C., Alembik, Y., Lesot, H., and Schmittbuhl, M. (2008) *J. Dent. Res.* 87, 1089-1099. 3. Bornert F, Choquet P, Gros C-I, Aubertin G, Perrin-Schmitt F, Clauss F, Lesot H, Constantinesco A, Schmittbuhl M. Subtle morphological changes in the mandible of Tabby mice revealed by micro-CT imaging and elliptical Fourier quantification. *Front Physiol.* 2:15.doi:10.3389/fphys.2011.00015.

poster #21

CORRELATIVE ANALYSIS OF RECURRENT MULTICOLOR FLUORESCENCE IMAGES TO CHARACTERIZE IN VIVO THE EFFECT OF ANTIVEGF DRUGS ON GLIOBLASTOMA TUMOR DEVELOPMENTRodriguez, T.^{1,2}, Stanchi, F.^{3,1}, Benesmanne, S.¹, Ricard, C.¹, Rougon, G.¹, Debarbieux, F.^{1,4}¹AMU-CNRS IBDML, Marseille Cedex 09, France ; ²CNRS Institut Génomique Fonctionnelle, Montpellier, France ; ³Vesalius Research Center, Leuven, Belgium ; ⁴AMU-CNRS CPPM, Marseille, France (debarbieux@univmed.fr)

Introduction: Glioblastoma multiforme (GBM) is the most aggressive and lethal primary brain tumor despite current standard care. GBM is highly vascularized and therefore represents attractive target for anti-angiogenic therapies. Recent investigations have revealed that treatments with agents targeting angiogenesis such as anti-VEGF antibodies (bevacizumab), inevitably fail. To clarify the effects of the treatment on tumor burden, recurrence, and vascular physiology we have established an orthotopic GBM xenograft model in mice suitable for repeated non invasive imaging using fluorescence two-photon microscopy (2P). We simultaneously followed the dynamics of tumor angiogenesis and growth at cellular resolution over several weeks in the same animal. Quantification of images stacks and correlative analysis of the data allow for real time evaluation of anti-VEGF treatment efficacy.

Methods: Green Fluorescent Protein expressing human U87 GBM spheroids are grafted in the superficial cortex of immuno-deficient mice. A glass cranial window is cemented on their skull to allow optical imaging. Prior every imaging session, red fluorescent dextran (70kD) is injected intravenously to highlight blood vessels. Thus in a given subject, tumor cells and blood vessels shine in different colors. Bicolor 3x3x0.5 mm³ image stacks are acquired at microscopic resolution. Starting 2 weeks post graft, the volume of interest is repeatedly imaged on a weekly basis with a <50 μ m repositioning accuracy thanks to careful placement of the animal under the objective. ImageJ 1.45g NIH software is used to analyze the data. Based on stable vascular landmarks images are manually registered using Align3TP pluggins. A revolution axis perpendicular to the image plane through the center of mass of the tumor is used to generate incremental cylindrical regions of interest on the first image stack. These regions of interest are relocated on the successive image stacks to assess tumor growth at different distances from its epicenter and to correlate growth with local blood supply. Mean fluorescence intensities respectively on the green and red channels are used as indexes of tumor density and blood supply. Linear correlation between these values are looked for in the different volumes of interest (VOI) at a given time point as well as between time points. Time evolution of indexes are compared between control and treated conditions.

Results: Quantification of the dynamics of tumor growth and of tumor vascularization over several weeks indicated that regions of highest tumor cell proliferation did not match with regions of highest vascular density. No correlation was indeed found between tumor density and vascular density or plasticity. The relative independence of tumor development with regard to blood supply was further confirmed *in vivo* by the modest and transient effect of angiogenesis blockade on tumor growth. Our data show that treatment escape was not associated with revascularisation of the tumor during anti-VEGF treatment and also suggest that angiogenesis is not the major player of GBM development.

Conclusions: More generally, this imaging and data analysis method shows potential to facilitate a better understanding of disease progression and response to therapy for GBM

Acknowledgement/References: Authors are thankful to PICSL Platform where images were acquired

poster #22

QUANTIFICATION OF BONE CELL CONNECTIONS FROM 3D NANO-CT IMAGESDong, P.^{1,2}, Pacureanu, A.^{1,2}, Zuluaga, M.^{1,2}, Peyrin, F.^{1,2}¹CREATIS, INSA Lyon Villeurbanne, France ; ²ESRF, Grenoble, France

(pdong@esrf.fr)

Introduction: The understanding of bone fragility involved in diseases such as osteoporosis is an active topic of research. At the cellular level, the crucial role of the osteocyte system in bone adaptation was recently highlighted [1]. Osteocytes are the most numerous bone cells embedded in the mineralized matrix. Their bodies are located in spaces called lacunae and they are interconnected through processes hosted in canaliculi. The assessment of the lacuno-canalicular network (LCN) is challenging: i) the LCN has mainly been imaged from 2D microscopic techniques and rarely from 3D techniques; ii) all quantification has been so far performed manually. In previous works, we proposed a unique imaging technique based on Synchrotron Radiation (SR) Computerized Tomography (CT) to image the LCN (isotropic voxel size: 280nm) [2]. Since this method can provide 3D images of LCN enclosing up to thousands of cells, automated quantification methods are needed.

Methods: Herein, we present an automatic 3D quantification method for calculating the number of canaliculi radiating from each osteocyte lacuna (Lc.NCa), which is important for bone permeability [3]. After segmentation of the LCN, based on a line-enhancement filter, the lacunae and canaliculi are discriminated by means of morphological operations and connected component analysis. Then, each lacuna is processed automatically. The number of canaliculi per lacuna, denoted Lc.NCa, is estimated by calculating topological parameters on a specific volume of interest. The mean, standard deviation and distribution of Lc.NCa at different distances from the lacuna surface are obtained for the whole population of lacunae in the image.

Results: The method was validated on a simple phantom and one isolated lacuna by comparison to manual counting. For the isolated lacuna, 22 and 32 canaliculi were calculated at two fixed distances. Then, the proposed method was successfully applied to a 3D SR-nanoCT image of a human femoral cortical bone. Statistical results on 167 lacunae are reported, showing a mean of 41.6 canaliculi per lacuna.

Conclusions: This is the first report of the number of canaliculi calculated directly from a 3D image, enclosing a large population of cells. The result is consistent with previous estimations extrapolated from 2D manual measurements [3]. The different numbers of canaliculi calculated on one isolated lacuna at different distances put in evidence the branching of canaliculi. Although the results rely on the quality of the acquired image and its segmentation, this method is expected to provide new data on the LCN with important impact on the understanding of bone strength. In addition, our method could also be applied to other similar 3D stellate biological objects from 3D images acquired in various modalities.

Acknowledgement/References: [1] L. Bonewald, "The amazing osteocyte" *J Bone Min Res*, 26(2), 229-38, 2011. [2] A. Pacureanu, M. Langer, E. Boller, P. Tafforeau, F. Peyrin, Nanoscale imaging of the bone cell network with synchrotron X-ray tomography: optimization of acquisition setup, *Med Phys*, submitted 2011. [3] T. Beno, Y. Yoon, S. Cowin, and S. Fritton, "Estimation of bone permeability using accurate microstructural measurements," *J Biomech*, 39(13), 2378-87, 2006.

poster #23

PROGRAMMED INFUSION FOR [¹¹C] FLUMAZENIL PET – A STEADY-STATE APPROACHFeng, L.¹, Svarer, C.¹, Madsen, K.¹, Ziebell, M.¹, Dyssegaard, A.¹, Arfan, H.², Ettrup, A.¹, Hansen, H.¹, Yndgaard, S.³, Paulson, O.^{1,4}, Knudsen, G.¹, Pinborg, L.^{1,5}¹Neurobiology Research Copenhagen ²Epilepsihospitalet Filadelfia, Dianalund; ³Department of Anaesthesia Copenhagen; ⁴Danish Research Centre Magnetic Resonance Copenhagen Hvidovre; ⁵Epilepsy Clinic, Copenhagen University Hospital, all Denmark (ling.feng@nru.dk)

Introduction: Full quantification with an arterial input is ideal in the evaluation of [¹¹C]FMZ PET (1). However, it is not feasible in a clinical setting due to the invasiveness and the time-consuming metabolites identification. A bolus infusion (BI) steady-state (SS) approach is appealing, and at SS the venous plasma concentration can be used as a representation of the input (2). However, it is challenging to attain SS with C-11 labeled tracers, due to its short half-life. The purpose of this study was to introduce a simulation system that captures the tracer kinetics from bolus studies, and together with an offline feedback proportional-controller to design programmed infusion (PI) experiments, aiming at describing a quantitative method with one blood sampling. This simulation system can also be used for BI design, and PI and BI comparison.

Methods: Five bolus, five BI, and three PI PET studies were conducted in healthy subjects with a HRRT scanner. Three subjects participated in both BI and PI experiments. The simulation system includes three models: (A) tracer administration to arterial plasma concentration; (B) conversion between radioactivity in whole-blood and plasma; (C) delivery of radioligand with arterial plasma to the brain tissue: one-tissue compartment model (3). For system verification a PI scheme was designed based upon the individual kinetics of a bolus study in one subject, and subsequently tested in the same subject. Population based PI and BI were designed based on the mean representation of system parameters across five bolus studies.

Results: The system verification proved that the system could reproduce the TACs for plasma and brain tissue from a bolus study. The system suggested that the B/I=55min outperformed other BI protocols, and PET studies confirmed the finding. SS was attained with B/I=55min within 51 min; with B/I=60min within 65 min; and with B/I=35min no SS was attained within 2 h. Comparisons between the experimental results from the optimal BI and the population based PI did not show significant difference w.r.t. SS attainment, which for most regions was attained within 59 min. Using PI the simulation, however, indicated an improvement of 16 min. The mean V_T across three BI studies correlated significantly with the ones across PI studies ($r = 0.9961$, $p=0.000$). They also correlated with the mean V_T from 1TC modelling of bolus studies: $r = 0.9964$, $p = 0.000$ (BI vs. 1TC); and $r = 0.9979$, $p=0.000$ (PI vs. 1TC).

Conclusions: The study showed that B/I=55min was the optimal BI protocol for [¹¹C]FMZ. The population based PI scheme provided similar performance. The discrepancy between the time of attaining SS in the simulation and PET data might be due to: 1) uncertainty in the estimated compartment parameters; 2) test-retest experimental variation; 3) inter-individual variation.

Acknowledgement/References: This study was supported by Østdansk Sundhedsvidenskabeligt Forskningsforum, The Danish Council for Independent Research, and Euripides. Authors thank the PET department, VUMC, for their experience sharing. 1. Hammers, A., et. al, *J Cereb Blood Flow Metab* 28, 207-216 (2008) 2. Carson R.E., et. al. *J Cereb Blood Flow Metab* 13(1):24-42 (1993) 3. Koeppe R.A., et. al. *J Cereb Blood Flow Metab* 11(5):735-44 (1991)

poster #24

QUANTIFICATION OF MYOCARDIAL BLOOD FLOW USING $^{13}\text{NH}_3$ AND PET: PARAMETRIC MAPS AND IMPACT OF DIFFERENT RECONSTRUCTION FRAMING ON THE FLOW RESERVE

Florea, I.¹, Berti, V.², Burger, C.¹, Sciagra, R.²

¹PMOD Technologies Ltd, Zürich, Switzerland; ²University of Florence Nuclear Medicine Unit, Florence, Italy

(ioana.florea@pmod.com)

Introduction: The aim of this study was to generate parametric maps (pm) of the myocardial blood flow (MBF) using ^{13}N labeled ammonia and positron emission tomography (PET) in patients studied for suspect coronary artery disease. The effect of different reconstruction protocols on flow reserve (CFR) estimates was also investigated.

Methods: The 8 patients enrolled in the study (4 females and 4 males) underwent two dynamic $^{13}\text{NH}_3$ PET scans at rest and under pharmacological stress. The data were acquired on a Philips Medical Systems, GEMINI TF TOF 16. The list mode data were reconstructed using two different framing protocols: 2 seconds versus 10 seconds. The images were analyzed using the PMOD 3.3 software. The MBF was calculated using the De Grado model [1] as implemented in the PCARD module. The CFR was quantified as the ratio between the Stress and the Rest MBF. The standard AHA 17 segment model was selected for the heart segmentation. The model crossing option for polar sampling was used for myocardium segmentation. The short axis (SA) re-oriented dynamic images, the right ventricle (RV), left ventricle (LV) and total myocardium (MYO) time activity curves were saved and used during the parametric mapping procedure. The parametric maps of the MBF for both Stress and Rest studies were generated using a basis function method (BFM) implementation [2] of the De Grado model [1] in PXMOM. The CFR was further quantified from the MBF parametric images using PCARD and the above settings for the MYO segmentation. The Bland Altman plot was used to compare the CFR in the 17 myocardial segments. Four scenarios were compared: 10s PCARD vs. 2s PCARD (S1), 10s PCARD vs. 10s PXMOM (S2), 2s PCARD vs. 2s PXMOM (S3), 10s PXMOM vs. 2s PXMOM (S4).

Results: The S3 and S4 CFR comparisons revealed the lowest values for mean difference and limits of agreement: 0.266 ([-0.6 1.2]) and 0.289 ([-0.4 1]). The apex segment and the mid infero-septal segment represent S3 and S4 outliers, respectively. The mean difference values identified for S1 (0.342) and S2 (0.360) were higher as compared to S3 and S4. The limits of agreement were broader for both S1 and S2 in comparison with S3 and S4: [-1.32 2.04] for S2 and [-1.11 1.80] for S1. The S1 and S2 analysis evidenced the basal infero-septal segment as the outlier.

Conclusions: The parametric MBF maps provide results comparable to the segmental analysis. The S1 analysis showed a tendency of 10s PCARD to result in higher estimates than 2s PCARD. This might be due to the inaccurate sampling of the bolus peak in the 10s data: a reduced input function results in higher MBF estimates. Further analysis is ongoing for the identification of the optimal reconstruction framing.

Acknowledgement/References: 1. DeGrado TR. et al, J Nucl Cardiol 1996;3:494-507.2. Harms H. et al, Eur J Nucl Med Mol Imaging 2011;38:930-9.

poster #25

PARTIAL VOLUME CORRECTION IN ^{18}F -FDG PET: IMPACT ON SUV DIAGNOSTIC VALUE IN BREAST CANCER

Gallivanone, F.¹, Canevari, C.², Stefano, A.³, Grosso, E.³, Zuber, V.², Sassi, I.², Gianolli, L.², Messa, C.^{1,3}, Gilardi, M. C.^{1,4}, Castiglioni, I.¹

¹IBFM - CNR, Milan, Italy ; ²Scientific Institute H. San Raffaele, Milan, Italy ; ³LATO HSR Giglio, Milan, Italy ; ⁴Tecnomed Foundation, University of Milan-Bicocca, Italy (gallivanone.francesca@hsr.it)

Introduction: *In vivo* quantitative biomarkers by ^{18}F -FDG PET can be important to characterize oncological pathologies and to predict survival and response to therapy non invasively, using an approach of personalized medicine. To obtain a reliable and accurate ^{18}F -FDG PET quantitative biomarker, quantification including Partial Volume Correction (PVC) is required. Aim of this work was to evaluate the impact of PVC on the Standardized Uptake Value (SUV) as potential *in vivo* quantitative biomarker for breast cancer, reflecting *ex vivo* histo-pathological and immune-histochemical characteristics.

Methods: 35 oncological patients with biopsy-proven breast cancer were recruited in a personalized medicine protocol involving Senology, Nuclear Medicine and Pathology departments of Scientific institute H San Raffaele, Milan, Italy . Patients underwent a ^{18}F -FDG PET-CT study before surgery. Accurate ^{18}F -FDG PET quantification using Averaged Body-Weighted SUV with PVC (PVC-SUV_{BW}) was performed [1]. After surgery, excised tissues were sectioned and classified according to the WHO guidelines[2]. Mann-Whitney and Kruskal-Wallis tests allowed to evaluate correlations of SUV_{BW} biomarker, obtained with and without PVC, with histopathological indices.

Results: Both SUV_{BW} and PVC-SUV_{BW} strongly correlated with histological type (p-value < 0.02 vs p-value_{PVC}<0.01) , histological grade (p-value < 0.042 vs p-value_{PVC}<0.029), hormone receptor status (p-value < 0.021 vs p-value_{PVC}<0.018), and MiB-1 proliferation index (p-value < 0.03 vs p-value_{PVC}<0.019). These results proved that the statistical significance of correlations always improved applying PVC. Considering c-erb-B2 index, the correlation analysis showed no correlations between SUV_{BW} and histo-pathological indices, while a strong correlation (p-value_{PVC}<<0.001) was found when PVC was applied.

Conclusions: A strong correlation between SUV PET biomarker and histo-pathological indices, such as histological type, histological grade, hormone receptor status, and MiB-1 proliferation index, was found, indicating that SUV has a prognostic value in breast cancer. The improvement of significance of statistical tests and the results of correlation of PVC-SUV_{BW} with c-erbB2 index suggest that PVC has an important impact in the evaluation of the diagnostic value of SUV as surrogate biomarker of *in vivo* histo-pathological indices.

Acknowledgement/References: [1] Gallivanone F. et al., (2011) "PVE Correction in PET-CT Whole-Body Oncological Studies From PVE-Affected Images", IEEE Transactions on nuclear Science [2] FA.Tavassoli and P. Devilee (2003) "World Health Organization Classification of Tumours: Pathology and Genetics of tumours of the Breast and Female Genital Organs". Lyon, France: IARC Press.

poster #26

PARTIAL VOLUME CORRECTION IN ^{18}F -FDG PET: IMPACT ON THE PROGNOSTIC VALUE OF ^{18}F FDG PET SUV IN HEAD AND NECK CANCER

Grosso, E.¹, Villa, E.², Mapelli, P.³, Dell'Oca, I.⁴, Picchio, M.^{5,6}, Gallivanone, E.⁶, Gianolli, L.⁷, Messa, C.^{1,6}, Gilardi, M. C.^{7,6}, Castiglioni, I.⁶

¹LATO HSR Giglio; ²University Milan-Bicocca, Italy; ³Nuclear Medicine Department, ⁴Radiation Oncology, ⁵Nuclear Medicine Department, ⁶IBFM - CNR, ⁷Scientific Institute all Milan, Italy

(gallivanone.francesca@hsr.it)

Introduction: Head and neck cancer (HNC) represents the 5% of whole malignant tumours worldwide. Treating HNC patient is complex and in continuous evaluation. Simultaneous Integrated Boost Intensity-Modulated Radiotherapy (SIB-IMRT) allows the simultaneous delivery of different doses to different target volumes that means less dose to critical organs, and treatment acceleration with reduced total treatment time. ^{18}F FDG PET studies are recommended for HNC patients at stages III-IV and for their follow-up after treatment. ^{18}F FDG PET/CT studies have been also used in HNC patients to guide treatment planning, to identify primary and secondary tumours and to assess involved lymphnodes. The aim of this work was to evaluate the impact of Partial Volume Correction (PVC) on the prognostic role of ^{18}F FDG PET Standard Uptake Value (SUV) in HNC patients treated with Biological Target Volume (BTV)-guided SIB-IMRT.

Methods: 22 HNC pts (median age 59.3 yrs, range: 23-81 yrs) treated with ^{18}F FDG PET/CT guided SIB-IMRT (69Gy, 30 fractions) between 2005 and 2011 were retrospectively included. Pre-therapy ^{18}F FDG PET images were analyzed. SUV, with and without PVC, and BTV (60% SUV_{max}) were calculated for both Primary (P) tumour and Lymphnodes (L) (SUV_P, SUV_L and BTV_P, BTV_L, respectively) to identify SUV thresholds for the assessment of patient outcome. A cluster analysis has been performed and two-year DFS was calculated for each cluster of patients.

Results: ^{18}F FDG PET/CT detected the primary tumor in all 22 pts and cervical nodes in 16/22 pts. The biological lesion diameter (sphere-equivalent) was < 3.1 cm, 1.5cm±0.5cm for P and 1.3cm±0.4cm L. SUV_P correlated with SUV_L, both with and without PVC (r=0.82, 0.76 respectively). G1 patients had SUV_P <14 with PVC (SUV_P <11 without PVC). G2 patients had SUV (both P and L) which resulted uncorrelated with their BTV. SUV_P was correlated with SUV_L (r=0.79) and correlation improved when PVC was applied (r=0.85). Two clusters of G2 patients were identified, the elements of the two clusters changed cluster when PVC was applied. Two thresholds were found selecting the two clusters:

A) SUV_P <17 and SUV_L <13 with PVC (SUV_P <14.6 and SUV_L <11 without PVC)

B) SUV_P >17 and SUV_L >13 with PVC (SUV_P >14.6 and SUV_L >13 without PVC)

These results prove that a high P tumor uptake (SUV_P >17) is always associated with the presence of ^{18}F FDG PET positive L. DFS for G1 was 83.3% either with or without PVC. DFS for G2 patients were 45.8% (cluster A) and 37.5% (cluster B) with PVC and 41.9% (cluster A) and 66.6% (cluster B) without PVC, proving a better prognosis for lower SUV_P.

Conclusions: PVC was found mandatory for accurate SUV measurement in HNC lesions. An high primary tumor uptake (SUV_T >17) was always associated with the presence of positive L. These results indicated that pretreatment ^{18}F FDG PET SUV has a prognostic value for DFS in HNC patients candidate to BTV-SIB-IMRT.

poster #27

THE EFFECT OF ISOFLURANE ANESTHESIA ON THE QUANTIFICATION OF IN VIVO BIOLUMINESCENT SIGNALS.

Keyaerts, M.^{1,2}, Remory, I.^{1,3}, Caveliers, V.^{1,2}, Lahoutte, T.^{1,2}

¹In Vivo Cellular and Molecular Imaging (ICMI) Jette, Belgium; ²Department of Nuclear Medicine Jette, Belgium; ³Department of Anesthesiology Jette, Belgium (mkeyaerts@gmail.com)

Introduction: Rodents are anesthetized during Bioluminescence imaging (BLI) and BLI cameras are routinely provided with an isoflurane anesthesia unit. Isoflurane is animal- and user-friendly because of its fast induction and recovery. However a direct inhibition of the Firefly luciferase (Fluc) enzyme by anesthetics has been described, and anesthetics are known to change cardiovascular state of mice, which can result in differences in in vivo quantification. Aim: To evaluate the effect of isoflurane anesthesia on in vivo BLI signal quantification.

Methods: 293T-Fluc cells (1 x 10⁶) were subcutaneously injected in mice at day 0. Mice were imaged at day 3, 5 and 7 post cell injection, alternating between isoflurane anesthesia (2%) and no anesthesia (unanesthetized), in a cross-over design (n=10). For the final signal intensity, the average of day 3 and day 7 was compared to day 5, to correct for cell growth. D-luciferin was injected intravenously at 150 mg/kg. Mice were imaged using the Photon Imager equipped with the *in actio* module (Biospace, France), on a heated platform. The photon emission was measured dynamically during 50 min. Identical elliptical ROIs were drawn over the mice and time activity curves were obtained using 5s intervals. For the calculation of the PE_{max} from the tumor, the 95th percentile was used. For the calculation of the time-to-peak, the same acquisition data were analyzed using 1min intervals, and the time point containing the highest photon emission was defined as time-to-peak. The area-under-the-curve (AUC) was calculated.

Results: There was a significant reduction of BLI signal in mice anesthetized with 2% Isoflurane compared to awake mice, on average to 45±13% of control values for the peak intensity and 70±16% of control values for the AUC. The shape of the time profile was also different, with a fast rise and a more rapid decline in awake animals, and a slower evolving kinetic profile in anesthetized mice.

Conclusions: Isoflurane anesthesia significantly reduces the intensity of the BLI signal in vivo, and also changes its kinetic profile, with important impact on its quantification.

Acknowledgement/References: Marleen Keyaerts is an aspirant and Tony Lahoutte is a senior clinical investigator of the Research Foundation - Flanders (Belgium) (FWO). The company Biospace lab (Paris, France) kindly provided the *in actio* camera to perform the isoflurane versus unanesthetized animal experiment during a period of 3 weeks.

poster #28

A DUAL TRACER TECHNIQUE TO SIMULTANEOUSLY QUANTIFY THE VASCULAR AND INTERSTITIAL VOLUME FRACTIONS IN SOLID TUMORS.Stapleton, S.¹, Allen, C.², Jaffray, D.^{1,3}¹University of Toronto Medical Biophysics, Canada ; ²Pharmaceutical Sciences, Canada ; ³Ontario Cancer Institute Radiation Medicine, Toronto Ontario, Canada (shawn.stapleton@rmp.uhn.on.ca)

Introduction: Tumour microvessels are spatially disorganized, tortuous, lack structural hierarchy, are often dilated, contain excessive branching and shunts, and are hyper-permeable. The tumour interstitium is collagen rich, fluid rich and lacks functional lymphatics [1]. These abnormalities form a barrier to optimal drug delivery [2]. We have developed a dual tracer imaging method to quantify the interstitial volume fraction (IVF) and vascular volume fraction (VVF) in solid tumours. These parameters are reflective of the tissue microenvironment and may be reflective of the ability to efficiently deliver drugs. The proposed method takes advantage of the differential transport properties of a high molecular weight liposome CT contrast agent compared a low molecular weight freely diffusible CT contrast agent.

Methods: A macro-molecular weight (MW) CT liposome contrast agent was injected into 6 orthotopic (OR) and 6 intramuscular (IM) cervix tumour bearing mice followed by the injection of a micro-MW iohexol agent. *In-vivo* kinetics of the two agents were simultaneously measured using micro CT. The VVF was quantified by taking the ratio of the tissue to arterial enhancement two minutes post liposome injection. The VVF was used to subtract the plasma signal from the time intensity curves obtained from the micro-MW agent. The ratio of tumour to arterial enhancement 2 minutes post administration of iohexol gave an estimate of the IVF. Measurements of IVF and VVF were made in both tumor and muscle tissue on a voxel by voxel basis. Results are reported as a grand median over all voxels for a specified tissue type, with minimum and maximum values shown in brackets. Results were compared to estimates made by fitting the iohexol time intensity curves to the modified Tofts model.

Results: There was no statistically significant difference in VVF for both tissues and tumor types; The grand median VVF for all mice was 0.08 (0.01 - 0.24). The IVF for muscle was similar in all mice; The grand median for all mice was 0.16 (0.01-0.45). The IVF was elevated in tumor tissue compared to muscle tissue in both tumor types; The grand median is IM tumors was 0.25 (0.03-0.63) and 0.28 (0.04-0.71) in OR tumours. No difference was observed in IVF between tumor types. Finally, there was a linear correlation between estimates of IVF when the dual tracer technique was compared to the Tofts model. No correlation was found for VVF.

Conclusions: This work demonstrates the potential of simultaneously detecting macro- and micro-MW CT contrast agents to non-invasively quantify the vascular and interstitial volume fractions. Quantification of VVF and IVF may provide an important tool to investigate barriers to drug delivery and monitor therapy.

Acknowledgement/References: 1. Vaupel P, Tumor microenvironmental physiology and its implications for radiation oncology. *Seminars in radiation oncology.*, 14(3):198-206 (2004). 2. Jain R. K. Transport of molecules in the tumor interstitium: A Review. *Cancer Res.* 47:3039-3051 (1987).

The authors would like to thank Dr. Naz Chaudary and Dr. Richard Hill for providing the tumor bearing mice.

poster #29

PHYSIOLOGICAL PARAMETERS AND TIME-ACTIVITY-CURVE FITTING OF DYNAMIC ¹⁸F-FDG SCANS IN MICEBerndsen, S.¹, Konijnenberg, M.¹, de Jong, M.^{1,2}, Groen, H.¹¹Erasmus MC Nuclear Medicine, Rotterdam, Netherlands; ²Erasmus MC Radiology, Rotterdam, Netherlands

(h.c.groen@erasmusmc.nl)

Introduction: ¹⁸F-FDG is widely used to estimate the metabolic activity in organs, tumors and to localize metastasis. Usually the metabolic activity is assessed by static imaging. Dynamic image studies, however, can provide physiological parameters. Plasma input-functions and glucose levels should then be obtained by blood-sampling, for small-animal studies this procedure is difficult and blood volume is limited though. We present a whole-body pharmacokinetic (PK) compartment model to estimate the input-function and as such the physiological parameters are determined without the need for repeated blood sampling in these small animals.

Methods: Experiments were performed in 6 over-night-fasted and pre-warmed healthy mice, where each mouse was used in 3 experiments:

- Intra-vascular (IV) injection of ¹⁸F-FDG under isoflurane anesthesia,
- IV injection awake,
- Intra-peritoneal (IP) injection under anesthesia.

On average 7.4±0.4 MBq ¹⁸F-FDG was administered and the mice were scanned with the Siemens Inveon PET scanner for 90 minutes under 2.5% isoflurane anesthesia. Images were reconstructed with filter-back-projection and the brain, heart, kidneys, bladder and brown-fat were manually segmented using the full-width-half-maximum method. Time-activity curves of each organ in each mouse were imported into the PK compartment model in software package SAAMII. Each organ, except the bladder, was modeled by two-compartments connected to the plasma compartment. The bladder was modeled by one trapping compartment. Additionally, for the IP group an additional peritoneal injection-compartment was added to the model for the transportation of the ¹⁸F-FDG into the plasma compartment. For comparison, the net transfer rate ($K_i = K_1 * k_3 / (k_2 + k_3)$), the binding potential ($BP = (k_3 / k_4)$) and the distribution volume ($DV = (K_1 / k_2) * (1 + BP)$) for each organ was calculated by compartment analysis (K_1 , k_2 , k_3 and k_4). Statistics was performed by paired Student's t-test with Bonferroni correction and the Akaike Information Criterion test.

Results: No statistical significant differences were found between the physiological parameters between the IV and the IP group that were injected under anesthesia. Administration of the ¹⁸F-FDG awake showed lower K_i , BP and DV brain values and lower K_i and DV kidney values compared to administration during anesthesia while heart and brownfat parameters remained equal.

Conclusions: We showed that a 2-compartment PK model is capable of fitting all time-activity curves of ¹⁸F-FDG uptake in organs of individual mice, physiological parameters can be calculated and compared for mice scanned under slightly different conditions. Since some physiological parameters were dependent on animal handling, care should be taken comparing results from animals scanned under different conditions.

AUTHOR'S INDEX

A

Alfaraj, A. 43
 Allan, C. 32
 Allen, C. 51, 56
 Arfan, H. 53
 Arranz, A. 46
 Arridge, S. 25
 Autret, G. 43

B

Babos, M. 35
 Backes, H. 14, 28, 35
 Balvay, D. 43
 Bandi, P. 35
 Benlloch, J. M. 23
 Benning, M. 48
 Bensemanne, S. 52
 Berndsen, S. 56
 Berti, V. 54
 Blackburn, C. 32
 Block, K. T. 24
 Boellaard, R. 17, 50
 Boffa, C. 39
 Boisgard, R. 36
 Bornert, F. 52
 Botha, C. P. 43, 49
 Buether, F. 13
 Bulte, D. 38
 Burel, J. - M. 32
 Burger, C. 54
 Burger, M. 44, 45, 48
 Buvat, I. 39

C

Camelliti, P. 51
 Camici, P. G. 18
 Canevari, C. 54
 Cardiology 18
 Carole, F. 47
 Caselles, O. 47
 Castano, M. 39
 Castiglioni, I. 44, 54, 55
 Cavelliers, V. 55
 Cerutti, S. 18
 Chalon, S. 39
 Chandarana, H. 24
 Charara, J. 39
 Chatzioannou, A. 34
 Choquet, P. 52
 Clément, O. 43
 Clustering 39
 Comtat, C. 36
 Constantinesco, A. 52
 Correcher, C. 23
 Correia, T. 25
 Courbon, F. 47
 Croprobe 43
 Cunningham, V. 13

D

David, R. 47
 Dawood, M. 33
 Debarbieux, F. 52
 de Jong, M. 46, 48, 56
 Dell Oca, I. 55
 de Swart, J. 48
 Didierlaurent, D. 47
 Dierickx, L. O. 47
 Di Grigoli, G. 44
 Dijkstra, J. 21, 43, 45, 49
 Di, Z. 26
 Dong, P. 53
 Dyssegaard, A. 53
 Dzyubachyk, O. 27, 49

E

Egri, G. 35
 Elceiri, K. 32
 Endepols, H. 35
 Engbers, R. 48
 Eriksson, J. 50
 Ettrup, A. 53

F

Feng, L. 24, 53
 Feuerstein, D. 14, 28
 Florea, I. 54
 Frohwein, L. 33
 Froklage, F. 50

G

Galbrun, E. 50
 Galineau, L. 39
 Gallivanone, F. 44, 54, 55
 Gämperli, O. 18
 Gazeau, F. 43
 Gebhard, C. 18
 Gianolli, L. 54, 55
 Gigengack, F. 44
 Gilardi, M. C. 44, 54, 55
 Girault, J. - M. 39
 Giustetto, P. 39
 Gonçalves Antunes, S. 18
 González, A. 23
 Graf, R. 14, 28
 Gramer, M. 14, 28
 Grandjean, J. 46
 Gremse, F. 25
 Groen, H. 46, 48, 56
 Gros, C. - I. 52
 Grosso, E. 44, 54, 55

H

Hansen, H. 53
 Heins, P. 48
 Hendrikse, N. 50
 Hill, E. 32

Hobor, S. 35
 Hoehn, M. 31
 Hüsken, A. 35

I

Imbert, L. 50
 Irani, M. 28

J

Jaffray, D. 51, 56
 Jähnen-Dechent, W. 25
 Jan, S. 20, 36
 Jaudet, C. 47
 Jelier, R. 27
 Jiang, X. 33, 44, 45
 Jones, T. 20, 29

K

Kalthoff, D. 31
 Karcher, G. 50
 Keyaerts, M. 55
 Khmelinskii, A. 46, 49
 Kiessling, F. 25
 Kinkeldey, A. 25
 Knudsen, G.M. 16, 53
 Kohl-Bareis, M. 28
 Kok, P. 43, 49
 Kolosnjaj-Tabi, J. 43
 Konijnenberg, M. 48, 56
 Koppe, J. 48
 Krüger, A. 27

L

Lahoutte, T. 55
 Lammers, T. 25
 Lammertsma, A.A. 12, 50
 Law, M. 13
 Lederle, W. 25
 Lehner, B. 27
 Lelieveldt, B. 21, 33, 43, 45, 46, 49
 Linkert, M. 32
 Littlewood, S. 32
 Loynton, S. 32

M

Madsen, K. 53
 Mapelli, P. 55
 Marlène, W. 47
 Maroy, R. 36
 Mathe, D. 35
 Mattout, J. 40
 Meerman, J. 26
 Meiburger, K. M. 39
 Meijering, E. 23, 26, 27, 49
 Messa, C. 54, 55
 Mezzanotte, L. 21
 Milosevic, M. 51

Molinari, F. 39
 Moliner, L. 23
 Moore, J. 32
 Moore, W. 32
 Moresco, R. M. 44
 Mouysset, S. 39

N

Neves, C. 32
 Niessen, W.J. 23, 31, 49
 Noel, A. 50
 Nuyts, J. 21

O

Odet, C. 51
 Otazo, R. 24
 Ourselin, S. 38

P

Pacureanu, A. 53
 Papp, L. 35
 Patterson, A. 32
 Paulson, O. 53
 Peyrin, F. 53
 Picchio, M. 55
 Pinborg, L. 53
 Plenge, E. 23, 49
 Poole, D. S. 23
 Poot, D. 23, 49
 Postnov, A. 50
 Poussier, S. 50
 Pracht, E. 31
 Price, L. 26
 Prieto, J. C. 51

R

Reijneveld, J. C. 50
 Reinhardt, D. 13
 Remory, I. 55
 Revol-Muller, C. 51
 Ribes, S. 47
 Ricard, C. 52
 Rimoldi, O. 18
 Ripoll, J. 12, 24, 46
 Rizzo, G. 18
 Rodriguez, T. 52
 Rougon, G. 52
 Rudin, M. 46
 Rueden, C. 32
 Ruthotto, L. 44

S

Salvatore, C. 44
 Sassi, I. 54
 Sawatzky, A. 45
 Schäfers, K. 13, 17, 33, 44, 48
 Schmid, S. 33

Schmittbuhl, M. 52
 Schuit, R. C. 50
 Sciagra, R. 54
 Stanchi, F. 52
 Stapleton, S. 51, 56
 Stefano, A. 54
 Steimers, A. 28
 Stout, D. 34
 Strömblad, S. 27
 Stute, S. 39
 Sué, M. 35
 Suidgeest, E. 49
 Svarer, C. 16, 53
 Swedlow, J. 32

T

Takagaki, M. 14, 28
 Tarkowska, A. 32
 Tauber, C. 39
 Tavitian, B. 36
 Tenbrinck, D. 45
 Terreno, E. 39
 Tofts, P. 19

U

Uecker, M. 24

V

Valtorta, S. 44
 van Berckel, B. N. M. 50
 van de Giessen, M. 21, 45, 49
 van der Weerd, L. 23, 49
 Verbeek, F. 26
 Villa, E. 55
 Vollmar, S. 31, 35

W

Wang, H. 34
 Wehrl, H. 34
 Wells, S. 32
 Wiedermann, D. 31
 Wilhelm, C. 43
 Windhorst, A. D. 50
 Wolf, D. 50
 Wolters, C. H. 44

Y

Yndgaard, S. 53

Z

Zacharopoulos, A. 46
 Zbib, H. 39
 Zerdoud, S. 47
 Zhang, S. 24
 Ziebell, M. 53
 Zuber, V. 54
 Zuluaga, M. 53

European Society for Molecular Imaging – ESMI
management office
Eupener Str. 57-59
50933 Cologne
Germany

telephone: +49 (0)2 21 28 20 68 32
email: office@e-smi.eu
web: www.e-smi.eu

Layout: Doris Kracht
printing: Hundt Druck GmbH, Cologne

